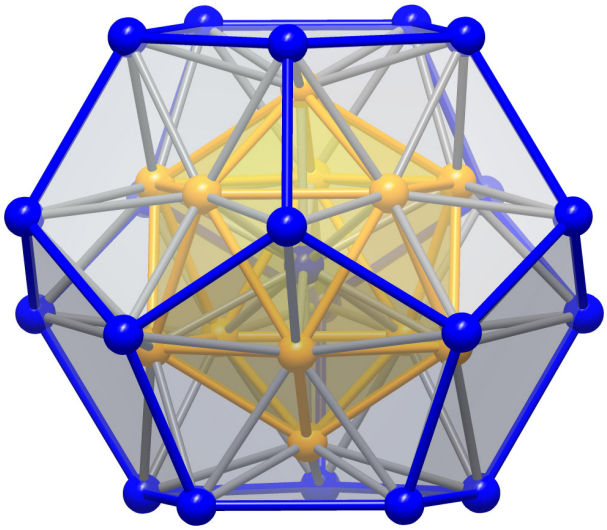

Clusters and Networks of Tetrel Elements and Late d Block Metals in Ternary Intermetallic Phases with Alkali and Alkaline Earth Metals

Saskia Stegmaier

Technische Universität München
Lehrstuhl für Anorganische Chemie
mit Schwerpunkt Neue Materialien

TECHNISCHE UNIVERSITÄT MÜNCHEN
Lehrstuhl für Anorganische Chemie mit Schwerpunkt Neue Materialien

Clusters and Networks of Tetrel Elements and Late d Block Metals in Ternary Intermetallic Phases with Alkali and Alkaline Earth Metals

Saskia Stegmaier

Vollständiger Abdruck der von der Fakultät für Chemie
der Technischen Universität München zur Erlangung des akademischen Grades eines
Doktors der Naturwissenschaften
genehmigten Dissertation.

Vorsitzender: Univ.-Prof. Dr. Lukas Hintermann
Prüfer der Dissertation:
1. Univ.-Prof. Dr. Thomas F. Fässler
2. Univ.-Prof. Dr. Karsten Reuter
3. Univ.-Prof. Dr. Hubert Schmidbaur (em.)

Die Dissertation wurde am 12.04.2012 bei der Technischen Universität München eingereicht und durch die Fakultät für Chemie am 25.05.2012 angenommen.

… – and yet – and yet – it's rather curious, you know, this sort of life!

Alice (in Wonderland) / Lewis Carroll

Dank sage ich

meinem Doktorvater

Prof. Dr. Thomas F. Fässler

für Vertrauen, Wohlwollen, Unterstützung und wissenschaftliche Freiheit.

Dr. Lisa Siggelkow für die Labor-, Büro- und Diskussionsgemeinschaft, für die sorgfältige Durchsicht und wertvolle Vorschläge zu Manuskripten dieser Arbeit sowie für Unterhaltung(en) in und außerhalb der Festkörperchemie. *Dr. Bernhard Wahl* für Interesse und Unterstützung nicht nur in speziellen kristallographischen Lagen. *Markus Waibel* für die Bürogemeinschaft, den Aufbau der neuen IT-Netzwerkstruktur am Lehrstuhl und insbesondere für das Auflösen meiner Cluster-Phasen. *Dr. M. Bele Boeddinghaus* für die SQUID-Betreuung und für gemeinsame Unternehmungen und die gute Zeit in München und anderswo. *Dr. Viktor Hlukhyy* für viele Gespräche und Anregungen zu festkörperchemischen Belangen. *Dr. Wilhelm Klein* insbesondere für die Diskussionsbereitschaft zu kristallographischen Fragen. *Dr. Sung-Jin Kim* für die Einführung in festkörperchemische Arbeitsweisen. *Manuela Donaubauer* für die Hilfe bei den organisatorischen Aspekten.

den *Gruppen Fässler*, *Kraus*, *Niewa* und *Nilges*.

meinem Bachelor- und später Master-Studenten *Alexander Henze* und meinen Forschungspraktikanten *Richard Brimioulle*, *Jürgen Kraus* und *Thomas Wagner*, sowie unserem Auszubildenden und später Laboranten *Fabian Krause* für ihr Engagement und die zu den jeweiligen Projekten geleisteten Beiträge.

der *Studienstiftung des Deutschen Volkes* für die Gewährung eines Promotionsstipendiums.
der *Technischen Universität München* für ein Promotionsstipendium im Rahmen des Hochschul- und Wissenschaftsprogramms (HWP).

Dank sage ich

Dr. Andreas Kaltzoglou unter anderem für die Einarbeitung an der DTA, *Priv.-Doz. Dr. Florian Kraus* für viele wertvolle Hinweise und Rubidium, *Dr. Sandra Scharfe* und *Volodymyr Baran* für geseigertes Natrium und Kalium, *Prof. Dr. Tom Nilges* für die stete Diskussionsbereitschaft, *Dr. Antti J. Karttunen* für Gespräche und Interesse nicht nur die theoretischen Teile dieser Arbeit betreffend, *Andrea Hoffmann* und *Ingrid Werner* für REM-Bilder, EDX- und SQUID-Messungen, *Laura-Alice Jantke* für die Zusammenarbeit an der gemeinsamen Publikation, *Dr.-Ing. Stephan D. Hoffmann* für die Einarbeitung am Oxford Diffraktometer.

Sebastian Baer, Christian Benda, Dr. Daniel Bräunling, Carina Dressel, Dr. Michael Evans, Dr. Frank Gäbler, Haiyan He, Thomas Henneberger, Dr. Florian Kiefer, Iryna Kurylyshyn, Dr. Prashanth W. Menezes, Dieter Rau, Dr. Annette Schier, Ursula Madan-Singh, Herta Slavik, Dr. Annette Spiekermann, Lorenzo Toffoletti, Dr. Jian-Qiang Wang, Patrick Woidy, Michael Zeilinger und allen anderen Mitgliedern der *Gruppen Fässler*, *Kraus*, *Niewa* und *Nilges* für die Zusammenarbeit, ihre Hilfsbereitschaft und gemeinsame Unternehmungen.

auch allen anderen, insbesondere Mitarbeitern der Fakultät für Chemie der Technischen Universität München, die zum Gelingen dieser Arbeit beigetragen haben.

meinen Freunden und *meiner Familie*.

Zusammenfassung

(Halb)metalle des p-Blocks (*E*) können zusammen mit späten d-Block-Metallen (*T*) und elektropositiven Metallen (*A*') intermetallische Phasen bilden, die als aus *A'*-Kationen und einer insgesamt negativ geladenen *T*–*E*-Teilstruktur bestehend beschrieben werden können. Diese *A'*–*T*–*E*-Phasen beeindrucken durch eine große Vielfalt an Strukturen und Bindungsverhältnissen. Gegenstand der vorliegenden Arbeit sind *A'*–*T*–*Tt*-Phasen (*E* = *Tt*; *Tt*: Tetrelelement), die Cluster, Clustersäulen oder Netzwerke als *T*–*Tt*-Teilstrukturen aufweisen.

$Na_{2.8}Cu_5Sn_{5.6}$ und ***$A_{12}Cu_{12}Sn_{21}$*** (*A* = Na, K, Rb, Cs), die ersten *A*–Cu–Sn-Phasen mit *A* = Na – Cs, weisen intermetalloide Cu–Sn-Clusterspezies auf, die in der Clusterchemie der (Halb)metalle der Gruppe 14 bislang einzigartig sind. In der Struktur von $Na_{2.8}Cu_5Sn_{5.6}$ liegen diskrete doppelwandige Cu–Sn-Säulen $^1_\infty\{Sn_{0.6}@Cu_5@Sn_5\}$ vor, die zu quasi-eindimensionalen metallischen Eigenschaften führen. Die isotypen $A_{12}Cu_{12}Sn_{21}$-Phasen enthalten mehrschalige Cluster $[Sn@Cu_{12}@Sn_{20}]^{12-}$ mit delokalisierter Clusterbindung. Die *A*–Cu–Sn-Verbindungen wurden durch Reaktion von Alkalimetallen mit zuvor hergestellten Cu–Sn-Legierungen synthetisiert und können – in Analogie zu Zintl-Verbindungen – als „salzartig", mit Alkalimetall-Kationen und intermetalloiden Cu–Sn-Polyanionen, angesehen werden.

$\{T@Tt_n\}$-Cluster mit einem endoedrischen *T*-Atom in einem $\{Tt_n\}$-Käfig sind aus der Chemie der Zintlanionen in Lösung bekannt. Im Rahmen dieser Arbeit wurden Berechnungen zur Analyse der (elektronischen) Struktur von $[Cu@Sn_9]^{3-}$, $[Ir@Sn_{12}]^{3-}$ und $[Co@Ge_{10}]^{3-}$ durchgeführt. Für einen Übersichtsartikel wurde ein Beitrag über theoretische Untersuchungen zu bestimmten Clusterspezies der Tetrelelemente verfasst. Die ternäre Phase **$Na_{12}NiSn_{17}$** mit den Clusteranionen $[Ni@Sn_9]^{4-}$ und $[Sn_4]^{4-}$ ist eine der ersten strukturell charakterisierten Festkörperphasen mit $\{T@Tt_n\}$-Clustern.

Die Verbindungen ***$A_{14}ZnGe_{16}$*** (*A* = K, Rb) weisen $[Ge_4]^{4-}$-Anionen und ein neues Isomer des Clusters $[(Ge_4)Zn(Ge_4)]^{6-}$ auf, welcher aus zwei tetraedrischen $\{Tt_4\}$-Einheiten und einem diese verknüpfenden *T*-Atom besteht. $\{(Tt_4)T(Tt_4)\}$-Strukturmotive sind von einer Reihe von Festkörperphasen bekannt. Besonderes Interesse verdienen die ternären $A_{14}ZnGe_{16}$-Verbindungen da sie zu den wenigen löslichen Zintl-Phasen mit $\{Tt_4\}$-Einheiten zählen.

Die *A*–Zn–*Tt*-Phasen (*A* = Li, Na; *Tt* = Ge, Sn) **Li_2ZnGe_3**, **$Li_3Zn_2Sn_4$**, **$Na_8Zn_4Ge_{42}$** und **Na_2ZnSn_5** weisen verschiedene Zn–*Tt*-Netzwerke vierbindiger Atome auf. Li_2ZnGe_3 und $Li_3Zn_2Sn_4$ bestehen aus Zn–*Tt*-Netzwerken mit diamant(polytyp)artigen Strukturen deren Zwischenräume mit Li-Atomen aufgefüllt sind. $Na_8Zn_4Ge_{42}$ besitzt eine Typ-I Clathrat-Struktur mit Na-Atomen in den käfigartigen Hohlräumen des Zn–Ge-Netzwerkes. Im Fall von *hP*- und *tI*-Na_2ZnSn_5 liegen offene Zn–Sn-Netzwerkstrukturen vor, die Kanäle aufweisen, welche mit Na-Atomen besetzt sind.

Der Polymorphismus der Zintl-Verbindung Na_2ZnSn_5 wurde im Rahmen dieser Arbeit aufgezeigt und untersucht. Der Phasenübergang von der metastabilen Modifikation *hP*-Na_2ZnSn_5 zur stabilen Modifikation *tI*-Na_2ZnSn_5 konnte mittels Röntgenbeugungs-experimenten am Pulver und am Einkristall *in situ* beobachtet werden. Des Weiteren wurde die Beziehung zwischen Na_2ZnSn_5 und $Na_5Zn_{2+x}Sn_{10-x}$ untersucht. Ausgehend von einer Analyse der Zn–Sn-Netzwerkstrukturen dieser Phasen wurde ein Konstruktionsprinzip für eine Serie von Netzwerken vierbindiger Atome entwickelt. Diese Netzwerke können, beispielsweise in theoretischen Studien, als Strukturen hypothetischer Allotrope der Tetrelemente C, Si, Ge und Sn betrachtet werden.

In den ternären *Ae*–Zn–Sn-Systemen mit den Erdalkalimetallen *Ae* = Ca und Sr wurden **$Ca_2Zn_3Sn_6$** und **$SrZn_2Sn_2$** erhalten. Diese Verbindungen sind typische polare intermetallische Phasen mit Zn–Sn-Netzwerken, die auch Atome mit Koordinationszahlen größer vier enthalten.

Die Synthese der intermetallischen Phasen erfolgte ausgehend von den Elementen über Hochtemperatur-Reaktionen. Kristallstrukturbestimmungen wurden mittels Röntgen-beugungsexperimenten an Einkristallen durchgeführt. Zu den verwendeten experimentellen Charakterisierungsmethoden zählen des Weiteren Röntgenpulverdiffraktometrie, energie-dispersive Röntgenspektroskopie (EDX) zur qualitativen und semi-quantitativen chemischen Analyse, thermische Analyse (DTA) und SQUID-Magnetometrie. Berechnungen der elektronischen Struktur von Festkörperverbindungen wurden mit dem Stuttgarter TB-LMTO-ASA Program durchgeführt. Für Berechnungen der (elektronischen) Struktur diskreter polyanionischer Cluster wurden GAUSSIAN und DGRID verwendet, letzteres für Berechnungen der Elektronenlokalisierungsfunktion (ELF).

Abstract

Intermetallic phases of p block (semi)metals (*E*), late d block metals (*T*), and electropositive metals (*A'*) which can be described in terms of *A'* cations and an overall negatively charged *T*–*E* substructure show an impressive variety of structures and bonding situations. The present thesis deals with *A'*–*T*–*Tt* ternary phases (*E* = *Tt*; *Tt*: tetrel element) that feature *T*–*Tt* clusters, rods or networks.

Intermetalloid Cu–Sn cluster species that are unprecedented in the cluster chemistry of the group 14 (semi)metals are exhibited by **$Na_{2.8}Cu_5Sn_{5.6}$** and ***A*$_{12}$Cu$_{12}$Sn$_{21}$** (*A* = Na, K, Rb, Cs), which represent the first *A*–Cu–Sn phases with *A* = Na to Cs. $Na_{2.8}Cu_5Sn_{5.6}$ shows discrete double-walled Cu–Sn columns $^1_\infty\{Sn_{0.6}@Cu_5@Sn_5\}$ giving rise to quasi-one-dimensional metallic characteristics. The isotypic $A_{12}Cu_{12}Sn_{21}$ phases feature onion-skin-like clusters $[Sn@Cu_{12}@Sn_{20}]^{12-}$ with delocalized cluster bonding. The phases, which were obtained via reactions of preformed Cu–Sn alloys with elemental alkali metals, may – in analogy to Zintl compounds – be considered as "salt-like" with alkali metal cations and intermetalloid Cu–Sn polyanions.

A number of $\{T@Tt_n\}$ clusters with an endohedral *T* atom in a $\{Tt_n\}$ cage are known from solution based Zintl anion chemistry. Computational studies on the (electronic) structures of $[Cu@Sn_9]^{3-}$, $[Ir@Sn_{12}]^{3-}$, and $[Co@Ge_{10}]^{3-}$ were performed as part of this thesis, and an overview on theoretical investigations on certain group 14 cluster species has been prepared as a contribution to a review article. The ternary phase **$Na_{12}NiSn_{17}$** with $[Ni@Sn_9]^{4-}$ and $[Sn_4]^{4-}$ clusters is among the first solid state phases with $\{T@Tt_n\}$ clusters that have been structurally characterized.

The ***A*$_{14}$ZnGe$_{16}$** compounds (*A* = K, Rb) show $[Ge_4]^{4-}$ anions and a new isomer of the $[(Ge_4)Zn(Ge_4)]^{6-}$ cluster, with two tetrahedral $\{Tt_4\}$ units linked by a *T* atom. $\{(Tt_4)T(Tt_4)\}$ structure motifs are known from a number of solid state phases. More importantly, the $A_{14}ZnGe_{16}$ compounds add to the sparse pool of soluble Zintl phases with $\{Tt_4\}$ cluster units.

The *A*–Zn–*Tt* phases (*A* = Li, Na*; Tt* = Ge, Sn) **Li_2ZnGe_3**, **$Li_3Zn_2Sn_4$**, **$Na_8Zn_4Ge_{42}$**, and **Na_2ZnSn_5** exhibit different four-connected Zn–*Tt* networks. The structures of Li_2ZnGe_3 and $Li_3Zn_2Sn_4$ represent Li-stuffed diamond polytype like Zn–*Tt* networks. $Na_8Zn_4Ge_{42}$ adopts a type-I clathrate structure with Na atoms in the cages of the Zn–Ge framework. In case of *hP*- and *tI*-Na_2ZnSn_5, Na atoms are situated in channels of Zn–Sn open network structures.

The polymorphism of the Zintl compound Na_2ZnSn_5 was revealed in the course of the present thesis, and the phase transition from metastable *hP*-Na_2ZnSn_5 to stable *tI*-Na_2ZnSn_5 was studied and observed in situ by means of powder and single crystal X-ray diffraction methods. Further, the relation between Na_2ZnSn_5 and $Na_5Zn_{2+x}Sn_{10-x}$ was investigated. Based on an analysis of the structural features of the Zn–Sn networks of these phases, a construction scheme for a series of four-connected networks was developed. These networks can be considered, for example in computational studies, as hypothetical allotrope structures of the group 14 elements C, Si, Ge, and Sn.

$Ca_2Zn_3Sn_6$ and **$SrZn_2Sn_2$** were obtained in the *Ae*–Zn–Sn systems with the alkaline earth metals *Ae* = Ca and Sr. These compounds represent typical polar intermetallic phases with Zn–Sn networks that comprise also atoms with coordination numbers higher than four.

The intermetallic phases were obtained via high temperature reactions of the elements. Single crystal X-ray diffraction methods were used for crystal structure determinations. Further methods of experimental characterization that were employed include powder X-ray diffraction, energy dispersive X-ray spectroscopy (EDX) for qualitative and semi-quantitative chemical analysis, thermal analysis (DTA), and SQUID magnetometer measurements. Solid state electronic structure calculations were performed with the Stuttgart TB-LMTO-ASA programs. Computational studies on discrete polyanionic clusters were carried out with GAUSSIAN and DGRID, which was used for calculations of the electron localization functions (ELF).

Abbreviations

0b	non-bonded
2c2e	two-center two-electron (bond)
3b	three-bonded
4b	four-bonded
5c6e	five-center six-electron (multicenter bond)
A	alkali metal
A'	electropositive alkali metal, alkaline earth metal, or rare earth metal
Ae	alkaline earth metal
ASA	atomic sphere approximation
bcc	body centered cubic
CCD	charge coupled device
COHP	crystal orbital Hamilton population
DFT	density functional theory
DTA	differential thermal analysis
E	p block (semi)metal
EDX	energy dispersive X-ray spectroscopy
E_F	Fermi energy
ELF	electron localization function
EN	electronegativity
fcc	face centered cubic
G	guest atom
HOMO	highest occupied molecular orbital
hP	primitive hexagonal
HP	high pressure (modification)
HT	high temperature (modification)
ICDD	International Centre for Diffraction Data
ICOHP	integrated crystal orbital Hamilton population
ICSD	Inorganic Crystal Structure Database
IDOS	integrated density of states
IPDS	imaging plate diffraction system
IP-PSD	imaging plate position sensitive detector

LDA	local density approximation
LMTO	linearized muffin-tin orbital
L-PSD	linear position sensitive detector
LT	low temperature (modification)
LUMO	lowest unoccupied molecular orbital
M	metal
MO	molecular orbital
N	network atom
NBO	natural bond orbital (analysis)
Occ.	occupancy
PDF	Powder Diffraction File
PDOS	partial density of states
R	rare earth metal
SEM	scanning electron microscopy
SQUID	superconducting quantum interference device
T	d block metal
TB	tight-binding
tI	body centered tetragonal
Tr	group 13 (semi)metal (triel element)
Tt	group 14 (semi)metal (tetrel element)
vec	valence electron concentration
XRD	X-ray diffraction

Table of Contents

1 Introduction **1**

1.1 Intermetallics, Zintl Compounds, and Polar Intermetallic Phases 1

1.2 Background, Scope, and Outline of this Work 3

1.3 References 6

2 Intermetalloid Clusters of Ge and Sn with Late d Block Metals **7**

2.1 Introduction and Outline 7

2.2 Discrete Multiply Endohedral Intermetalloid Cu–Sn Columns and Clusters in Novel Solid State Phases Related to Zintl Compounds 10

2.2.1 $^{1}_{\infty}\{Sn_{0.6}@Cu_5@Sn_5\}$ Cluster Columns in $Na_{2.8}Cu_5Sn_{5.6}$ 10

2.2.2 $[Sn@Cu_{12}@Sn_{20}]^{12-}$ Clusters in $A_{12}Cu_{12}Sn_{21}$ (A = Na, K, Rb, Cs) 11

2.2.3 Structural Relations 13

2.3 Tetrel Element Cages Filled with an Endohdral Late d Block Metal Atom 15

2.3.1 Computational Studies on $[Cu@Sn_9]^{3-}$, Icosahedral $[Ir@Sn_{12}]^{3-}$ and Non-Deltahedral $[Co@Ge_{10}]^{3-}$ 15

2.3.2 The Solid State Phase $Na_{12}NiSn_{17}$ with $[Ni@Sn_9]^{4-}$ and $[Sn_4]^{4-}$ Clusters 18

2.4 Zn-Linked Tetrahedral Ge Clusters 20

2.4.1 $A_{14}ZnGe_{16}$ (A = K, Rb) with $[(Ge_4)Zn(Ge_4)]^{6-}$ and $[Ge_4]^{4-}$ Clusters 20

2.5 Discussion 21

2.6 References 23

3 Zintl Phases and Polar Intermetallics with Zn–Ge and Zn–Sn Networks 25

3.1 Introduction 25

3.2 *Tt*-Rich *A*–Zn–*Tt* Phases with Networks of Four-Bonded Atoms (*A* = Li, Na; *Tt* = Ge, Sn) 29

3.2.1 Introduction and Outline 29

3.2.2 Li_2ZnGe_3 and $Li_3Zn_2Sn_4$ with Diamond Polytype Analogous Zn–*Tt* Networks 30

3.2.3 The Clathrate $Na_8Zn_4Ge_{42}$ 31

3.2.4 Polymorphs and Phase Transitions of the Zintl Compound Na_2ZnSn_5 33

3.2.5 Topological Relationships of Four-Connected Networks Based on Structures of Sn-Rich Na–Zn–Sn Phases 34

3.3 *Ae*–Zn–Sn Phases with Networks of Interconnected Layers (*Ae* = Ca, Sr) 36

3.3.1 The Polar Intermetallic Phases $SrZn_2Sn_2$ and $Ca_2Zn_3Sn_6$ 36

3.4 Discussion 37

3.5 References 38

4 Summary and Conclusion 41

5 Methods 47

5.1 General Experimental Procedures 47

5.2 Synthesis 47

5.2.1 Starting Materials 47

5.2.2 Reaction Containers 48

5.2.3 Furnaces 48

5.3 Experimental Characterization 48

5.3.1 Powder X-ray Diffraction 48

5.3.2 Single Crystal X-ray Diffraction and Crystal Structure Determination 49

5.3.3 Scanning Electron Microscopy and Energy Dispersive X-ray Spectroscopy 50

5.3.4 Differential Thermal Analysis 51

5.3.5 Magnetic Measurements 51

5.4 Computational Studies 51

5.4.1 Solid State Electronic Structure Calculations 51

5.4.2 Molecular Electronic Structure Calculations 52

5.5 References 52

6 Publications and Manuscripts 55

6.1 $Na_{2.8}Cu_5Sn_{5.6}$: A Crystalline Alloy Featuring Intermetalloid $^1{}_\infty\{Sn_{0.6}@Cu_5@Sn_5\}$ Double-Walled Nanorods with Pseudo-Five-Fold Symmetry 57
S. Stegmaier, T. F. Fässler,
Angew. Chem. Int. Ed. **2012**, *51*, 2647; *Angew. Chem.* **2012**, *124*, 2701.

6.2 A Bronze Matryoshka: The Discrete Intermetalloid Cluster $[Sn@Cu_{12}@Sn_{20}]^{12-}$ in the Ternary Phases $A_{12}Cu_{12}Sn_{21}$ (A = Na, K) 59
S. Stegmaier, T. F. Fässler, *J. Am. Chem. Soc.* **2011**, *133*, 19758.

6.3 $[Cu@Sn_9]^{3-}$ and $[Cu@Pb_9]^{3-}$: Intermetalloid Clusters with Endohedral Cu Atoms in Spherical Environments 61
S. Scharfe, T. F. Fässler, S. Stegmaier, S. D. Hoffmann, K. Ruhland,
Chem. Eur. J. **2008**, *14*, 4479.

6.4 Step-by-Step Synthesis of the Endohedral Stannaspherene $[Ir@Sn_{12}]^{3-}$ via the Capped Cluster Anion $[Sn_9Ir(cod)]^{3-}$ 63
J.-Q. Wang, S. Stegmaier, B. Wahl, T. F. Fässler,
Chem. Eur. J. **2010**, *16*, 1793.

6.5 $[Co@Ge_{10}]^{3-}$: An Intermetalloid Cluster with Archimedean Pentagonal Prismatic Structure 65
J.-Q. Wang, S. Stegmaier, T. F. Fässler,
Angew. Chem. Int. Ed. **2009**, *48*, 1998; *Angew. Chem.* **2009**, *121*, 2032.

6.6 *Chapter on Theoretical Investigations in the Review Article:* Zintl Ions, Cage Compounds, and Intermetalloid Clusters of Group 14 and Group 15 Elements 67
S. Scharfe, F. Kraus, S. Stegmaier, A. Schier, T. F. Fässler, *Angew. Chem. Int. Ed.* **2011**, *50*, 3630; *Angew. Chem.* **2011**, *123*, 3712.

6.7 Intermetalloid Ni-Filled Sn Clusters $[Ni@Sn_9]^{4-}$ and Tetrahedral $[Sn_4]^{4-}$ in the Solid State Phase $Na_{12}NiSn_{17}$ 69
S. Stegmaier, T. F. Fässler, *manuscript in preparation.*

6.8 The Soluble Zintl Phases $A_{14}ZnGe_{16}$ (A = K, Rb) Featuring $[(\eta^3\text{-}Ge_4)Zn(\eta^2\text{-}Ge_4)]^{6-}$ and $[Ge_4]^{4-}$ Clusters and the Isolation of $[(MesCu)_2(\eta^3,\eta^3\text{-}Ge_4)]^{4-}$ – the Missing Link in the Solution Chemistry of Tetrahedral Group 14 Element Zintl Clusters 81
S. Stegmaier, M. Waibel, A. Henze, L.-A. Jantke, A. J. Karttunen, T. F. Fässler, *J. Am. Chem. Soc.* **2012**, *134*, 14450.

6.9 Lithium-Stuffed Diamond Polytype Zn–*Tt* Structures (*Tt* = Sn, Ge): The Two Lithium-Zinc-Tetrelides $Li_3Zn_2Sn_4$ and Li_2ZnGe_3 83
S. Stegmaier, T. F. Fässler, *Inorg. Chem.*, http://dx.doi.org/10.1021/ic3011037.

6.10 The Intermetallic Type-I Clathrate $Na_8Zn_4Ge_{42}$ 85
S. Stegmaier, T. F. Fässler, *manuscript for publication.*

6.11 Reorientation of Hexagonal Helical Channels in Tetrahedral Framework Structures – Phase Transitions of the Zintl Phase Na_2ZnSn_5 and its Relation to $Na_5Zn_{2+x}Sn_{10-x}$ 97
S. Stegmaier, S.-J. Kim, A. Henze, T. F. Fässler, *manuscript for publication.*

6.12 Topological Relationships of Four-Connected Networks Based on Structures of Sn-Rich Na–Zn–Sn Phases 133
S. Stegmaier, T. F. Fässler, *manuscript for publication.*

6.13 $SrZn_2Sn_2$ and $Ca_2Zn_3Sn_6$ – Two New *Ae*–Zn–Sn Polar Intermetallic Compounds (*Ae*: Alkaline Earth Metal) 143
S. Stegmaier, T. F. Fässler, *J. Solid State Chem.* **2012**, *192*, 312.

Note

This work is composed as a paper style thesis. For articles which are already published in peer-reviewed journals the bibliographic data are given, manuscripts prepared for submission are included in chapter 6.

A general introduction to the research field as well as an overview of the results of this thesis is provided in chapter 1. Chapters 2 and 3 comprise more specific introductions, summaries of the articles or, in case of joint publications, the respective contributions which originated from this thesis project, and some more detailed comparative discussions. An overall summary and concluding discussion is presented in chapter 4. Brief descriptions of employed experimental and computational methods are given in chapter 5.

1 Introduction

1.1 Intermetallics, Zintl Compounds, and Polar Intermetallic Phases

In the interdisciplinary area of materials research, the prime domain of chemistry is the synthesis and characterization of both known and new materials. The term "materials design" can refer to optimizing the properties of a given material for a certain application, for example by gradually changing the chemical composition. In a most ambitious sense it might imply that there is a rational way to a new material with desired properties. Such "designing" requires knowledge that enables first to anticipate the structure and composition of a substance which exhibits these properties, and then to obtain it. Yet a corresponding comprehensive understanding of the relations between chemical composition, structure, and properties, as well as generally applicable strategies for synthesis planning and reaction control are, to date, not available in many fields. This is also the case for intermetallics,[1] which belong to the domain of inorganic solid state chemistry.

Intermetallics are chemical substances, with a defined composition or narrow homogeneity range, which comprise atoms of two or more (semi)metallic elements and usually adopt a crystal structure different from that of the constituting (semi)metals. The terms "intermetallics", "intermetallic compounds", and "intermetallic phases" are generally used interchangeably. Among the metallic elements, which represent the vast majority of chemical elements, there is great diversity. Consider for example the high chemical reactivity of the alkali metals in contrast to the inert behavior of the coinage metals, which can be found in their elemental state in nature, or the melting points of the two metals mercury (–39 °C) and tungsten (3410 °C). While for most s and d block metals at least delocalized metallic bonding and structures based on sphere packings are common features, most of the p block (semi)metals of groups 13 to 16 exhibit different structures and bonding characteristics. Tin stands out with its metallic β-modification and its α-form with a cubic diamond structure and covalent bonding, which are stable above or below 13.2 °C, respectively. Obviously, there is a plethora of combinations of (semi)metals that can lead to the formation of intermetallic compounds, and the great variety of intermetallics – in terms of crystal and

electronic structures, chemical and physical properties – is no surprise. Their properties qualify certain intermetallics for various applications,[2, 3] including magnetic and superconducting materials, phase-change materials for data storage,[4] or thermoelectrics for power generation from waste heat or energy efficient cooling and heating devices,[5] to name just a few examples. A number of schemes exist for the classification of intermetallic phases.[6] Emphasis may be put on the types of constituting elements, chemical bonding, crystal structure, structure determining factors, physical properties etc. Of course all these aspects are mutually dependent, but often the classification of a certain intermetallic compound is not unambiguous. There are examples which fit to one or more groups by some but not all criteria.

Zintl compounds are formed by the combination of (semi)metals that have very different electronegativities, namely electropositive alkali, alkaline earth or rare earth metals (*A'*) and more electronegative p block (semi)metals (*E*). Within the Zintl concept, formally a full charge transfer from *A'* to *E* is assumed, and the interactions between the resulting cations of *A'* and the polyanions of *E* are considered to have ionic character, implying a "salt-like" description. Within the polyanionic parts, localized covalent two-center *E*–*E* bonding as well as localized lone pairs of *E* atoms can be present, and the structures of the polyanions follow the 8–*N* rule. An extension of the definition for Zintl compounds includes Wade's rules for the electron count and structure of clusters for the polyanionic part. Due to their bonding characteristics, Zintl phases are expected to be semiconducting, and usually no phase widths occur. The bonding features become more involved for ternary phases with mixed *E*–*E'* polyanions of two different p block (semi)metals, or *T*–*E* polyanions including a late d block metal *T* (like Zn from group 12), since then there can also be heteronuclear, polar covalent bonds within the polyanionic part.

Polar intermetallics are closely related to Zintl compounds. They, too, are formed by electropositive metals and p block and/or transition metals and they are also commonly described in terms of positively charged atoms and a negatively charged network. However, a "salt-like" description is not applicable for polar intermetallics, and they are fairly good conductors. The substructures that are built up by the more electronegative metal atoms can involve atoms with coordination numbers exceeding four, and they cannot be described with the 8–*N* rule for covalent two-center bonding, but require to take e.g. also multicenter and delocalized bonds into account. Generally, the interplay of structure determining factors – including the electron count, size and packing effects – is considered to be far more

complicated for polar intermetallics, as compared to Zintl compounds. Deviations from ideal electron counts, which are established for certain structures, occur frequently.

The boundary between Zintl compounds and polar intermetallics is diffuse, and especially compounds at the borderline of localized covalent and metallic bonds often show interesting bonding patterns, crystal structures and physical properties. A motivation for fundamental research concerned with the synthesis and characterization of new Zintl phases and polar intermetallic compounds is to contribute to the understanding of relations between composition, structures, and properties – which has been mentioned as a prerequisite for rational materials design at the beginning of this section. Any new intermetallic compound adds to the pool of potential materials, and its characterization can contribute to the knowledge base on intermetallics – by corroborating or challenging classification schemes and concepts, or by just not fitting in.

1.2 Background, Scope, and Outline of this Work

Ternary phases of p block (semi)metals and d block metals with electropositive alkali, alkaline earth, or rare earth metals, which can be described in terms of cations of the electropositive metals and an overall negatively charged substructure that is formed by the p and d block element atoms, show a variety of different structures and bonding situations. There are representatives of electron precise Zintl compounds as well as polar intermetallic phases among them, and these ternary systems are a fertile ground to further explore the borderline between these types of compounds in search for new structures and bonding features in intermetallics.

In this area, a focus of the Fässler group's research is set on compounds of the group 14 (semi)metals (*Tt*) with alkali (*A*) and alkaline earth metals (*Ae*). The present thesis contributes to this field with studies on ternary phases in the systems Na–Ni–Sn, *A*–Cu–Sn (*A* = Na, K, Rb, Cs), *A*–Zn–Sn (*A* = Li, Na), *A*–Zn–Ge (*A* = Li, Na, K, Rb), and *Ae*–Zn–Sn (*Ae* = Ca, Sr). While the corresponding binary *A*–*Tt* and *Ae*–*Tt* systems have been studied intensively in the last decades, and also *A*–*T*, *Ae*–*T* and *T*–*Tt* (*T*: d block metal) phase diagrams are available, little to nothing was known about most of the ternary systems under consideration. Prior to this work, no *A*–*T*–Sn phases with *A* = Na to Cs and *T* = Ni or Cu have been reported. Lists of known *A*–Zn–*Tt* phases with *A* = Li to Cs and *Tt* = Ge or Sn, as well as *Ae*–Zn–Sn phases

with *Ae* = Ca, Sr, Ba are given in Tables 3.1 and 3.2. The manifold Na–Zn–Sn phases are all due the PhD project of S.-J. Kim in the Fässler group.[7] One of the most obvious structural features that show the diversity of (binary and ternary) Zintl compounds and polar intermetallic phases is the dimensionality of the polyanionic structure parts. There can be one-, two-, or three-dimensionally extended polymeric chains or rods, layers, or networks, respectively, as well as smaller units, from isolated atoms to finite chains or discrete clusters ("zero-dimensional").

The phases that are presented in this work feature *T*–*Tt* metal clusters, metal rods or metal networks as substructures in *A*–*T*–*Tt* and *Ae*–*T*–*Tt* intermetallic compounds.

Heterometallic *T*–*Tt* cluster species are the subject of **chapter 2** (**publications and manuscripts 6.1 to 6.8**). Homoatomic cage cluster anions $\{Tt_n\}$ (n = 4, 9) of the group 14 (semi)metals are known both in solid state Zintl phases and as Zintl anions in solution.[8] But while a number of clusters with *Tt* cages filled with endohedral *T* atoms $\{T_m@Tt_n\}$ (n = 9, 10, 12 with m = 1; n = 17 with m = 2; n = 18 with m = 2 or 3) have been obtained from reactions with soluble A_4Tt_9 phases and metallorganic d block metal compounds,[8] no neat solid state phases with such discrete *T*–*Tt* clusters were known prior to this work. The intent to find *A*–*T*–*Tt* phases with *T*–*Tt* cluster species in the course of the present thesis project is set in this context. The objective was achieved with the synthesis of new phases in the systems *A*–Cu–Sn (*A* = Na to Cs) and Na–Ni–Sn. The obtained Cu–Sn cluster species are unprecedented in the cluster chemistry of the group 14 (semi)metals: Discrete double-walled $^1{}_\infty\{Sn_{0.6}@Cu_5@Sn_5\}$ columns and onion-skin-like $[Sn@Cu_{12}@Sn_{20}]^{12-}$ clusters are the *T*–*Tt* polyanions in $Na_{2.8}Cu_5Sn_{5.6}$ and the series of $A_{12}Cu_{12}Sn_{21}$ phases (*A* = Na, K, Rb, Cs), respectively (chapters 2.2.1 and 2.2.2; publications 6.1 and 6.2). The electronic structure of the solid state phases and the discrete $[Sn@Cu_{12}@Sn_{20}]^{12-}$ cluster anion were analyzed by means of band structure and molecular orbital calculations, respectively. In contrast to the cage clusters filled with a single endohedral atom, the bonding situation of the multiply endohedral intermetalloid cluster species with a high *T* metal content is clearly beyond a simple extension of common concepts for p block clusters such as Wade's rules. Computational studies on the $\{T@Tt_n\}$ clusters $[Cu@Sn_9]^{3-}$,[9] $[Ir@Sn_{12}]^{3-}$,[10] and $[Co@Ge_{10}]^{3-}$,[11] which have been synthesized in the Fässler group via reactions in solution, were also performed as a part of the present thesis (chapter 2.3.1; contributions to publications 6.3, 6.4, 6.5). Furthermore, a chapter on theoretical investigations on certain group 14 cluster species as part of a review article (contribution to publication 6.6) originates from this work. With $Na_{12}NiSn_{17}$, which features $[Ni@Sn_9]^{4-}$ and $[Sn_4]^{4-}$ cluster anions, a ternary phase with

a {T@Tt_9} nine-vertex cage cluster centered by a single T atom was identified (chapter 2.3.2; manuscript 6.7). Finally, the $A_{14}ZnGe_{16}$ compounds (A = K, Rb) presented in chapter 2.4 (publication 6.8) show a new isomer of the $[(Ge_4)Zn(Ge_4)]^{6-}$ cluster and $[Ge_4]^{4-}$ anions. Also in this case electronic structure calculations were carried out both for the solid state phases as well as for the discrete clusters. In the field of solid state chemistry, the $A_{14}ZnGe_{16}$ phases add to a group of compounds with heterometallic polyanions built of {Tt_4} tetrahedra linked by other (mostly late d block) metal atoms. Moreover, in cooperation with other coworkers in the Fässler group it was found that the $A_{14}ZnGe_{16}$ phases dissolve in liquid ammonia and add to the sparse pool of precursors for solution based group 14 Zintl anion chemistry. A reaction with mesitylcopper (MesCu) yielded the cluster $[(MesCu)_2Ge_4]^{4-}$ which represents the first $[Ge_4]^{4-}$ species obtained from solution (see joint publication 6.8).

Chapter 3 (**publications and manuscripts 6.9 to 6.13**) deals with Zintl phases and polar intermetallics featuring T–Tt networks with T = Zn and Tt = Ge or Sn. Two Sn-rich Na–Zn–Sn phases with open Zn–Tt frameworks with hexagonal channels which are occupied by Na atoms have been described prior to this thesis.[7] Channel structures are often related to potential ion conducting properties, and an intent of the present work was to study whether such or related structures could also be realized with Tt = Ge instead of Sn in the framework and with A = Li instead of Na as guest atoms. The corresponding attempts yielded the Li phases Li_2ZnGe_3 and $Li_3Zn_2Sn_4$ which show Li-stuffed diamond polytype like Zn–Tt networks (chapter 3.2.2; publication 6.9), and the type-I clathrate $Na_8Zn_4Ge_{42}$ with Na atoms in the cages of a Zn–Ge framework (chapter 3.2.3; manuscript 6.10). The results of further studies on the two previously identified Sn-rich Na–Zn–Sn phases already mentioned above are described in chapter 3.2.4 (manuscript 6.11). In the course of the present project, the synthesis of the phases has been optimized and it is established that actually both are modifications of the Zintl compound Na_2ZnSn_5. The phase transition from metastable *hP*-Na_2ZnSn_5 to stable *tI*-Na_2ZnSn_5 was studied and observed in situ by means of powder and single crystal X-ray diffraction methods. Furthermore, the relation between Na_2ZnSn_5 and $Na_5Zn_{2+x}Sn_{10-x}$[12] was investigated. Based on an analysis of the structural relations between the polyanionic networks of these Sn-rich Na–Zn–Sn phases, a construction scheme for a series of four-connected networks has been developed (chapter 3.2.5; manuscript 6.12), which might serve as input for computational studies on hypothetical allotropes of the group 14 elements. Na_2ZnSn_5, $Na_8Zn_4Ge_{42}$ and Li_2ZnGe_3 qualify as electron precise Zintl phases with four-bonded polyanionic Zn–Tt networks which follow the 8–N rule. $Li_3Zn_2Sn_4$ still exhibits a network of four-bonded Zn and Sn atoms though it falls short of the expected electron count

for a valence compound. Typical polar intermetallic phases were obtained with the alkaline earth metals *Ae* = Ca and Sr. $Ca_2Zn_3Sn_6$ and $SrZn_2Sn_2$ have Zn–Sn networks that comprise also atoms with coordination number five and electron counts which can be rationalized with models that include both covalent and multicenter bonding (chapter 3.3; publication 6.13).

1.3 References

[1] T. F. Fässler, G. J. Miller, *Z. Anorg. Allg. Chem.* **2011**, *637*, 1935.

[2] J. H. Westbrook, R. L. Fleischer, Eds., *Intermetalic Compounds*, John Wiley & Sons.

[3] G. Sauthoff, *Intermetallics*, Wiley-VCH, **1995**.

[4] M. Wuttig, N. Yamada, *Nat. Mater.* **2007**, *6*, 824.

[5] G. J. Snyder, E. S. Toberer, *Nat. Mater.* **2008**, *7*, 105.

[6] R. Nesper, *Angew. Chem. Int. Ed. Engl.* **1991**, *30*, 789; *Angew. Chem.* **1991**, *103*, 805.

[7] S.-J. Kim, Dissertation, Technische Universität München, **2007**.

[8] S. Scharfe, F. Kraus, S. Stegmaier, A. Schier, T. F. Fässler, *Angew. Chem. Int. Ed.* **2011**, *50*, 3630; *Angew. Chem.* **2011**, *123*, 3712.

[9] S. Scharfe, T. F. Fässler, S. Stegmaier, S. D. Hoffmann, K. Ruhland, *Chem. Eur. J.* **2008**, *14*, 4479.

[10] J.-Q. Wang, S. Stegmaier, B. Wahl, T. F. Fässler, *Chem. Eur. J.* **2010**, *16*, 1793.

[11] J.-Q. Wang, S. Stegmaier, T. F. Fässler, *Angew. Chem. Int. Ed.* **2009**, *48*, 1998; *Angew. Chem.* **2009**, *121*, 2032.

[12] S. Ponou, S.-J. Kim, T. F. Fässler, *J. Am. Chem. Soc.* **2009**, *131*, 10246.

2 Intermetalloid Clusters of Ge and Sn with Late d Block Metals

2.1 Introduction and Outline

Interdisciplinary interest in *intermetalloid*[1] clusters extends across the fields of gas phase cluster science, solution based cluster chemistry, and solid state chemistry of intermetallic systems. Among other things, intermetalloid clusters are ascribed to contribute to a better understanding of the transition (in terms of bonding, structure, and properties) from aggregates of a few metal atoms to bulk solid state materials.[2, 3] Ligand-free cluster chemistry of the group 14 (semi)metals in the condensed state basically is Zintl anion chemistry. And this is a genuine meeting point of solid state and solution based chemistry. The description of Zintl phases as "salt-like" proves truly appropriate for a number of representatives with polyanionic clusters of the group 14 (semi)metals. These phases dissolve in polar solvents, such as liquid ammonia, ethylenediamine, and N,N-dimethylformamide, and salts of the polyanions can crystallize from solution. In the last decades the field of solution based Zintl anion chemistry of the group 14 (semi)metals has developed rapidly, with K_4Tt_9 Zintl phases as the most commonly used precursor phases providing nine-atom cage cluster anions $\{Tt_9\}$ with Tt = Ge, Sn, and Pb. The $\{Tt_9\}$ clusters were not only found to be stable in solution, but also to be able to undergo a variety of different reactions. Dimers and oligomeric or polymeric chains of $\{Tt_9\}$ cluster units result from oxidative coupling reactions (in case of Tt = Ge), main-group or transition-metal organometallic fragments can be added to the clusters, and also ligand-free heterometallic clusters can be obtained from reactions with metallorganic complexes or other coordination compounds of d block metals.[4, 5]

Generally, most of the ligand-free *T*–*Tt* clusters with *Tt* and other (mostly late d block) metal atoms *T* , which have been structurally characterized by means of X-ray diffraction methods, fit into a classification scheme with two types.[4] Representatives of the first type comprise group 14 cages filled with endohedral *T* atoms $\{T_m@Tt_n\}$. The others show (empty) group 14 cages linked by *T* atoms and (in most cases) no direct intercluster *Tt*–*Tt* bonds. The term

intermetalloid cluster has firstly been coined for the filled clusters,[1] but it has also been used for the others.[6]

For the group of linked empty cage clusters, $\{(Tt_n)T_m(Tt_n)\}$ units, $\{[(Tt_n)T]_p(Tt_n)\}$ chains, and $^1_\infty\{(Tt_n)T\}$ polymers are actually known both from solution based cluster chemistry as well as from solid state chemistry. There is, however, a certain discrepancy: Up to now, polyanions with linked $\{Tt_9\}$ cages have only been obtained from reactions in solution, while cluster species with linked tetrahedral $\{Tt_4\}$ units are reported to occur as polyanions in neat solid state phases. For example, Cs_6ZnGe_8[7] and A_5InPb_8 (A = K, Rb)[8] show $[(Ge_4)Zn(Ge_4)]^{6-}$ and $[(Pb_4)In(Pb_4)]^{5-}$ units, respectively, A_6CdPb_8 (A = K, Rb)[9] features $[(Pb_4)Cd(Pb_4)Cd(Pb_4)$-$Cd(Pb_4)]^{10-}$ oligomeric chains and single $[Pb_4]^{4-}$ clusters, and linear polymeric chains $^1_\infty\{[(Tt_4)Au]^{3-}\}$ are found for the isotypic A_3AuTt_4 phases (Tt = Ge[10] and Sn[11] with A = K, Rb, Cs; Tt = Pb[11] with A = Rb, Cs).

In contrast, prior to this project, all structurally characterized compounds with filled cage clusters $\{T_m@Tt_n\}$ were obtained from solution based Zintl anion chemistry, and no neat solid state phases with discrete *T*–*Tt* clusters of this kind had been reported. The group of known $\{T_m@Tt_n\}$ polyanions from solution comprises clusters with different cage sizes and up to three endohedral atoms (n = 9, 10, 12 with m = 1; n = 17 with m = 2; n = 18 with m = 2 or 3).[4, 5] The filled nine-atom cage cluster anions among them are $[Ni@Tt_9]^{3-}$ with Tt = Ge[12] and Sn,[13] $[Ni@Sn_9]^{4-}$,[14] and $[Cu@Tt_9]^{3-}$ with Tt = Sn and Pb.[15]

For the group of filled cage clusters, the *A*–*T*–Sn phases (T = Cu, Ni) with polyanionic Cu–Sn and Ni–Sn cluster species that are presented in this thesis are in the front line of solid state phases catching up with compounds from solution based chemistry. With the *A*–Cu–Sn phases presented herein the solid state phases actually get a head start as it comes to *T*–*Tt* cluster species with a high T metal content. $Na_{2.8}Cu_5Sn_{5.6}$ and the series of $A_{12}Cu_{12}Sn_{21}$ phases (A = Na, K, Rb, Cs) feature discrete double-walled $^1_\infty\{Sn_{0.6}@Cu_5@Sn_5\}$ columns and onion-skin-like $[Sn@Cu_{12}@Sn_{20}]^{12-}$ clusters, respectively (chapter 2.2; publications 6.1 and 6.2). The description of these phases with discrete Cu–Sn polyanions and alkali metal cations is supported by the results of electronic structure calculations.

Computational studies on the related smaller clusters $[Cu@Sn_9]^{3-}$,[15] $[Ir@Sn_{12}]^{3-}$,[16] and $[Co@Ge_{10}]^{3-}$[17] were also carried out in the course of the present project (chapter 2.3.1; contributions to joint publications 6.3, 6.4, 6.5). In this context, a chapter on theoretical investigations on certain group 14 cluster species as part of a review article was prepared (contribution to publication 6.6). See the subsection “Wade’s Rules, Shell Models, Spherical

Aromaticity, and Cluster MOs" for a brief introduction on theoretical concepts that are commonly used in the discussion of the structure and chemical bonding of group 14 (semi)metal clusters.

In chapter 2.3.2 (manuscript 6.7), the ternary phase $Na_{12}NiSn_{17}$ is presented. It features $[Ni@Sn_9]^{4-}$ and $[Sn_4]^{4-}$ cluster anions, and thus represents a solid state phase with a $\{T@Tt_9\}$ cluster species that is already known from solution based chemistry.[14] Together with related phases that have been characterized very recently by other coworkers of the Fässler group,[18] it starts a new series of neat solid state phases with $\{T@Tt_9\}$ cluster polyanions.

The $A_{14}ZnGe_{16}$ phases described in chapter 2.4.1 (joint publication 6.8) show a new isomer of the $[(Ge_4)Zn(Ge_4)]^{6-}$ cluster and $[Ge_4]^{4-}$ anions, and thus join the group of known solid state phases with tetrahedral $\{Tt_4\}$ units linked by *T* atoms that have been mentioned above. As for the relation between solid state and solution based Zintl anion cluster chemistry, the $A_{14}ZnGe_{16}$ phases turned out to be a suitable precursor to obtain the first tetrahedral $\{Tt_4\}$ species with *Tt* = Ge from solution. As shown by other coworkers in the Fässler group, the $A_{14}ZnGe_{16}$ phases dissolve in liquid ammonia, and a reaction of $K_{14}ZnGe_{16}$ with mesitylcopper (MesCu) yielded the cluster $[(MesCu)_2Ge_4]^{4-}$ (see joint publication 6.8).

The ternary solid state phases that are presented in this chapter were obtained via high temperature reactions (resistance tube furnaces) in argon-atmosphere using sealed niobium or tantalum ampoules as reaction containers. For the synthesis of the *A*–Cu–Sn phases and $Na_{12}NiSn_{17}$, binary *T*–Sn alloys were pre-prepared (by arc-melting elemental Cu and Sn or Ni and Sn, respectively), and then used for reactions with the corresponding alkali metals. The $A_{14}ZnGe_{16}$ phases were synthesized by direct reactions of the elements. The crystal structures of the ternary phases were determined by means of single crystal X-ray diffraction methods. Further methods of experimental characterization that were used (in all or selected cases) include powder X-ray diffraction, qualitative and semi-quantitative chemical analysis (EDX), thermal analysis (DTA), and SQUID magnetometer measurements. Solid state electronic structure calculations were carried out with the Stuttgart TB-LMTO-ASA programs.[19] The GAUSSIAN package of programs[20] was used for computational studies on discrete polyanions.

2.2 Discrete Multiply Endohedral Intermetalloid Cu–Sn Columns and Clusters in Novel Solid State Phases Related to Zintl Compounds

2.2.1 $^1_\infty\{Sn_{0.6}@Cu_5@Sn_5\}$ Cluster Columns in $Na_{2.8}Cu_5Sn_{5.6}$

see publication 6.1 — $Na_{2.8}Cu_5Sn_{5.6}$: A Crystalline Alloy Featuring Intermetalloid $^1_\infty\{Sn_{0.6}@Cu_5@Sn_5\}$ Double-Walled Nanorods with Pseudo-Five-Fold Symmetry
S. Stegmaier, T. F. Fässler, *Angew. Chem. Int. Ed.* **2012**, *51*, 2647; *Angew. Chem.* **2012**, *124*, 2701.

$Na_{2.8}Cu_5Sn_{5.6}$ was synthesized via a reaction of a preformed Cu–Sn alloy with elemental Na. The crystal structure of the phase shows discrete one-dimensional Cu–Sn columns $^1_\infty\{Sn_{0.6}@Cu_5@Sn_5\}$ with pseudo-five-fold symmetry (Figure 2.1a,c). The columns are arranged in style of a hexagonal rod packing (Figure 2.1b), and they are separated from each other by a substructure of Na atoms that appears as a matrix which provides dodecagonal channels (Figure 2.1b), thus breaking the pseudo-five-fold symmetry. The $^1_\infty\{Sn_{0.6}@Cu_5@Sn_5\}$ rods can be described as filled double-walled tubes, with an outer Sn shell enclosing an inner Cu tube and Sn atoms situated on the central column axis with disorder.

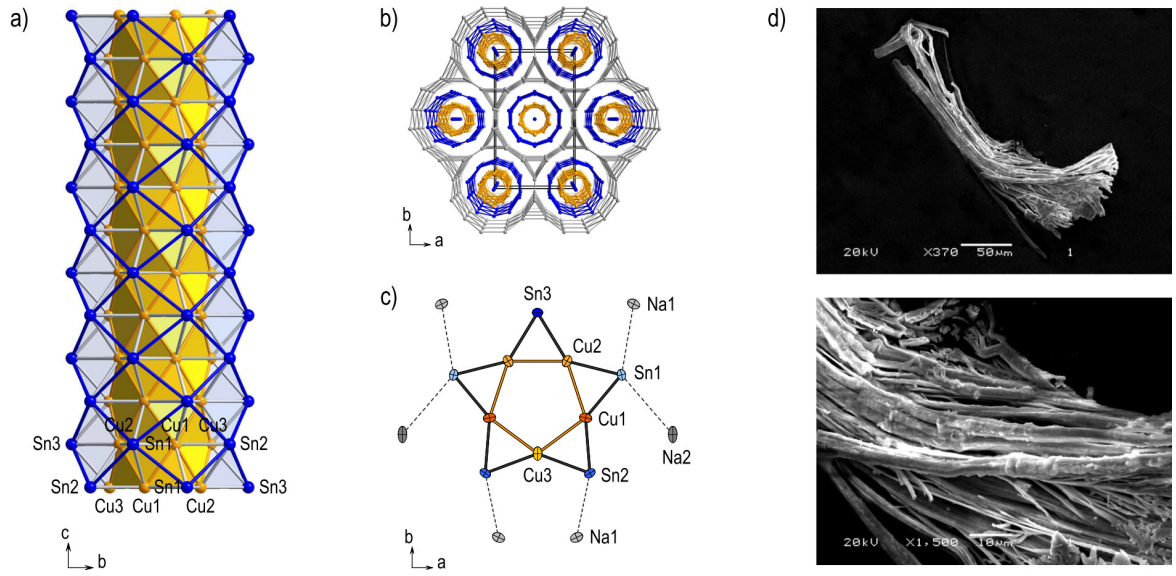

Figure 2.1.[21] a) $^1_\infty\{Sn_{0.6}@Cu_5@Sn_5\}$ rods in $Na_{2.8}Cu_5Sn_{5.6}$. b) Arrangement of the Cu–Sn wires in style of a hexagonal rod packing and separation of the wires by a Na substructure that provides dodecagonal channels. c) Segment of the rods with surrounding Na sites. d) SEM images of a bundle of needle-shaped crystals of $Na_{2.8}Cu_5Sn_{5.6}$.

This structure brings about high coordination numbers, especially for the inner Sn and Cu atoms. And with an almost equal ratio of Cu to Sn, the composition of the $^1_\infty\{Sn_{0.6}@Cu_5@Sn_5\}$ rods is close to that of the Sn-richest binary Cu–Sn bronze Cu_6Sn_5. Thus, this one-dimensionally extended Cu–Sn polyanion of $Na_{2.8}Cu_5Sn_{5.6}$ can be seen as an exemplary intermetalloid species. In accord with the columnar structure at the atomic scale, $Na_{2.8}Cu_5Sn_{5.6}$ forms needle-shaped crystals, and samples of the phase contain bundles of fibrous crystals (Figure 2.1d).

Furthermore, the parallel alignment of the Cu–Sn wires is associated with a highly anisotropic band structure, indicating one-dimensional metallic behavior. Electronic structure calculations were performed for a model "$Na_3Cu_5Sn_{5.5}$" with a slightly higher Na and lower Sn content than the title phase and an ordered arrangement of Sn atoms in the column centers. The calculated band structure shows steep bands crossing the Fermi level along directions which correspond to the orientation of the columns. In contrast, along perpendicular symmetry lines flat bands occur and (within a rigid band model) a band gap opens for the composition "$Na_{2.8}Cu_5Sn_{5.5}$". This relates to the results of the crystal structure refinement, with partial occupancy of the Na sites leading to the composition $Na_{2.78(4)}Cu_5Sn_{5.62(1)}$. Representations of the electron localization function (ELF) are dominated by lone pair type valence basins of the outer Sn atoms, and also indicate multicenter interactions within the intermetalloid Cu–Sn rods.

2.2.2 $[Sn@Cu_{12}@Sn_{20}]^{12-}$ Clusters in $A_{12}Cu_{12}Sn_{21}$ (A = Na, K, Rb, Cs)

see publication 6.2 A Bronze Matryoshka: The Discrete Intermetalloid Cluster $[Sn@Cu_{12}@Sn_{20}]^{12-}$ in the Ternary Phases $A_{12}Cu_{12}Sn_{21}$ (A = Na, K)
S. Stegmaier, T. F. Fässler, *J. Am. Chem. Soc.* **2011**, *133*, 19758.

The series of isotypic $A_{12}Cu_{12}Sn_{21}$ phases (A = Na, K, Rb, Cs) features the 33-atom Cu–Sn cluster $\{Sn@Cu_{12}@Sn_{20}\}$ which has an onion-skin-like structure with a $\{Sn_{20}\}$ pentagonal dodecahedron enclosing a $\{Cu_{12}\}$ icosahedron and a Sn atom at the center (Figure 2.2a). Obviously the cluster is closely related to the Cu–Sn columns of $Na_{2.8}Cu_5Sn_{5.6}$, and represents another exemplary intermetalloid cluster species. In the structure of the $A_{12}Cu_{12}Sn_{21}$ phases the clusters are arranged in style of a face centered cubic packing (Figure 2.2b), and they are surrounded and separated from each other by the alkali metal atoms. The pseudo-five-fold

symmetry thereby reaches out in the surroundings of the clusters to such a degree as the twelve pentagonal faces of the {Sn_{20}} polyhedra are capped by *A* atoms (Figure 2.2c).

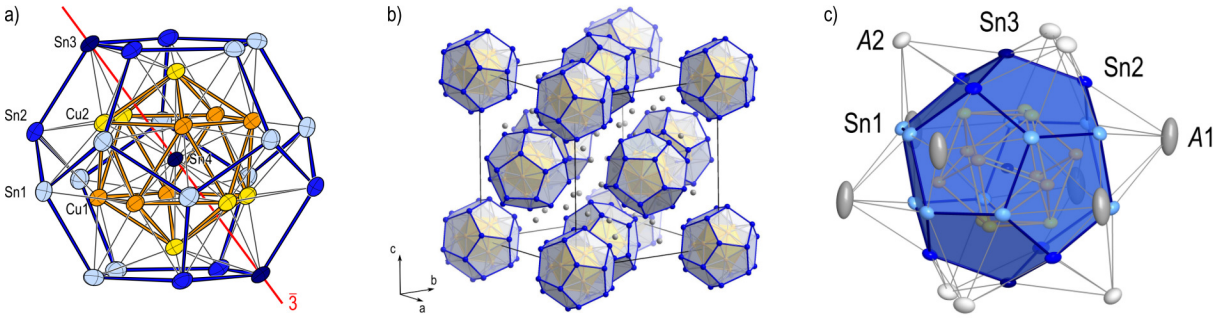

Figure 2.2.[22] a) $[Sn@Cu_{12}@Sn_{20}]^{12-}$ cluster. b) Arrangement of the clusters in style of a face centered cubic packing in the structure of the $A_{12}Cu_{12}Sn_{21}$ phases. c) Pentagonal faces of the cluster capped by surrounding alkali metal sites.

Both solid state electronic structure calculations for the *A*–Cu–Sn phases as well as molecular orbital calculations for the $[Sn@Cu_{12}@Sn_{20}]^{12-}$ anion were carried out. The results support the description of the compounds as salt-like intermetallic phases with alkali metal cations and discrete $[Sn@Cu_{12}@Sn_{20}]^{12-}$ cluster polyanions. Hence they are placed close to Zintl phases. Band structure calculations reveal, within a rigid band approximation, a band gap for the composition $A_{12}Cu_{12}Sn_{21}$. The calculated band gap increases in the series with increasing size of the *A* atoms und thus increasing intercluster distances. The molecular orbitals (MOs) of the $[Sn@Cu_{12}@Sn_{20}]^{12-}$ cluster anion can be classified – in the style of spherical shell models for cluster bonding – with labels indicating the numbers of radial and angular nodes (cf. contribution to publication 6.6). An appreciable HOMO–LUMO gap (1.3 eV) is calculated for $[Sn@Cu_{12}@Sn_{20}]^{12-}$, and thus the cluster's electronic requirements are exactly met by the composition and total electron count of $A_{12}Cu_{12}Sn_{21}$. The density of states (DOS) curves for the *A*–Cu–Sn phases are very structured with gaps and pseudogaps reflecting the energetic ordering of the cluster MOs. A detailed analysis reveals a clear correspondence between individual DOS peaks and sets of MOs (Figure 2.3), and also the partial DOS contributions are in good agreement with the atomic contributions found in the MO analysis for the $[Sn@Cu_{12}@Sn_{20}]^{12-}$ cluster. Several MOs comprise contributions of two or all three structural shells. Cu-p (and some Cu-s) type participation is found for MOs that show

important in-phase mixing involving such contributions from different structural shells which supposedly plays a part for the stability of the cluster.

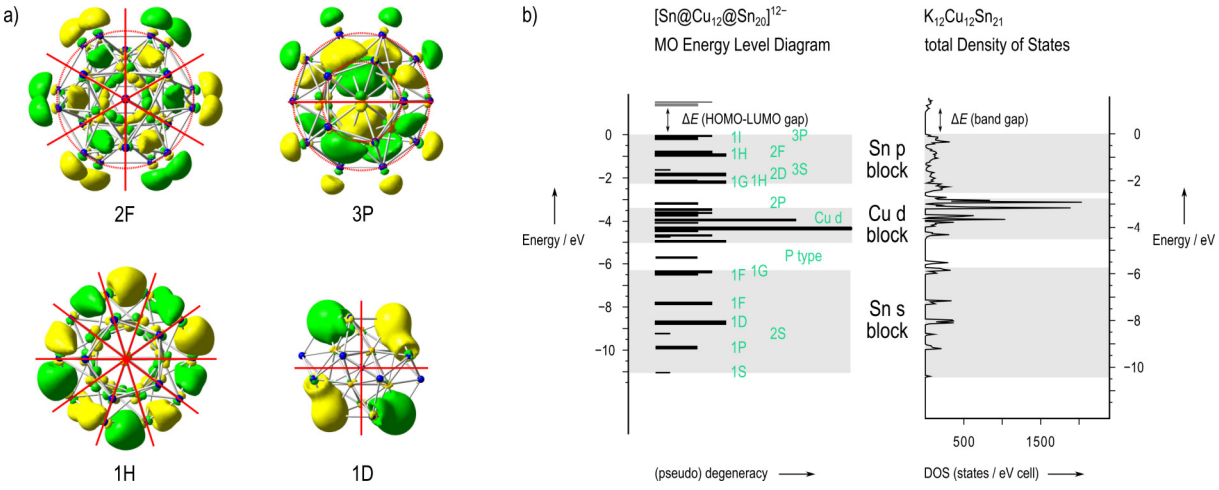

Figure 2.3.[22] a) Selected cluster MOs of $[Sn@Cu_{12}@Sn_{20}]^{12-}$, labeled in style of spherical shell models for cluster bonding. b) MO energy level diagram for $[Sn@Cu_{12}@Sn_{20}]^{12-}$ and total DOS curve for $K_{12}Cu_{12}Sn_{21}$.

2.2.3 Structural Relations

The structures of the ${}^{1}_{\infty}\{Sn_{0.6}@Cu_5@Sn_5\}$ rods in $Na_{2.8}Cu_5Sn_{5.6}$ and the $\{Sn@Cu_{12}@Sn_{20}\}$ clusters in the $A_{12}Cu_{12}Sn_{21}$ phases are closely related. Dual pentagonal antiprismatic $\{Cu_{10}@Sn_{10}\}$ fragments can be identified for both the column and the cluster (Figure 2.4). This suggests a description of the ${}^{1}_{\infty}\{Sn_{0.6}@Cu_5@Sn_5\}$ polyanions as "condensed cluster columns". A formal relation between the alignment of the columns in style of a hexagonal rod packing in $Na_{2.8}Cu_5Sn_{5.6}$ and the arrangement of the Cu–Sn clusters in style of a face centered cubic packing in $A_{12}Cu_{12}Sn_{21}$ is indicated in Figure 2.5.

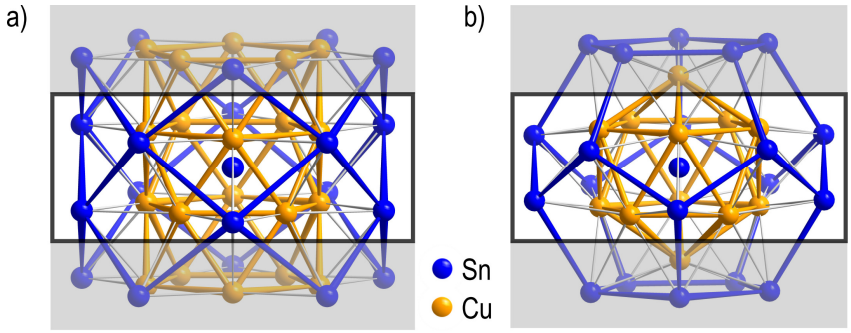

Figure 2.4.[21] Cu–Sn columns and clusters in ternary *A*–Cu–Sn phases. a) Section of $^{1}_{\infty}\{Sn_{0.6}@Cu_5@Sn_5\}$ column in $Na_{2.8}Cu_5Sn_{5.6}$. b) $\{Sn@Cu_{12}@Sn_{20}\}$ cluster in the $A_{12}Cu_{12}Sn_{21}$ phases.

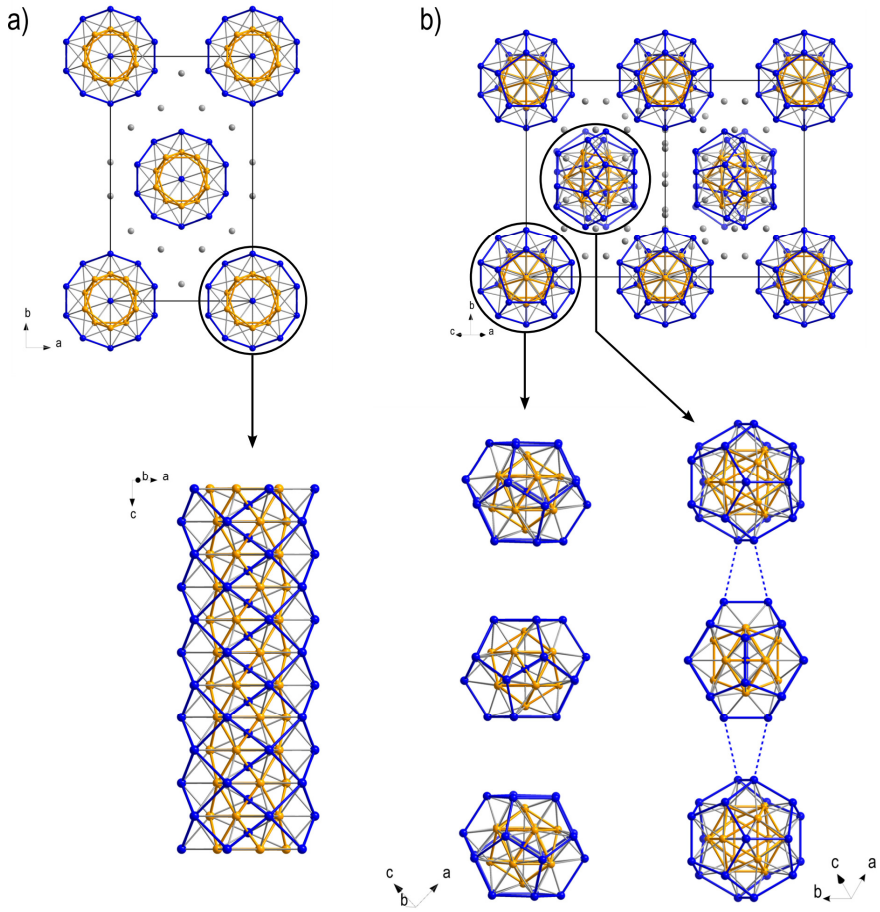

Figure 2.5. Representations of the structures of $Na_{2.8}Cu_5Sn_{5.6}$ and the $A_{12}Cu_{12}Sn_{21}$ phases. a) Cu–Sn cluster columns in $Na_{2.8}Cu_5Sn_{5.6}$ arranged in style of a hexagonal rod packing. b) Face centered cubic like arrangement of Cu–Sn clusters in the $A_{12}Cu_{12}Sn_{21}$ phases. Shortest intercluster Sn–Sn distances in $A_{12}Cu_{12}Sn_{21}$ are indicated with dotted lines, these are 4.002(1) Å for *A* = Na and 4.644(1) Å for *A* = K.

2.3 Tetrel Element Cages Filled with an Endohedral Late d Block Metal Atom

2.3.1 Computational Studies on $[Cu@Sn_9]^{3-}$, Icosahedral $[Ir@Sn_{12}]^{3-}$, and Non-Deltahedral $[Co@Ge_{10}]^{3-}$

see contributions to publication 6.3 — $[Cu@Sn_9]^{3-}$ and $[Cu@Pb_9]^{3-}$: Intermetalloid Clusters with Endohedral Cu Atoms in Spherical Environments
S. Scharfe, T. F. Fässler, S. Stegmaier, S. D. Hoffmann, K. Ruhland,
Chem. Eur. J. **2008**, *14*, 4479.

publication 6.4 — Step-by-Step Synthesis of the Endohedral Stannspherene $[Ir@Sn_{12}]^{3-}$ via the Capped Cluster Anion $[Sn_9Ir(cod)]^{3-}$
J.-Q. Wang, S. Stegmaier, B. Wahl, T. F. Fässler,
Chem. Eur. J. **2010**, *16*, 1793.

publication 6.5 — $[Co@Ge_{10}]^{3-}$: An Intermetalloid Cluster with Archimedean Pentagonal Prismatic Structure
J.-Q. Wang, S. Stegmaier, T. F. Fässler,
Angew. Chem. Int. Ed. **2009**, *48*, 1998; *Angew. Chem.* **2009**, *121*, 2032.

This chapter outlines computational studies on the intermetalloid *T*–*Tt* cluster polyanions $[Cu@Sn_9]^{3-}$, $[Ir@Sn_{12}]^{3-}$, and $[Co@Ge_{10}]^{3-}$ that were performed as part of the present thesis. The clusters with single endohedral *T* atoms in differently sized $\{Tt_n\}$ cages were synthesized (via reactions in solution) and experimentally characterized by other coworkers in the Fässler group. Schematic representations of the experimentally determined structures of the cluster anions are shown in Figure 2.6. In all cases, structure optimizations led to ground state structures in good agreement with the experimental data. $[Cu@Sn_9]^{3-}$, $[Ir@Sn_{12}]^{3-}$, and $[Co@Ge_{10}]^{3-}$ may formally be described, in the sense of a fragment analysis, as group 14 element cages filled with endohedral d block metal atoms with closed-shell d^{10} configurations (cf. contribution to publication 6.6). This implies the formulations $[Cu^{+}@Sn_9^{4-}]$, $[Ir^{-}@Sn_{12}^{2-}]$, and $[Co^{-}@Ge_{10}^{2-}]$.

The cage structure of $[Cu@Sn_9]^{3-}$ is close to a tricapped trigonal prism, with elongated prism heights. The tricapped trigonal prism is the deltahedral nine-vertex *closo* cluster structure which is, if Wade's rules are adhered to, adopted by species with $2n+2$ skeletal electrons (n: number of vertex-atoms). A $[Sn_9]^{4-}$ polyanion, however, has the electron count of a *nido* cluster ($2n+4$ skeletal electrons). The nine-vertex *nido* cluster structure is the monocapped square antiprism, and structure optimizations for the empty $[Sn_9]^{4-}$ cluster led to a corresponding ground state.

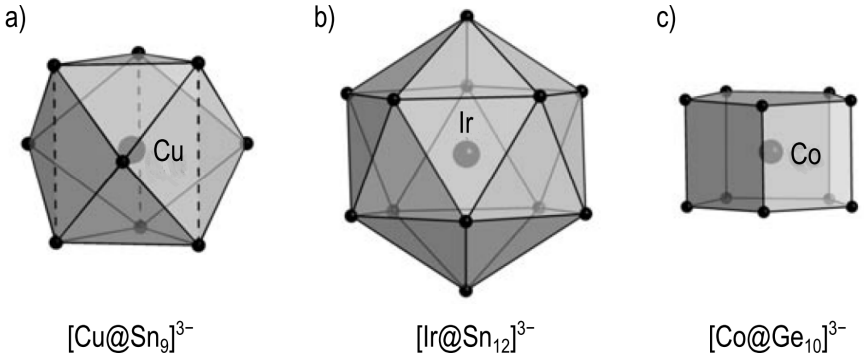

Figure 2.6. Schematic representations of the cluster structures of a) $[Cu@Sn_9]^{3-}$ (tricapped trigonal prism with elongated heights), b) $[Ir@Sn_{12}]^{3-}$ (icosahedron), and c) $[Co@Ge_{10}]^{3-}$ (pentagonal prism).

Thus, the incorporation of the endohedral Cu atom seems to have quite an influence on the nine-atom Sn cage. However, it must be noted that the nine-vertex *nido* and *closo* cage structures are closely related,[23] and both $\{Tt_9\}$ and $\{T@Tt_9\}$ clusters are found to be quite flexible, often showing intermediate shapes in the crystal structures of their salts.[4] For $[Cu@Sn_9]^{3-}$, also examples with cluster cages close to the *nido* structure have been characterized during subsequent investigations following the first report.[4, 24] The bonding situation for $[Cu@Sn_9]^{3-}$ was studied by means of molecular orbital (MO) analyses. An MO interaction diagram for the cluster is shown in Figure 2.7. The cluster MOs are classified with labels indicating the numbers of radial and angular nodes (cf. contribution to publication 6.6 for an introduction to this scheme). Selected cluster MOs of $[Cu@Sn_9]^{3-}$ which show the interaction of Cu-s, Cu-p, and Cu-d type orbitals with suitable $\{Sn_9\}$ cage based orbitals are depicted in Figure 2.7. The main stabilizing contribution is attributed to the interactions involving Cu-s and Cu-p states.

$[Ir@Sn_{12}]^{3-}$ displays an icosahedral structure close to perfect I_h symmetry. The icosahedron is the twelve-vertex *closo* cluster structure which is, according to Wade's rules, expected for a $[Sn_{12}]^{2-}$ cluster. The structure optimization for $[Sn_{12}]^{2-}$ also agrees with this. The Sn–Sn distances for the optimized structures of $[Ir@Sn_{12}]^{3-}$ and $[Sn_{12}]^{2-}$ differ only slightly. So in this case, the filling with an Ir atom seems to have hardly any effect on the cage structure (which might also be interpreted as a perfect fit). An MO diagram for $[Ir@Sn_{12}]^{3-}$ is included in the contribution to publication 6.6.

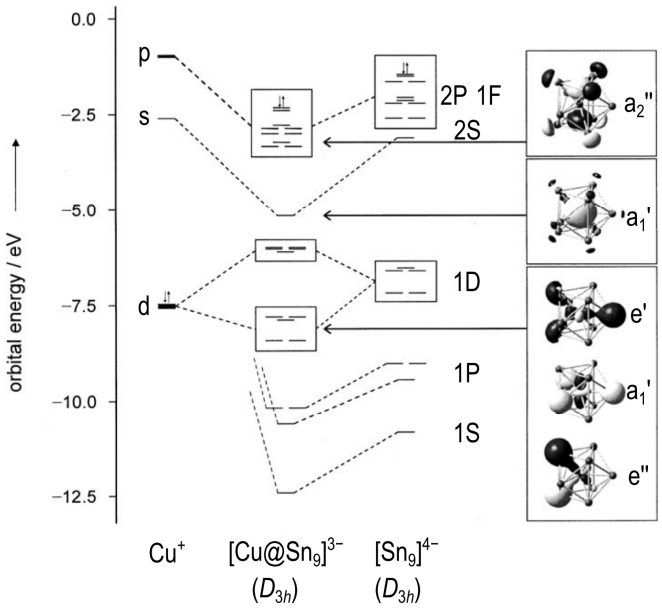

Figure 2.7.[15] Molecular orbital interaction diagram for $[Cu@Sn_9]^{3-}$ in fragments of Cu^+ and $[Sn_9]^{4-}$.

The shape of $[Co@Ge_{10}]^{3-}$ is a pentagonal prism, that is a fully non-deltahedral structure, which is beyond a rationalization within the framework of Wade's rules. $[Ge_{10}]^{2-}$ qualifies as a *closo* cluster, and the ten-vertex deltahedral *closo* structure, a bicapped square antiprism, was also reached in structure optimizations. For the empty $[Ge_{10}]^{2-}$ cluster it corresponds to a ground state which is energetically clearly favored compared to alternative ten-vertex structures, in line with Wade's rules. For $[Co@Ge_{10}]^{3-}$, structure optimizations led to a pentagonal prism as a ground state structure, in accordance with the experimental findings. Furthermore, the calculations indicate that the *closo* bicapped square antiprism does not correspond to a ground state for $[Co@Ge_{10}]^{3-}$, though the energetic differences between the two structures are rather small. For comparison, structure optimizations were also performed for isoelectronic $[Ni@Ge_{10}]^{2-}$, which may be described as $[Ni^0@Ge_{10}^{2-}]$ including an endohedral Ni^0 atom with a d^{10} configuration. For this (experimentally unknown) cluster, the energy differences between the deltahedral *closo* structure and the pentagonal prism are very small. This indicates that some sort of border concerning the applicability of Wade's rules for filled cage clusters is crossed when changing from $[Ni@Ge_{10}]^{2-}$ to $[Co@Ge_{10}]^{3-}$.[25]

For $[Co@Ge_{10}]^{3-}$, the bonding situation was analyzed by means of the electron localization function (ELF). The main features of the ELF of $[Co@Ge_{10}]^{3-}$ (Figure 2.8) are lone pair like monosynaptic valence basins ① at each Ge atom, and disynaptic basins above all Ge–Ge direct neighbor connecting lines, that is above all prism base edges (②) and prism

heights (③). No distinct valence basins occur for the Co–Ge interactions, corresponding to the high coordination number and the presumably delocalized nature of the Co–Ge bonding.

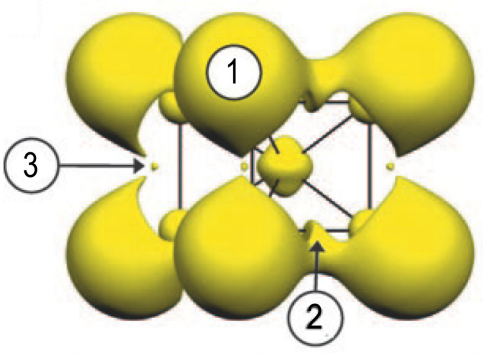

Figure 2.8.[17] ELF isosurface representation for $[Co@Ge_{10}]^{3-}$ (isovalue 0.635). Monosynaptic basins ① at each Ge atom, and disynpatic basins ② and ③ above the Ge–Ge edges.

2.3.2 The Solid State Phase $Na_{12}NiSn_{17}$ with $[Ni@Sn_9]^{4-}$ and $[Sn_4]^{4-}$ Clusters

see manuscript 6.7 — Intermetalloid Ni-Filled Sn Clusters $[Ni@Sn_9]^{4-}$ and Tetrahedral $[Sn_4]^{4-}$ in the Solid State Phase $Na_{12}NiSn_{17}$
S. Stegmaier, T. F. Fässler, *manuscript in preparation*.

$Na_{12}NiSn_{17}$ was obtained by a reaction of a preformed Ni–Sn alloy with elemental Na. Its crystal structure was determined by means of single crystal X-ray diffraction methods. $Na_{12}NiSn_{17}$ contains filled nine-vertex $[Ni@Sn_9]^{4-}$ (Figure 2.9a) and tetrahedral $[Sn_4]^{4-}$ polyanions (Figure 2.9b) in ratio 1:2. The phase represents a ternary derivative to the series of binary $A_{12}Tt_{17}$ phases with empty $[Tt_9]^{4-}$ cage clusters,[26-29] for which notably no member with A = Na and Tt = Sn has been reported. The arrangement of the two types of clusters in the crystal structure of $Na_{12}NiSn_{17}$ can be described as a hierarchical replacement variant[30] of the $MgZn_2$ hexagonal Laves phase structure (C14), with the larger $\{Ni@Sn_9\}$ clusters taking the role of Mg and the smaller $\{Sn_4\}$ replacing Zn (Figure 2.9c,d).

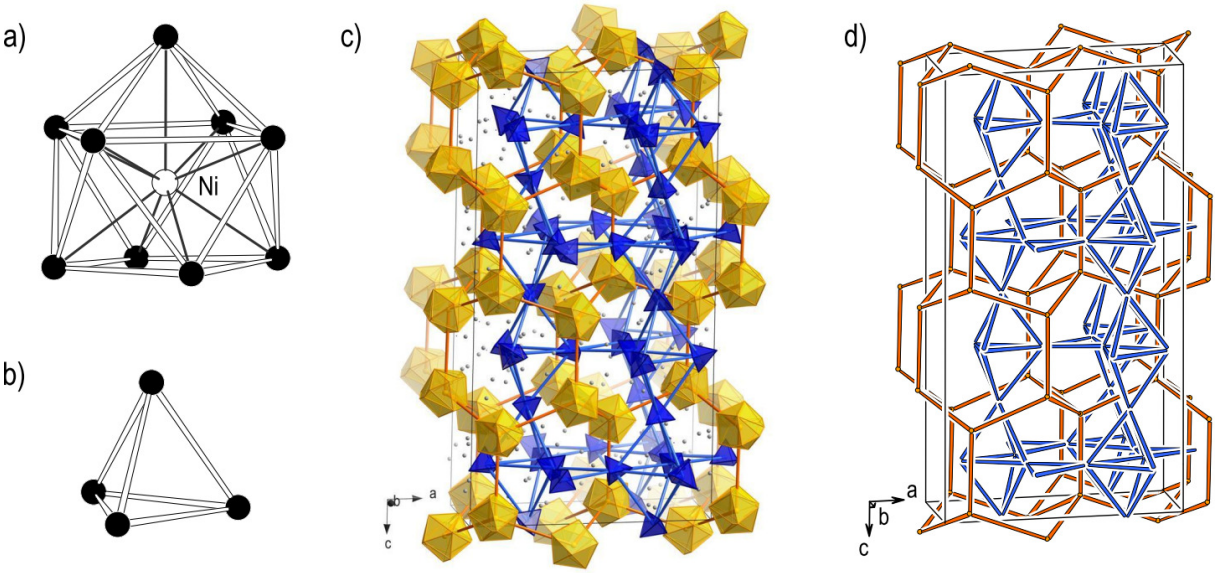

Figure 2.9. a) One of the $[Ni@Sn_9]^{4-}$ clusters in $Na_{12}NiSn_{17}$. b) Tetrahedral $[Sn_4]^{4-}$ cluster. c) Arrangement of the $\{Ni@Sn_9\}$ clusters (orange) and $\{Sn_4\}$ clusters (blue). d) Schematic representation illustrating the relation to the $MgZn_2$ structure.

The $[Ni@Sn_9]^{4-}$ clusters can formally be described as $[Ni^0@Sn_9^{4-}]$ with an endohedral Ni^0 atom with a closed-shell d^{10} configuration. According to Wade's rules for the electron count and structure of clusters, $[Sn_9]^{4-}$ classifies as a *nido* species, and the expected structure of the cluster is that of a mono-capped square antiprism. This *nido* structure has one square face – as opposed to the all deltahedral nine-vertex *closo* cluster structure, namely the tricapped trigonal prism. The crystal structure analysis for $Na_{12}NiSn_{17}$ led to a structure model with four crystallographically independent $\{Ni@Sn_9\}$ clusters, two of which are subject to disorder. The structure of one of the ordered clusters is close to a mono-capped square antiprism (Figure 2.9a), while the other one shows an intermediate structure between the ideal nine-vertex *nido* and *closo* polyhedra. Generally, such intermediate structures are often found for $\{Tt_9\}$ and $\{T@Tt_9\}$ clusters, which are considered to be structurally quite flexible, and no conclusions concerning the clusters' charge (i.e. the electron count) can be drawn from subtle structural differences.[4] The $[Ni@Sn_9]^{4-}$ polyanion was recently obtained from solution via the extraction of a precursor that was prepared by a reaction of K, Ni and Sn in ratio K:Ni:Sn = 4:3:9.[14] That precursor was not further characterized, only a XRD powder pattern was reported which shows elemental Sn as the main phase and some unindexed reflections.

2.4 Zn-Linked Tetrahedral Ge Clusters

2.4.1 $A_{14}ZnGe_{16}$ (A = K, Rb) with $[(Ge_4)Zn(Ge_4)]^{6-}$ and $[Ge_4]^{4-}$ Clusters

see contribution to joint publication 6.8

The Soluble Zintl Phases $A_{14}ZnGe_{16}$ (A = K, Rb) Featuring $[(\eta^3\text{-}Ge_4)Zn(\eta^2\text{-}Ge_4)]^{6-}$ and $[Ge_4]^{4-}$ Clusters and the Isolation of $[(MesCu)_2(\eta^3,\eta^3\text{-}Ge_4)]^{4-}$ – the Missing Link in the Solution Chemistry of Tetrahedral Group 14 Element Zintl Clusters
S. Stegmaier, M. Waibel, A. Henze, L.-A. Jantke, A. J. Karttunen, T. F. Fässler, *J. Am. Chem. Soc.* **2012**, *134*, 14450.

The two isotypic $A_{14}ZnGe_{16}$ phases (A = K, Rb) show heterometallic $[(Ge_4)Zn(Ge_4)]^{6-}$ (Figure 2.10a) and tetrahedral $[Ge_4]^{4-}$ clusters (Figure 2.10b) in ratio 1:2. The alignment of the two types of clusters is – in a hierarchical sense[30] – related to the packing of Al and B atoms in the AlB_2 structure (Figure 2.10c). The $[(\eta^3\text{-}Ge_4)Zn(\eta^2\text{-}Ge_4)]^{6-}$ cluster comprises two $\{Ge_4\}$ tetrahedra linked by a Zn atom, with one $\{Ge_4\}$ unit coordinating to the Zn atom with a face, the other one with an edge. It represents a new isomer of the cluster that is known in Cs_6ZnGe_8 as $[(\eta^3\text{-}Ge_4)Zn(\eta^3\text{-}Ge_4)]^{6-}$, with both $\{Ge_4\}$ face-coordinating.[7]

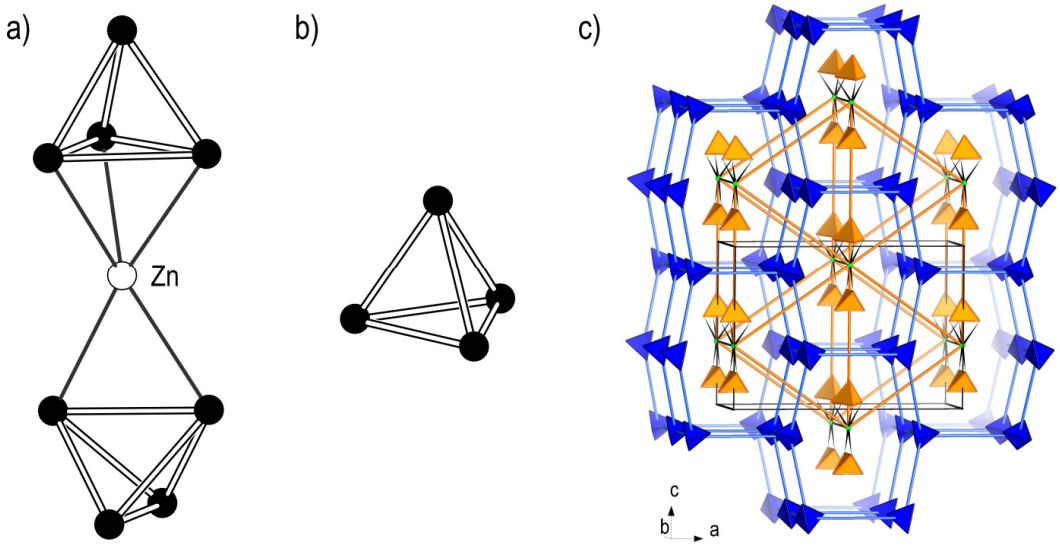

Figure 2.10. a) $[(\eta^3\text{-}Ge_4)Zn(\eta^2\text{-}Ge_4)]^{6-}$ cluster in the $A_{14}ZnGe_{16}$ phases. b) Tetrehahedral $[Ge_4]^{4-}$ cluster. c) Alignment of the two types of clusters, which is related to the AlB_2 structure type.

Computational studies were performed both for the solid state phases and for the discrete polyanions. Various isomers of the $[(Ge_4)Zn(Ge_4)]^{6-}$ cluster were considered in structure optimizations and four different ground state structures were identified, indicating that the clusters are quite flexible. The electronic structures of the two known isomers were studied in terms of MO (molecular orbital) and ELF (electron localization function) analyses and compared to that of the bare tetrahedral $[Ge_4]^{4-}$ cluster. Main features of bare $[Ge_4]^{4-}$ are still recognizable for the $\{Ge_4\}$ units in $[(Ge_4)Zn(Ge_4)]^{6-}$ but also significant differences for the bonding situation come along with the structural distortions and the coordination to the Zn atom. The MO analysis for $[(Ge_4)Zn(Ge_4)]^{6-}$ shows significant Zn-s and Zn-p orbital involvement. This contributes to the stability of the heterometallic cluster, similar to the situation for clusters with endohedral atoms. Electronic structure calculations for the $A_{14}ZnGe_{16}$ solid state phases show the expected band gap and structured DOS (density of states) curves that relate to the MO diagrams for the bare polyanions.

The description of the $A_{14}ZnGe_{16}$ (A = K, Rb) phases as salt-like Zintl compounds with alkali metal cations and discrete $[(Ge_4)Zn(Ge_4)]^{6-}$ and tetrahedral $[Ge_4]^{4-}$polyanions is not only supported by the results of computational studies: As it was shown by other coworkers in the Fässler group, the phases dissolve in liquid ammonia and can be used as precursors for solution based Zintl anion chemistry. A reaction with $K_{14}ZnGe_{16}$, MesCu, and [18]-crown-6 in liquid ammonia yielded a salt of the complex $[(MesCu)_2Ge_4]^{4-}$, which is the first example of a homoatomic tetrahedral $\{Ge_4\}$ cluster anion that has been isolated from solution.

2.5 Discussion

Already a first glance at the crystal structures of the ternary $A_{12}Cu_{12}Sn_{21}$, $Na_{12}NiSn_{17}$ and $A_{14}ZnGe_{16}$ phases with polyanionic clusters shows an intriguing common feature. They all exhibit arrangements of the clusters that can be described in analogy to basic structure types. In case of $A_{12}Cu_{12}Sn_{21}$, which contains only one cluster type with an almost spherical shape, this is the face centered cubic packing. $Na_{12}NiSn_{17}$ and $A_{14}ZnGe_{16}$ which each contain two different cluster types, relate to the hexagonal Laves phase $MgZn_2$ and AlB_2, respectively. Thus, the $A_{12}Cu_{12}Sn_{21}$, $Na_{12}NiSn_{17}$ and $A_{14}ZnGe_{16}$ phases are nice examples for hierarchical cluster replacement variants.[30]

A common characteristic concerning the bonding situation of the intermetalloid *T*–*Tt* clusters is illustrated by the MO analyses for $[(Ge_4)Zn(Ge_4)]^{6-}$, $[Cu@Sn_9]^{3-}$, and $[Sn@Cu_{12}@Sn_{20}]^{12-}$. In all cases, significant *T*-s and -p orbital contributions are found, indicative for bonding interactions which presumably contribute to the stability of the clusters. At this point it is worth noting that formulations like $[Cu^{+}@Sn_9^{4-}]$ or $[(Ge_4^{4-})(Zn^{2+})(Ge_4^{4-})]$, which are commonly used for the description of the clusters, do not account for these interactions and the involved occupancy of *T*-s and -p states. They may still be useful at certain points of a discussion, for example to emphasize the closed-shell d^{10} configuration of an endohedral atom, or in the sense of a fragment analysis (see chapter 2.3.1). But in general, the intermetalloid clusters should be viewed as a whole, rather than partitioned – as it has also been pointed out for the multiply endohedral $[Sn@Cu_{12}@Sn_{20}]^{12-}$ cluster (publication 6.2). This point of view can be supported by labeling the cluster MOs in style of spherical shell models for cluster bonding.

The results of solid state electronic structure calculations for the ternary $A_{12}Cu_{12}Sn_{21}$ and $A_{14}ZnGe_{16}$ phases have been compared with those of computational studies on the discrete polyanionic clusters $[Sn@Cu_{12}@Sn_{20}]^{12-}$ or $[(Ge_4)Zn(Ge_4)]^{6-}$ and $[Ge_4]^{4-}$, respectively. In both cases there is a band gap for the solid state phases, and a clear correspondence is found between the DOS curves (and PDOS contributions) for the solid state phases and the MO energy level diagrams (and atomic orbital contributions) for the clusters. This supports the description of the phases as "salt-like" with discrete cluster polyanions and alkali metal cations. However, the PDOS analyses also show some contributions of the alkali metal atoms, and of course, the environment of the clusters in the solid state structures has an influence on the polyanions – as it is also illustrated by a detailed ELF analysis for the clusters in $K_{14}ZnGe_{16}$. Various aspects concerning "cation effects" in polar intermetallic phases with cluster polyanions have been discussed for example in reference [31], and the term "cluster solvation" (by cations) has been coined in this context.

The polyanionic *T*–*Tt* cluster species that are presented in this thesis span quite a range, both in terms of structure and novelty. The $[(Ge_4)Zn(Ge_4)]^{6-}$ polyanion of the $A_{14}ZnGe_{16}$ phases, with Zn-linked {Ge_4} units, represents a new isomer of a cluster that is known from Cs_6ZnGe_8.[7] $Na_{12}NiSn_{17}$ is the first structurally characterized neat solid state phase featuring the $[Ni@Sn_9]^{4-}$ anion with a single endohedral Ni atom in a nine-vertex Sn cage – a cluster that has just recently been obtained from solution.[14] The onion-skin-like $[Sn@Cu_{12}@Sn_{20}]^{12-}$

clusters and the double-walled $^1_\infty\{Sn_{0.6}@Cu_5@Sn_5\}$ rods of the $A_{12}Cu_{12}Sn_{21}$ phases and $Na_{2.8}Cu_5Sn_{5.6}$, respectively, are unprecedented in the cluster chemistry of the group 14 (semi)metals. An analogy may still be drawn within group 14 – to the carbon fullerenes and nanotubes. However, there are more closely related heterometallic cluster species in other systems. $[Sn@Cu_{12}@Sn_{20}]^{12-}$ is iso(valence)electronic and isostructural to the $[As@Ni_{12}@As_{20}]^{3-}$ polyanion that was obtained from a reaction with K_3As_7 and a Ni complex in ethylendiamine solution.[32] An isostructural polycationic counterpart to the $^1_\infty\{Sn_{0.6}@Cu_5@Sn_5\}$ columns is known from the field of partially oxidized intermetallics, namely the $^1_\infty\{Bi_{0.6}@Ni_5@Bi_5\}$ rods in $Bi_{5.6}Ni_5I$.[33] Further, there are the smaller (single-walled) polyanionic $^1_\infty\{Cd_2@Tl_{11}\}$ cluster chains in $A_5Cd_2Tl_{11}$ (A = Cs, Rb),[34] and the related icosahedral $[M@Tl_{12}]^{12-}$ cluster anions with single endohedral atoms e.g. in $Na_{14}K_6Tl_{18}T$ (T = Zn, Cd, Hg).[35, 36] So the Cu–Sn polyanions presented in this work complete an intriguing series of group 12–group 13 (Cd–Tl), group 11–group 14 (Cu–Sn), group 10–group 15 (Ni–Bi; Ni–As) heterometallic (multiply) endohedral clusters and columns (with pseudo-five-fold symmetry).

2.6 References

[1] T. F. Fässler, S. D. Hoffmann, *Angew. Chem. Int. Ed.* **2004**, *43*, 6242; *Angew. Chem.* **2004**, *116*, 6400.

[2] J. M. Goicoechea, S. C. Sevov, *Angew. Chem. Int. Ed.* **2006**, *45*, 5147.

[3] J. M. Goicoechea, S. C. Sevov, *Angew. Chem.* **2006**, *118*, 5271.

[4] S. Scharfe, F. Kraus, S. Stegmaier, A. Schier, T. F. Fässler, *Angew. Chem. Int. Ed.* **2011**, *50*, 3630; *Angew. Chem.* **2011**, *123*, 3712.

[5] S. C. Sevov, J. M. Goicoechea, *Organometallics* **2006**, *25*, 5678.

[6] S. Scharfe, T. F. Fässler, *Phil. Trans. R. Soc. A* **2010**, *368*, 1265.

[7] V. Queneau, S. C. Sevov, *J. Am. Chem. Soc.* **1997**, *119*, 8109.

[8] M. T. Klem, J. D. Corbett, *Inorg. Chem.* **2005**, *44*, 5990.

[9] E. Todorov, S. C. Sevov, *Angew. Chem. Int. Ed.* **1999**, *38*, 1775.

[10] U. Zachwieja, M. Wlodarski, *Z. Anorg. Allg. Chem.* **2004**, *630*, 993.

[11] U. Zachwieja, J. Müller, J. Wlodarski, *Z. Anorg. Allg. Chem.* **1998**, *624*, 853.

[12] J. M. Goicoechea, S. C. Sevov, *J. Am. Chem. Soc.* **2006**, *128*, 4155.

[13] D. Rios, M. M. Gillett-Kunnath, J. D. Taylor, A. G. Oliver, S. C. Sevov, *Inorg. Chem.* **2011**, *50*, 2373.

[14] M. M. Gillett-Kunnath, J. I. Paik, S. M. Jensen, J. D. Taylor, S. C. Sevov, *Inorg. Chem.* **2011**, *50*, 11695.

[15] S. Scharfe, T. F. Fässler, S. Stegmaier, S. D. Hoffmann, K. Ruhland, *Chem. Eur. J.* **2008**, *14*, 4479.

[16] J.-Q. Wang, S. Stegmaier, B. Wahl, T. F. Fässler, *Chem. Eur. J.* **2010**, *16*, 1793.

[17] J.-Q. Wang, S. Stegmaier, T. F. Fässler, *Angew. Chem. Int. Ed.* **2009**, *48*, 1998; *Angew. Chem.* **2009**, *121*, 2032.

[18] V. Hlukhyy, H. He, L.-A. Jantke, T. F. Fässler, *Chem. Eur. J.* **2012**, *18*, 12000.

[19] O. Jepsen, A. Burkhardt, O. K. Andersen, *The Stuttgart TB-LMTO-ASA Program (Version 4.7)*, Max-Planck-Institut für Festkörperforschung, Stuttgart, **1998**.

[20] M. J. Frisch et al., *Gaussian*, Gaussian, Inc., Wallingford CT.

[21] S. Stegmaier, T. F. Fässler, *Angew. Chem. Int. Ed.* **2012**, *51*, 2647; *Angew. Chem.* **2012**, *124*, 2701.

[22] S. Stegmaier, T. F. Fässler, *J. Am. Chem. Soc.* **2011**, *133*, 19758.

[23] T. F. Fässler, *Coord. Chem. Rev.* **2001**, *215*, 347.

[24] S. Scharfe, Dissertation, Technische Universität München, **2010**.

[25] N. Korber, *Angew. Chem. Int. Ed.* **2009**, *48*, 3216; *Angew. Chem.* **2009**, *121*, 3262.

[26] H. G. von Schnering, M. Baitinger, U. Bolle, W. Carrillo-Cabrera, J. Curda, Y. Grin, F. Heinemann, J. Llanos, K. Peters, A. Schmeding, M. Somer, *Z. Anorg. Allg. Chem.* **1997**, *623*, 1037.

[27] V. Quéneau, E. Todorov, S. C. Sevov, *J. Am. Chem. Soc.* **1998**, *120*, 3263.

[28] W. Carrillo-Cabrera, R. Cardoso Gil, M. Somer, Ö. Persil, H. G. von Schnering, *Z. Anorg. Allgem. Chem.* **2003**, *629*, 601.

[29] C. Hoch, M. Wendorff, C. Röhr, *J. Alloy. Compd.* **2003**, *361*, 206.

[30] W. Carrillo-Cabrera, N. Caroca-Canales, H. G. von Schnering, *Z. Anorg. Allgem. Chem.* **1994**, *620*, 247.

[31] J. D. Corbett, *Angew. Chem. Int. Ed.* **2000**, *39*, 670; *Angew. Chem.* **2000**, *112*, 682.

[32] M. J. Moses, J. C. Fettinger, B. W. Eichhorn, *Science* **2003**, *300*, 778.

[33] M. Ruck, *Z. Anorg. Allg. Chem.* **1995**, *621*, 2034.

[34] S. Kaskel, J. D. Corbett, *Inorg. Chem.* **2000**, *39*, 3086.

[35] Z.-C. Dong, J. D. Corbett, *Angew. Chem. Int. Ed. Engl.* **1996**, *35*, 1006.

[36] Z.-C. Dong, J. D. Corbett, *Angew. Chem.* **1996**, *108*, 1073.

3 Zintl Phases and Polar Intermetallics with Zn–Ge and Zn–Sn Networks

3.1 Introduction

In the scope of this thesis, *Tt*-rich *A*–Zn–Ge and *A*–Zn–Sn phases with the light alkali metals *A* = Li and Na (chapter 3.2; publications and manuscripts 6.9 to 6.11), and *Ae*–Zn–Sn phases with the alkaline earth metals *Ae* = Ca, Sr (chapter 3.3; publication 6.13) have been studied. Tables 3.1 and 3.2 list the hitherto known *A*–Zn–*Tt* phases with *A* = Li to Cs and *Tt* = Ge or Sn, and the *A*e–Zn–Sn phases with *Ae* = Ca, Sr, Ba, respectively. The phases that have been discovered or have been subject to further investigations in the course of the present work are highlighted (bold face type). Overall, the listings appear quite sparse, indicating that most of these systems have been rather neglected up to now. The many Na–Zn–Sn phases with a rich diversity of polyanionic Zn–Sn substructures have all been characterized by S.-J. Kim within his PhD project in the Fässler group – previous to that work no ternary Na–Zn–Sn phases were known. The recent reports on Li-rich phases in the Li–Zn–Ge system can be seen in the context of research on lithium-ion battery materials. The current interest in intermetallic clathrates like the $A_8Zn_4Tt_{42}$ phases is mainly due to the promising thermoelectric properties of some representatives of this class of compounds.[1]

The ternary zinc-stannides and -germanides of alkali metals (*A*) and alkaline earth metals (*Ae* = Ca, Sr, Ba) can basically be described in terms of cations of the electropositive metals and an overall negatively charged Zn–*Tt* part – as it has been noted in chapter 1 in general for ternary *A'*–*T*–*E* or *A'*–*E*–*E'* phases (*A'*: electropositive alkali metal, alkaline earth metal or rare earth metal; *T*: d block metal; *E, E'*: p block (semi)metal). And also among the ternary zinc-tetrelides, there are Zintl compounds and polar intermetallic phases.

Since the group 12 metal Zn has a closed-shell $3d^{10}$ configuration and the Zn 3d orbitals are low in energy, Zn–*E* polyanions and the electronic structure of *A'*–Zn–*E* phases are more closely related to that of ternary *A'*–*E*–*E'* phases of main group elements than to that of *A'*–*T*–*E* phases with d block transition metals *T*. Zn–*E* networks in polar intermetallic phases can

therefore be described as s-p bonded, like networks of binary Zn–*E* phases such as the zinc-antimonides.[2, 3]

For the purpose of formal electron counting for the Zn–*Tt* part of the ternary zinc-germanides and -stannides one may employ two extreme pictures: One counting scheme assumes a Zn–*Tt* network of exclusively covalently four-bonded (4b) atoms, which leads to (4b-Sn^0) and negatively charged (4b-Zn^{2-}). At first sight this may seem unfamiliar because Zn is commonly associated with its role as a divalent cation Zn^{2+} in salts or coordination compounds. The other counting scheme implies Zn^{2+} and purely ionic interactions. But a strong charge separation is not in accord with the rather similar electronegativites (*EN*) of Zn, Ge, and Sn (Pauling scale: *EN*(Zn) = 1.6, *EN*(Ge) = 1.8, *EN*(Sn) = 1.8; Allred-Rochow: *EN*(Zn) = 1.66, *EN*(Ge) = 2.02, *EN*(Sn) = 1.72)[4]. This seeming discrepancy underlines the formal character of the electron counting based on "purely covalent" or "purely ionic" pictures. Intermediate types of chemical bonds between the two extremes are commonly described as "polar covalent" or "polarized ionic".

However, the formal electron counting has certainly proved to be a useful tool in the rationalization of the structures and corresponding electron requirements of the polyanions of Zintl phases and polar intermetallics. As a specific example, the electron count of the $A_8Zn_4Tt_{42}$ clathrates with Zn–*Tt* substructures of four-connected atoms can be discussed as follows: The counting scheme with (4b-Tt^0) and (4b-Zn^{2-}) leads to the description as electron precise Zintl phases according to the charge balanced formulation $(A^+)_8$(4b-Zn^{2-})$_4$(4b-Sn^0)$_{42}$. The alternative (equally charge balanced) formulation with Zn^{2+} cations is $(A^+)_8(Zn^{2+})_4$(3b-Sn^-)$_{16}$(4b-Sn^0)$_{26}$, because each Zn atom is coordinated by four (3b-Sn^-) that are covalently bonded to three other Sn atoms. Since this leads to a picture with four Sn atoms that can each donate a lone pair to the Zn^{2+} cation, the description may also be seen to arrive at "polarized ionic"/"polar covalent".

As described in chapter 1.1, polar intermetallic phases have electron counts and polyanionic substructures that cannot be described within the simple concepts for two-center covalent bonding (8–*N* rule) that hold for the polyanionic part of classic Zintl compounds. Other concepts, such as multicenter bonding need to be taken into account. But of course, the questions concerning the nature of the Zn–*Tt* interactions arise equally for both Zintl compounds and polar intermetallic phases with Zn–*Tt* polyanions.

Table 3.1. Known *A*–Zn–*Tt* phases with *A* = Li to Cs and *Tt* = Ge or Sn. Phases that have been discovered or further investigated within the present thesis are highlighted (bold face type).

ternary system	known phases	Zn–*Tt* structure part
Li–Zn–Ge	$LiZnGe$[5-7]; former "$Li_{1.25}ZnGe$"[8, 9]	interconnected puckered and planar layers of six-membered rings with alternating Zn and Ge atoms
	α-Li_2ZnGe[7, 10]	diamond polytype like (zinc blende)[7]
	β-Li_2ZnGe[11]	slightly puckered hexagonal layers of six-membered rings with alternating Zn and Ge atoms
	$Li_8Zn_2Ge_3$[7]	planar atom-defective hexagonal layers (α-BN-like Zn–Ge layer with one third of Zn missing)
	$Li_{17-\varepsilon}Zn_\varepsilon Ge_4$[12]	isolated Ge atoms (Zn-doped $Li_{17}Ge_4$, Zn on Li site)
	Li_2ZnGe_3[8]	diamond polytype like (hexagonal diamond)
Na–Zn–Ge	Na_2ZnGe[13]	{ZnGe} zig-zag chains
	$Na_8Zn_4Ge_{42}$	type-I clathrate (open four-connected framework with cages)
K–Zn–Ge	**$K_{14}ZnGe_{16}$**	{Ge_4} and {(Ge_4)Zn(Ge_4)} clusters
	$K_8Zn_4Ge_{42}$[14]	type-I clathrate
Rb–Zn–Ge	**$Rb_{14}ZnGe_{16}$**	{Ge_4} and {(Ge_4)Zn(Ge_4)} clusters
	$Rb_8Zn_4Ge_{42}$[15]	type-I clathrate
Cs–Zn–Ge	Cs_6ZnGe_8[16]	{(Ge_4)Zn(Ge_4)} cluster
	$Cs_8Zn_4Ge_{42}$[15]	type-I clathrate
Li–Zn–Sn	Li_2ZnSn [17, 18]	diamond polytype like (zinc blende)
	$Li_3Zn_2Sn_4$	diamond polytype like (ordered coloring variant of 6H polytype)
Na–Zn–Sn	**Na_2ZnSn_5**[19]	open four-connected framework with channels
	$Na_5Zn_{2+x}Sn_{10-x}$ [20]	four-connected network with realgar like motifs
	Na_6ZnSn_2[21] $Na_{4.24}K_{1.76(1)}ZnSn_2$[21]	linear {Sn–Zn–Sn} slightly bent {Sn–Zn–Sn} (variant with K for Na substitution)
	$Na_{20}Zn_8Sn_{11}$[21]	networks of interconnected icosahedra and other structural motifs (clusters or others)
	$Na_{29}Zn_{24}Sn_{32}$[22]	
	$Na_{16}Zn_{13.54}Sn_{13.46(5)}$[23]	
	$Na_{22}Zn_{20}Sn_{19(1)}$[23]	
	$Na_{34}Zn_{66}Sn_{38(1)}$[23]	
K–Zn–Sn	$K_8Zn_4Sn_{42}$[24]	type-I clathrate
Rb–Zn–Sn	$Rb_8Zn_4Sn_{42}$[25]	
Cs–Zn–Sn	$Cs_8Zn_4Sn_{42}$[25, 26]	

Table 3.2. Known *Ae*–Zn–Sn phases with *Ae* = Ca, Sr, Ba. Phases that are described in this work are highlighted (bold face type).

ternary system	known phases	structure type; Zn–*Tt* structure part
Ca–Zn–Sn	$CaZnSn$[27]	LiGaGe type; diamond polytype like (wurtzite) / network of puckered layers of six-membered rings (for CaZnSn: interlayer distance > intralayer distance)
	$Ca_2Zn_3Sn_6$	isotypic to $R_2Zn_3Ge_6$ (R = La, Ce, Pr, Nd)[28]; network of interconnected PbO-like $\{ZnSn_{4/4}\}$ layers and $\{Sn_4Zn\}$ slabs
	$Ca_{4.66}Zn_{0.70}Sn_3$[29]	related to W_5Si_3 type
Sr–Zn–Sn	$SrZnSn$[30]	BeZrSi type; graphite-like / α-BN-like layers
	$SrZn_2Sn_2$	$SrPd_2Bi_2$[31] type (monoclinc variant of $CaBe_2Ge_2$ type); network of interconnected PbO-like $\{ZnSn_{4/4}\}$ and anti-PbO-like $\{SnZn_{4/4}\}$ layers
Ba–Zn–Sn	$BaZnSn$[30]	BeZrSi type; graphite-like / α-BN-like layers
	$BaZn_2Sn_2$[32]	$CaBe_2Ge_2$ type; network of interconnected PbO-like $\{ZnSn_{4/4}\}$ and anti-PbO-like $\{SnZn_{4/4}\}$ layers

The ternary solid state phases that are presented in this chapter were obtained via direct reactions of the elements at high temperatures (high frequency induction furnace for $SrZn_2Sn_2$, resistance tube furnaces in all other cases) in argon-atmosphere using sealed niobium or tantalum ampoules as reaction containers. The crystal structures of the phases were determined by means of single crystal X-ray diffraction methods. Further methods of experimental characterization that were used (in all or selected cases) include powder X-ray diffraction, qualitative and semi-quantitative chemical analysis (EDX), thermal analysis (DTA), and SQUID magnetometer measurements. Solid state electronic structure calculations were carried out with the Stuttgart TB-LMTO-ASA programs.[33]

3.2 *Tt*-Rich *A*–Zn–*Tt* Phases with Networks of Four-Bonded Atoms (*A* = Li, Na; *Tt* = Ge, Sn)

3.2.1 Introduction and Outline

Four-connected networks with covalent bonds between tetrahedrally connected atoms are native to the structural chemistry of the group 14 elements C, Si, Ge, and Sn. Extended network types of exclusively four-bonded atoms that are represented by at least one allotrope structure of C, Si, Ge, or Sn include the series of diamond polytype structures,[34, 35] clathrate structures,[36-39] and the so-called (*m*)-*allo*-Ge[34, 40] structure models. Four-connected networks with tetrel element atoms are also found for a number of ternary silicides, germanides and stannides. These are either electron precise Zintl compounds or closely related polar intermetallic phases with alkali metal, alkaline earth metal, or rare earth metal cations as guests in the voids of polyanionic networks. A charge balanced situation, with a four-bonded network structure that follows the 8–*N* rule, can be reached if the tetrel element atoms are joined by electron poorer group 13 (*Tr*: triel element) or late d block metal (*T*) atoms to build *Tr*–*Tt* or *T*–*Tt* polyanions, respectively. Concerning the network type that is adopted by the polyanions, a structure determining influence can be attributed to the size of the cations.[41] As a general trend, among the ternary alkali metal-germanides and -stannides with four-connected *Tr*–*Tt* or *T*–*Tt* networks, Li phases show structures with Li-stuffed diamond polytype like networks, while open clathrate structures are realized with K, Rb, and Cs as guests in the cages. With intermediate sized Na, only few phases with diamond polytype like and (with *Tt* = Ge) clathrate structures are known,[42] but (with *Tt* = Sn) there are some phases with different network structures of four-bonded atoms which are not known for elemental modifications.[20, 43-45]

The *Tt*-rich *A*–Zn–*Tt* phases (*A* = Li, Na; *Tt* = Ge, Sn) that were first obtained or further investigated in the course of the present work are in line with this: Li_2ZnGe_3 and $Li_3Zn_2Sn_4$ show Li-stuffed diamond polytype like structures (chapter 3.2.2; publication 6.9), $Na_8Zn_4Ge_{42}$ is an intermetallic type-I clathrate (chapter 3.2.3; manuscript 6.10), and the two modifications of Na_2ZnSn_5 feature Zn–Sn open framework structures with hexagonal channels occupied by the Na atoms (chapter 3.2.4; manuscript 6.11). In chapter 3.2.5 (manuscript 6.12) a construction scheme for networks of four-connected atoms is described which emerged from an analysis of the structural relations between the Zn–Sn network structures of the Sn-rich Na–Zn–Sn phases.

3.2.2 Li_2ZnGe_3 and $Li_3Zn_2Sn_4$ with Diamond Polytype Analogous Zn–*Tt* Networks

see publication 6.9 Lithium-Stuffed Diamond Polytype Zn–*Tt* Structures (*Tt* = Sn, Ge): The Two Lithium-Zinc-Tetrelides $Li_3Zn_2Sn_4$ and Li_2ZnGe_3
S. Stegmaier, T. F. Fässler,
Inorg. Chem., http://dx.doi.org/10.1021/ic3011037.

Li_2ZnGe_3 and $Li_3Zn_2Sn_4$ show rare examples of 2H and 6H, respectively, diamond polytype like *T*–*Tt* network structures (see Figure 3.1). $Li_3Zn_2Sn_4$ further stands out due to its ordered structure with no mixed occupancy on the network sites. The Zn atoms take the site that allows to avoid homonuclear Zn–Zn contacts and there are only Sn–Sn and Zn–Sn bonds in the 6H polytype like network of $Li_3Zn_2Sn_4$. For Li_2ZnGe_3, no indication for an ordering of Zn and Ge was deduced from the X-ray diffraction data, and the structure is described with a model that comprises only one Ge/Zn mixed occupied network site. The existence of a Ge-rich Li–Zn–Ge phase with a Li-stuffed 2H diamond-like Zn–Ge network has been reported before,[8] but a full structure determination (including atomic coordinates) has not yet been published.

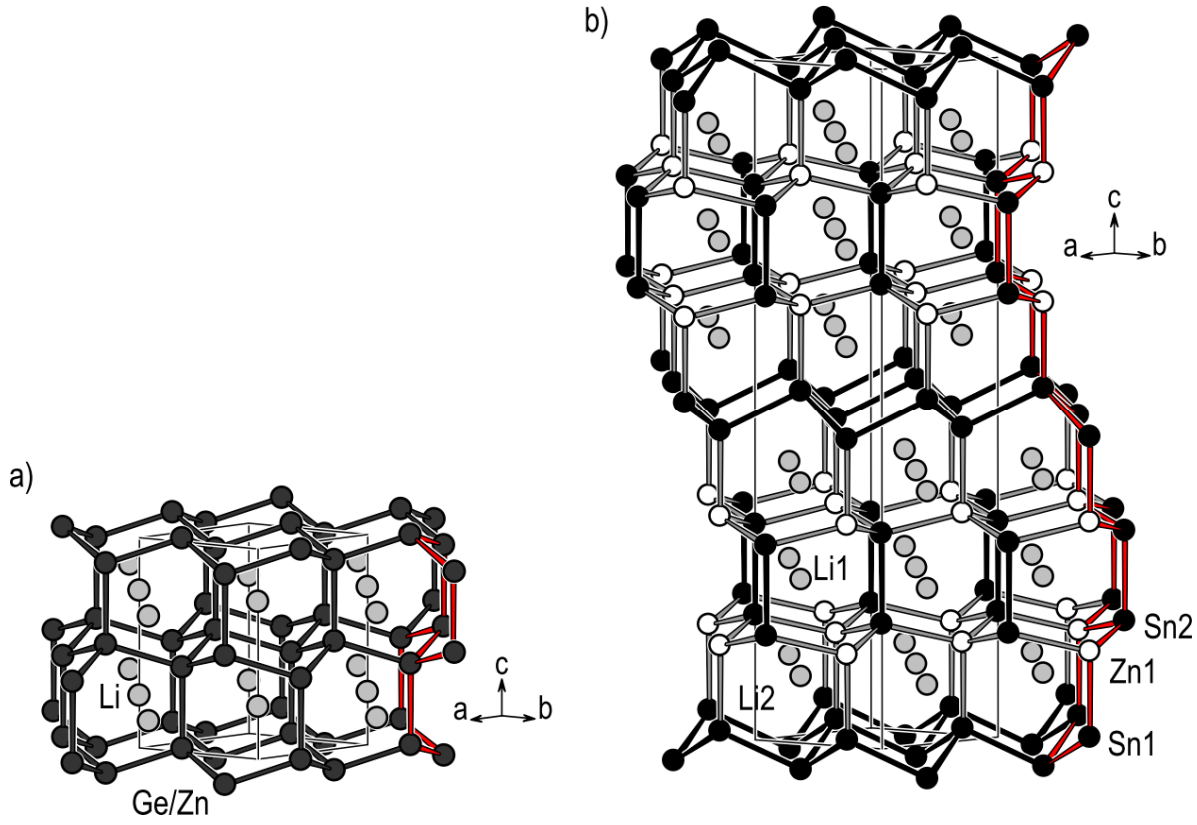

Figure 3.1. Li-stuffed diamond polytype like structures of a) Li_2ZnGe_3 and b) $Li_3Zn_2Sn_4$.

While both Li_2ZnGe_3 and $Li_3Zn_2Sn_4$ show Zn–*Tt* networks with exclusively four-bonded atoms, only the electron count for Li_2ZnGe_3 corresponds to a Zintl phase, according to $(Li^+)_2(4b\text{-}Zn^{2-})(4b\text{-}Ge^0)_3$. $Li_3Zn_2Sn_4$ falls short of the expected electron count.

The results of electronic structure calculations indicate that the Fermi level (E_F) for $Li_3Zn_2Sn_4$ is at the flank of a pseudo gap in the DOS (density of states) curve, and the IDOS (integrated DOS) value which relates to the Zintl phase composition "$Li_4Zn_2Sn_4$" (= "Li_2ZnSn_2") lies in the range of the pseudo gap (within a rigid band model). An inspection of the −(I)COHP curves reveals that also the bonding interactions would be optimized for an electron count corresponding to a composition close to "$Li_4Zn_2Sn_4$". This suggests that a Zintl phase "Li_2ZnSn_2" might exist, or a possible phase width according to "$Li_{3+x}Zn_2Sn_4$".

Generally, the −(I)COHP curves and high −ICOHP (at E_F) values indicate covalent Sn–Sn and Zn–Sn bonds. The analysis of the chemical bonding by means of the electron localization function (ELF) clearly confirmed the presence of covalent two-center Sn–Sn bonds. In contrast, the heteronuclear Zn–Sn contacts were not found to be associated with ELF basins that can unambiguously be related to covalent two-center bonds. Instead, the results indicate that multicenter bonding or even directed Li–Sn interactions should be considered.

3.2.3 The Clathrate $Na_8Zn_4Ge_{42}$

see manuscript 6.10 The Intermetallic Type-I Clathrate $Na_8Zn_4Ge_{42}$
S. Stegmaier, T. F. Fässler, *manuscript for publication.*

$Na_8Zn_4Ge_{42}$ represents an intermetallic type-I clathrate and can be described as an electron precise Zintl phase with Na cations in the voids (20- and 24-vertex cages) of a polyanionic host network of four-connected Zn and Ge atoms (see Figure 3.2). Zn/Ge mixed occupancy is found exclusively for the 6*c* network site. In the type-I clathrate structure this is the only network site which involves only bonds to atoms on other sites. The free refinement of the occupancy parameters for Zn and Ge on this site (with the sum fixed to 1) matches the ideal value that leads to the composition $Na_8Zn_4Ge_{42}$.

$Na_8Zn_4Ge_{42}$ shows that a Zn-substituted Ge type-I clathrate framework with encaged *A* atoms can also be realized with the light alkali metal Na. A binary $A_8Ge_{46-y}\square_y$ phase (□: vacancy) with *A* = Na has not been reported, and the only other known Ge type-I clathrates with

Na atoms as guests are the $Na_8Tr_xGe_{46-x}$ phases with *Tr* = Al and Ga.[42] This is noteworthy because Na is generally considered not to fit well in the larger cages of a Ge type-I clathrate host framework.[46] The displacement parameters for the Na atoms in the 24-vertex cages of the Zn–Ge network of $Na_8Zn_4Ge_{42}$ are indeed large, comparable to that reported for the corresponding K atoms in $K_8Hg_4Sn_{42}$.[47]

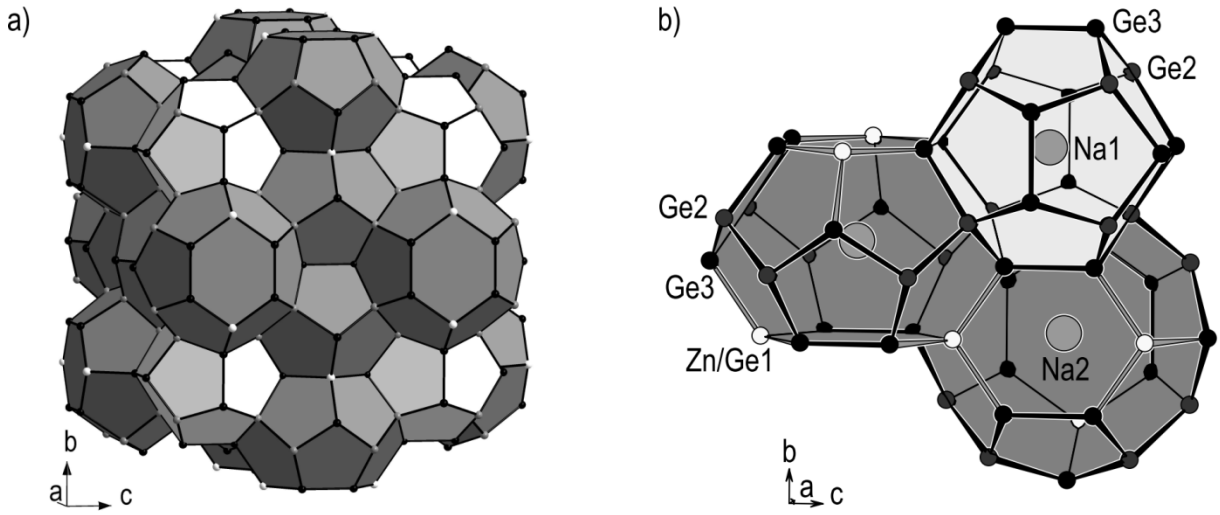

Figure 3.2. Structure of the intermetallic type-I clathrate $Na_8Zn_4Ge_{42}$. a) Space filling arrangement of tetrakaidecahedra (dark gray) and pentagonal dodecahedra (light gray). b) Na sites in the cages of the Zn–Ge framework.

3.2.4 Polymorphs and Phase Transitions of the Zintl Compound Na_2ZnSn_5

see manuscript 6.11 Reorientation of Hexagonal Helical Channels in Tetrahedral Framework Structures – Phase Transitions of the Zintl Phase Na_2ZnSn_5 and its Relation to $Na_5Zn_{2+x}Sn_{10-x}$
S. Stegmaier, S.-J. Kim, A. Henze, T. F. Fässler,
manuscript for publication.

Sn-rich Na–Zn–Sn phases show two other, closely related, possibilities for open four-bonded Zn–Sn framework structures, both with hexagonal channels in which the Na atoms are situated.[19] *tI*-Na_2ZnSn_5 has a structure with channels in two perpendicular directions (see Figure 3.3a). Zn and Sn are fully ordered on three different sites, and again there are Sn–Sn and Zn–Sn but no Zn–Zn bonds in the network. The other phase shows a network with Sn/Zn mixed occupancy and channels in only one direction (see Figure 3.3b), analogous to several Na–*Tr*–Sn phases (*Tr* = Ga, In).[43-45]

In the course of the present thesis, further studies on these phases have been performed. The synthesis of the phases has been optimized and it was found that there are two modifications of the Zintl compound Na_2ZnSn_5. *tI*-Na_2ZnSn_5 with an ordered Zn–Sn structure is the stable modification at standard conditions. For the metastable polymorph *hP*-Na_2ZnSn_5 with Sn/Zn mixed occupancy in the network, a revised structure model is given. Furthermore, the phase transition from metastable *hP*-Na_2ZnSn_5 to stable *tI*-Na_2ZnSn_5 was studied and observed in situ by means of temperature dependent powder and single crystal X-ray diffraction experiments. It was also shown that Na_2ZnSn_5 does not melt congruently but decomposes to form $Na_5Zn_{2+x}Sn_{10-x}$. A topological description of a mechanism for the interchange between the structures of the two Na_2ZnSn_5 polymorphs has been elaborated, and also the relation to the network structure of $Na_5Zn_{2+x}Sn_{10-x}$[20] is discussed. Electronic structure calculations were performed for ordered model structures for the two modifications of Na_2ZnSn_5. A band gap was found at the Fermi level for the stable polymorph *tI*-Na_2ZnSn_5, as expected for a Zintl phase, and in accord with previous calculations employing a slightly different model structure.[19]

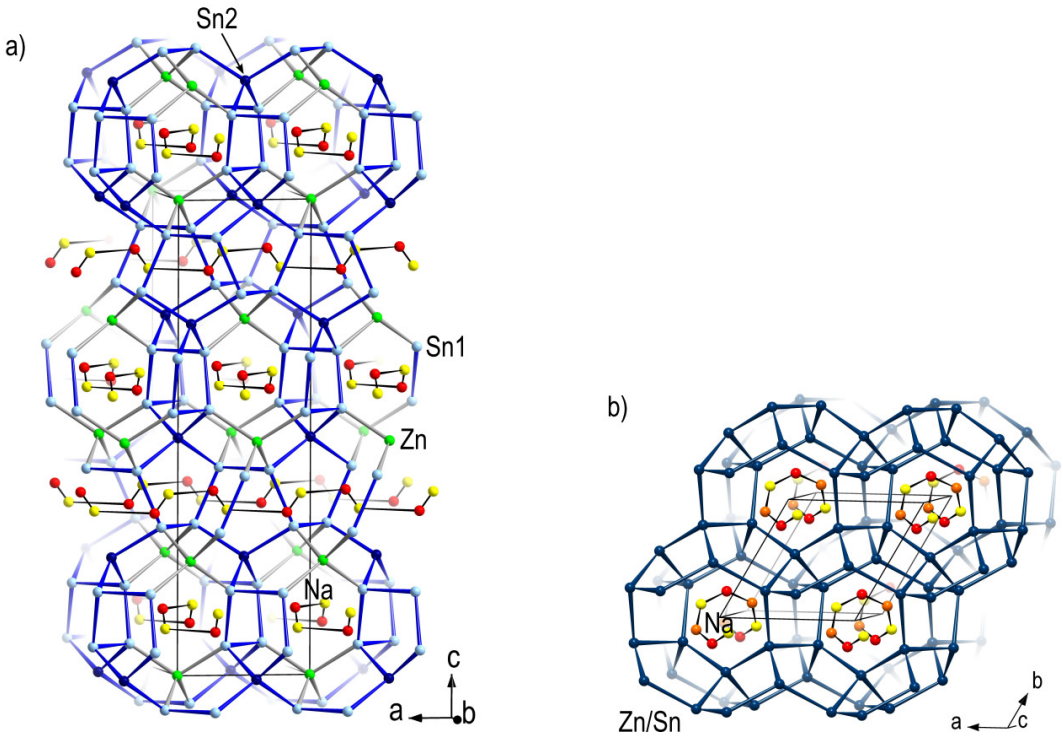

Figure 3.3. Structures of a) *tI*-Na_2ZnSn_5 and b) *hP*-Na_2ZnSn_5.

3.2.5 Topological Relationships of Four-Connected Networks Based on Structures of Sn-Rich Na–Zn–Sn Phases

see manuscript 6.12 Topological Relationships of Four-Connected Networks Based on Structures of Sn-Rich Na–Zn–Sn Phases
S. Stegmaier, T. F. Fässler, *manuscript for publication.*

Based on an analysis of the structural relations between the Zn–Sn frameworks of the Sn-rich Na–Zn–Sn phases a construction scheme for networks of four-connected atoms has been developed. The basic module is a layer of four- and two-connected atoms that can be seen as a cutout of the cubic diamond structure. Via the formation of intralayer bonds between the two-connected atoms, layers of four- and three-connected atoms can be obtained (see Figure 3.4). Two modes for the stacking and interconnection of these layers are available which lead to networks of exclusively four-bonded atoms. The construction scheme allows to anticipate a series of four-connected networks. Furthermore, there is an elegant transformation pathway for any two networks with the same stacking mode sequence.

Besides providing a description of the relations between the Zn–Sn structures of the Sn-rich Na–Zn–Sn phases, this construction scheme might be interesting in the context of studies on hypothetical allotropes of the group 14 elements. Acutally, the (empty) four-connected framework structure that is adopted by the Zn–Sn network of *hP*-Na_2ZnSn_5 (and was first described for $NaGaSn_5$[43]) has been considered in theoretical studies as a possible allotrope structure for C,[48, 49] Si,[48-51] Ge,[48, 50] and Sn.[48] It was found to be comparable in energy to type-I and type-II clathrate structures,[48, 50, 51] and lower in energy than any of the considered (Si and Ge) *allo*-structures.[50, 51] (Note that the cubic diamond structure is always established to be energetically most favorable.) So, this type of open framework structure seems to be a promising candidate for new group 14 element allotrope structures.

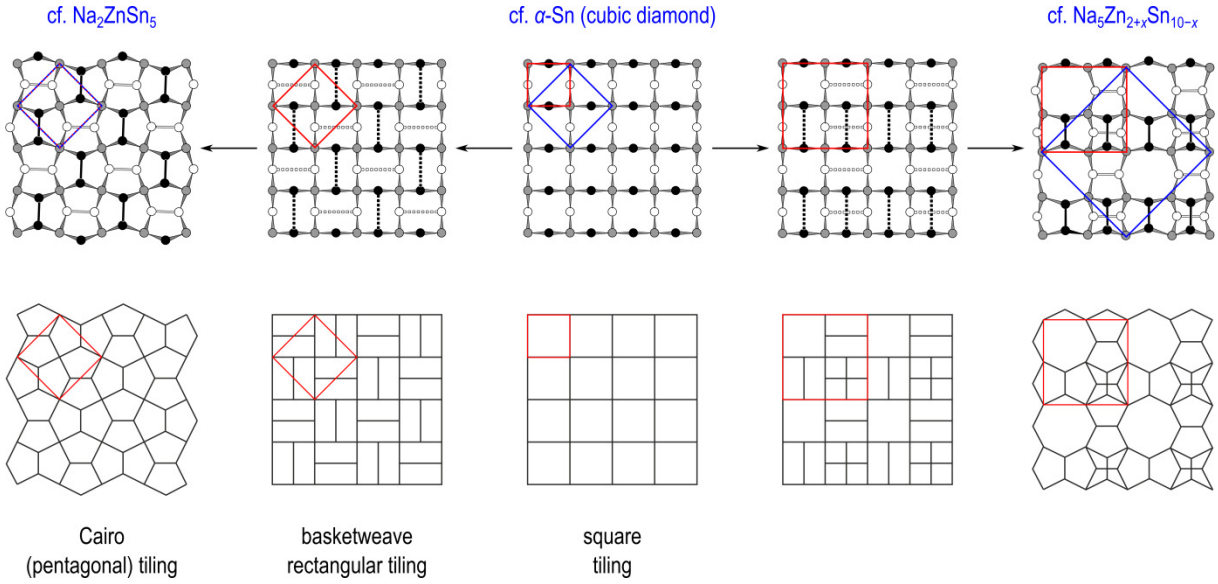

Figure 3.4. Relation between a two-dimensional section of the cubic diamond structure and the layers in the Zn–Sn structure parts of the Na_2ZnSn_5 polymorphs and $Na_5Zn_{2+x}Sn_{10-x}$. In the upper part of the figure schematic representations of the layers are shown in projection along the stacking directions, in the bottom part the related tessellations of the plane are depicted. Red squares show the repeating units of the layers and tessellations, respectively, blue squares indicate the unit cell dimensions of α-Sn, *hP*- and *tI*-Na_2ZnSn_5, and $Na_5Zn_{2+x}Sn_{10-x}$.

3.3 *Ae*–Zn–Sn Phases with Networks of Interconnected Layers (*Ae* = Ca, Sr)

3.3.1 The Polar Intermetallic Phases $SrZn_2Sn_2$ and $Ca_2Zn_3Sn_6$

see publication 6.13 $SrZn_2Sn_2$ and $Ca_2Zn_3Sn_6$ – Two New *Ae*–Zn–Sn Polar Intermetallic Compounds (*Ae*: Alkaline Earth Metal)
S. Stegmaier, T. F. Fässler, *J. Solid State Chem.* **2012**, *192*, 312.

Zn–Sn networks with coordination numbers higher than four are realized by the *Ae*–Zn–Sn phases $SrZn_2Sn_2$ and $Ca_2Zn_3Sn_6$. These are two closely related polar intermetallic compounds with Zn–Sn network structures, which can both be described as built up of two types of layers that are alternately stacked and interconnected via Zn–Sn bonds (see Figure 3.5). $SrZn_2Sn_2$ shows PbO-like $\{ZnSn_{4/4}\}$ and anti-PbO-like $\{SnZn_{4/4}\}$ layers. $Ca_2Zn_3Sn_6$ exhibits PbO-like $\{ZnSn_{4/4}\}$ layers and $\{Sn_4Zn\}$ slabs with a covalently bonded Sn scaffold and capping Zn atoms. Both network structures comprise Zn and Sn atoms with coordination numbers four and five. In case of $SrZn_2Sn_2$, only heteroatomic Zn–Sn contacts are associated with short interatomic distances. For $Ca_2Zn_3Sn_6$, there are corresponding Zn–Sn contacts, homoatomic two-center Sn–Sn bonds, and also a quite short Zn–Zn distance. The structure of $SrZn_2Sn_2$ is a monoclinic distortion variant of the $CaBe_2Ge_2$ type which represents a coloring variant of the $BaAl_4$ type. For s-p bonded networks of $BaAl_4$ type structures, a bonding picture is available which associates the interlayer contacts with 2c2e bonds and describes multicenter bonding within the layers.[52, 53] This scheme can be applied directly for $SrZn_2Sn_2$, and the ideas can also be adapted to rationalize the electron count of $Ca_2Zn_3Sn_6$. Analyses of the chemical bonding with the electron localization function (ELF) show lone pair like basins at Sn atoms and Zn–Sn bonding interactions between the layers for both title phases, and covalent Sn–Sn bonding within the $\{Sn_4Zn\}$ layers of $Ca_2Zn_3Sn_6$. No intralayer two-center Zn–Sn bonding interactions are apparent from the ELF analyses, in accordance with the assumption of multicenter bonding. The DOS curves for both phases reveal a pseudogap close to the Fermi level (E_F), and the band structures show bands crossing E_F both along lines that correspond to directions parallel to the layers as well as along lines that relate to the stacking directions. Sr- or Ca-d states, respectively, are found to make important contributions to conducting bands.

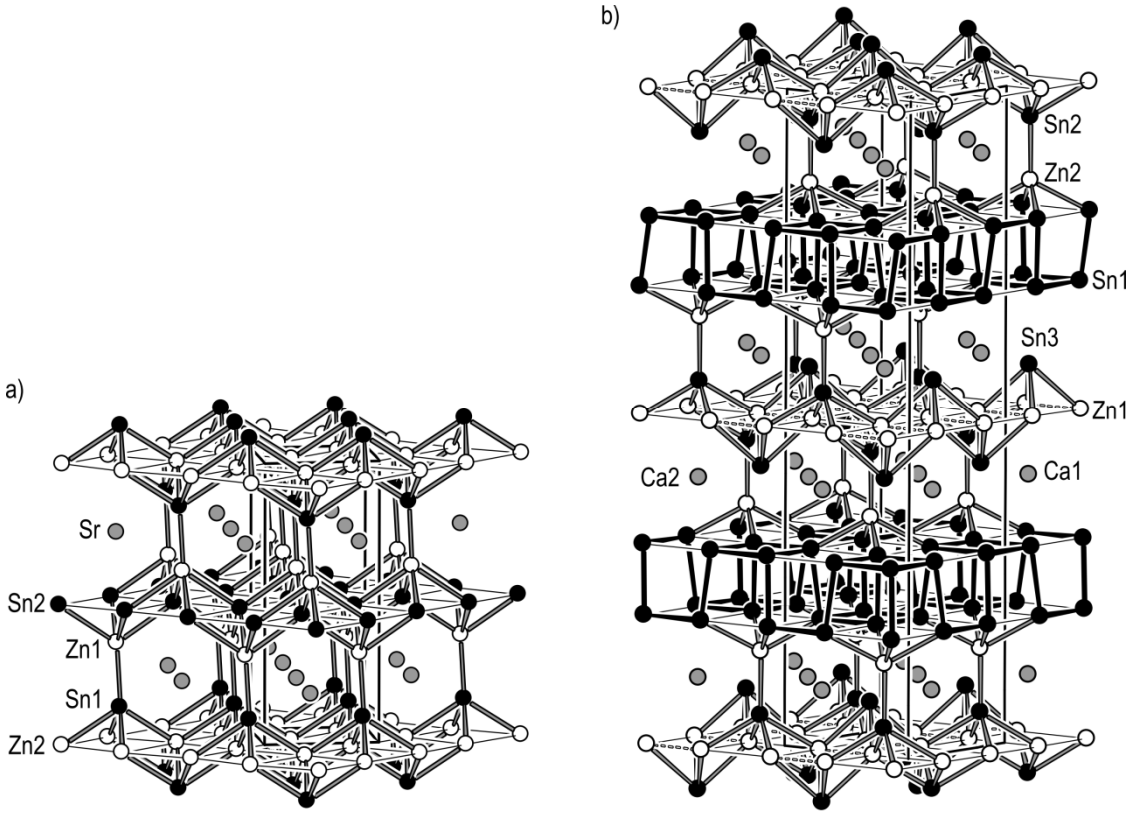

Figure 3.5. Structures of a) $SrZn_2Sn_2$ and b) $Ca_2Zn_3Sn_6$.

3.4 Discussion

The phases presented in this chapter show s-p bonded Zn–Ge and Zn–Sn networks. Concerning the Zn–*Tt* bonding, it is worth to point to the relation to the MO analysis for the cluster bonding of $[(Ge_4)Zn(Ge_4)]^{6-}$ which reveals Zn-s and -p orbital contributions (chapter 2.4.1). In this context, one may further note that a formal description of the networks with Zn^{2+} cations (cf. the example discussed in chapter 3.1) relates to employing the formula $[(Ge_4^{4-})(Zn^{2+})(Ge_4^{4-})]$ for the cluster – it may fit to rationalize the total electron count of the species, but it does not properly represent the Zn–*Tt* bonding situation.

The structural chemistry of the alkali metal-zinc-germanides and -stannides (*A*–Zn–*Tt*), which are described in this chapter, shows marked similarities to that of ternary alkali metal-trielide-tetrelides (*A*–*Tr*–*Tt*). The analogues are: LiGaGe[54] for Li_2ZnGe_3 (Li-stuffed 2H diamond-like network), Li_2Ga_2Sn[41] for $Li_3Zn_2Sn_4$ (Li-stuffed 6H diamond polytype like network),

$Na_8Tr_xGe_{46-x}$[42] for $Na_8Zn_4Ge_{42}$ (type-I clathrate), and the three Na–*Tr*–*Tt* phases $NaGaSn_2$,[45] $NaInSn_2$,[44] and $NaGaSn_5$[43] for (*hP*-)Na_2ZnSn_5 (open framework with channels). $SrZn_2Sn_2$ is iso(valence)electronic with binary $AeTr_4$ alkaline earth metal-trielides, and $BaAl_4$ represents the aristotype for the structure adopted by $SrZn_2Sn_2$.

Another common feature of the Zn–*Tt* network structures of the phases described herein concerns the site preference of the Zn atoms. For the *Tt*-rich phases it is possible to avoid direct homonuclear Zn–Zn contacts, and in the ordered Zn–*Tt* networks Zn atoms take sites that do not lead to Zn–Zn contacts. Furthermore it is notable that the environment of the Zn site in the structure of *tI*-Na_2ZnSn_5 is similar to that of the site occupied by Zn atoms in the type-I clathrate $Na_8Zn_4Ge_{42}$. For the clathrate this site is also the one that is avoided by *Tt* atoms in related binary $A_8Tt_{44}\square_2$ compounds (□: vacancy).

Cation size effects have already been mentioned in chapter 3.2.1 for the *A*–Zn–*Tt* phases with four-bonded networks and are discussed in publication 6.13 for the *Ae*–Zn–Sn phases. Aspects concerning the valence electron count of the phases are addressed in chapter 4.

3.5 References

[1] M. Christensen, S. Johnsen, B. B. Iversen, *Dalton Trans.* **2010**, *39*, 978.

[2] U. Häussermann, S. Amerioun, L. Eriksson, C.-S. Lee, G. J. Miller, *J. Am. Chem. Soc.* **2002**, *124*, 4371.

[3] U. Häussermann, A. S. Mikhaylushkin, *Dalton Trans.* **2010**, *39*, 1036.

[4] A. E. Holleman, E. Wiberg, N. Wiberg, *Lehrbuch der anorganischen Chemie / Holleman-Wiberg*, 101 ed., de Gruyter, Berlin, New York, **1995**.

[5] C. Belin, S. Sportouch, M. Tillard-Charbonnel, *C. R. Acad. Sci. II* **1993**, *317*, 769.

[6] S. Sportouch, C. Belin, M. Tillard-Charbonnel, M. C. Rovira, E. Canadell, *New J. Chem.* **1995**, *19*, 243.

[7] L. Lacroix-Orio, M. Tillard, C. Belin, *Solid State Sciences* **2006**, *8*, 208.

[8] H. Schönemann, H.-U. Schuster, *Rev. Chim. Miner.* **1976**, *13*, 32.

[9] H. Schönemann, H.-U. Schuster, *Z. Anorg. Allg. Chem.* **1977**, *432*, 87.

[10] H.-U. Schuster, *Z. Anorg. Allg. Chem.* **1969**, *370*, 149.

[11] H.-O. Cullmann, H.-W. Hinterkeuser, H.-U. Schuster, *Z. Naturforsch. B* **1981**, *36*, 917.

[12] L. Lacroix-Orio, M. Tillard, C. Belin, *J. Alloy. Compd.* **2008**, *465*, 47.

[13] F. Cheviré, F. J. DiSalvo, *Acta Cryst. E* **2007**, *63*, i62.

[14] Q. Xie, Dissertation, Eidgenössische Technische Hochschule Zürich, **2004**.

[15] H. Wang, Master Thesis, Technische Universität München, Ludwig-Maximilians-Universität München, Universität Augsburg, **2009**.

[16] V. Queneau, S. C. Sevov, *J. Am. Chem. Soc.* **1997**, *119*, 8109.

[17] H.-U. Schuster, *Naturwissenschaften* **1966**, *53*, 361.

[18] W. Pobitschka, H.-U. Schuster, *Z. Naturforsch. B* **1978**, *33*, 115.

[19] S.-J. Kim, Dissertation, Technische Universität München, **2007**.

[20] S. Ponou, S.-J. Kim, T. F. Fässler, *J. Am. Chem. Soc.* **2009**, *131*, 10246.

[21] S.-J. Kim, F. Kraus, T. F. Fässler, *J. Am. Chem. Soc.* **2009**, *131*, 1469.

[22] S.-J. Kim, S. D. Hoffmann, T. F. Fässler, *Angew. Chem. Int. Ed.* **2007**, *46*, 3144.

[23] S.-J. Kim, T. F. Fässler, *J. Solid State Chem.* **2009**, *182*, 778.

[24] V. Baran, T. F. Fässler, *unpublished results*.

[25] G. S. Nolas, J. L. Cohn, J. S. Dyck, C. Uher, J. Yang, *Phys. Rev. B* **2002**, *65*, 165201.

[26] G. S. Nolas, T. J. R. Weakley, J. L. Cohn, *Chem. Mater.* **1999**, *11*, 2470.

[27] A. K. Ganguli, J. D. Corbett, *J. Solid State Chem.* **1993**, *107*, 480.

[28] J. R. Salvador, D. Bilc, J. R. Gour, S. D. Mahanti, M. G. Kanatzidis, *Inorg. Chem.* **2005**, *44*, 8670.

[29] A. K. Ganguli, S. Gupta, J.-T. Zhao, E. Alejandro Leon-Escamilla, J. D. Corbett, *J. Solid State Chem.* **2005**, *178*, 2959.

[30] F. Merlo, M. Pani, M. L. Fornasini, *J. Less-Common Met.* **1991**, *171*, 329.

[31] L. Frik, D. Johrendt, A. Mewis, *Z. Anorg. Allg. Chem.* **2006**, *632*, 1514.

[32] B. Eisenmann, H. Schäfer, N. May, W. Müller, *Z. Naturforsch. B* **1972**, *27*, 1155.

[33] O. Jepsen, A. Burkhardt, O. K. Andersen, *The Stuttgart TB-LMTO-ASA Program (Version 4.7)*, Max-Planck-Institut für Festkörperforschung, Stuttgart, **1998**.

[34] A. Grüttner, R. Nesper, H. G. von Schnering, *Angew. Chem. Int. Ed. Engl.* **1982**, *21*, 912.

[35] F. Kiefer, V. Hlukhyy, A. J. Karttunen, T. F. Fässler, C. Gold, E.-W. Scheidt, W. Scherer, J. Nylen, U. Häussermann, *J. Mater. Chem.* **2010**, *20*, 1780.

[36] J. Gryko, P. F. McMillan, R. F. Marzke, G. K. Ramachandran, D. Patton, S. K. Deb, O. F. Sankey, *Phys. Rev. B* **2000**, *62*, R7707.

[37] A. Ammar, C. Cros, M. Pouchard, N. Jaussaud, J.-M. Bassat, G. Villeneuve, M. Duttine, M. Ménétrier, E. Reny, *Solid State Sciences* **2004**, *6*, 393.

[38] A. M. Guloy, R. Ramlau, Z. Tang, W. Schnelle, M. Baitinger, Y. Grin, *Nature* **2006**, *443*, 320.

[39] T. F. Fässler, *Angew. Chem. Int. Ed.* **2007**, *46*, 2572; *Angew. Chem.* **2007**, *119*, 2624.

[40] F. Kiefer, A. J. Karttunen, M. Döblinger, T. F. Fässler, *Chemistry of Materials* **2011**, *23*, 4578.

[41] W. Blase, G. Cordier, R. Kniep, *Z. Anorg. Allg. Chem.* **1993**, *619*, 1161.

[42] W. Westerhaus, H.-U. Schuster, *Z. Naturforsch. B* **1977**, *32*, 1365.

[43] W. Blase, G. Cordier, *Z. Naturforsch. B* **1988**, *43*, 1017.

[44] W. Blase, G. Cordier, R. Kniep, R. Schmidt, *Z. Naturforsch. B* **1989**, *44*, 505.

[45] J. T. Vaughey, J. D. Corbett, *J. Am. Chem. Soc.* **1996**, *118*, 12098.

[46] A. J. Karttunen, T. F. Fässler, M. Linnolahti, T. A. Pakkanen, *Inorg. Chem.* **2011**, *50*, 1733.

[47] A. Kaltzoglou, S. Ponou, T. F. Fässler, *Eur. J. Inorg. Chem.* **2008**, 538.

[48] C. J. Pickard, R. J. Needs, *Phys. Rev. B* **2010**, *81*, 014106.

[49] D. Connétable, *Phys. Rev. B* **2011**, *83*, 035206.

[50] J. C. Conesa, *J. Phys. Chem. B* **2002**, *106*, 3402.

[51] M. A. Zwijnenburg, K. E. Jelfs, S. T. Bromley, *Phys. Chem. Chem. Phys.* **2010**, *12*, 8505.

[52] C. Zheng, R. Hoffmann, *Z. Naturforsch. B* **1986**, *41*, 292.

[53] G. J. Miller, F. Li, H. F. Franzen, *J. Am. Chem. Soc.* **1993**, *115*, 3739.

[54] W. Bockelmann, H. Jacobs, H.-U. Schuster, *Z. Naturforsch. B* **1970**, *25*, 1305.

4 Summary and Conclusion

An overview for a summarizing analysis of the ternary Zintl compounds and polar intermetallics that are presented in this work is given in Figure 4.1. Figure 4.1a provides a graphical abstract for the present thesis, showing the network structures or the *T*–*Tt* polyanionic cluster species of the phases (*T* = Ni, Cu, Zn; *Tt* = Ge, Sn). The average valence electron count per atom of the *T*–*Tt* polyanionic parts, which is referred to as vec(*T*–*Tt*) in the following discussion, is indicated in Figure 4.1b.

The reduction of a more electronegative p block (semi)metal *E* by an electropositive metal *A'*, which can yield a binary *A'*–*E* Zintl compound, may be pictured as *A'* scissoring the elemental structure of *E*, thus leading to a more open network or a lower dimensional (layer or cluster) polyanionic structure of *E* in the resulting binary *A'*–*E* phase. Using this depicting, some important aspects may be illustrated citing the ternary phases presented in this thesis as examples.

By the reduction of the group 14 elements with alkali metals *A*, the *Tt* structure can be "cut down" to deltahedral cluster polyanions $[Tt_9]^{4-}$ and/or $[Tt_4]^{4-}$. The most common binary phases with such anions have the compositions A_4Tt_9 (vec(*Tt*) = 4.44; $[Tt_9]^{4-}$ anions), $A_{12}Tt_{17}$ (vec(*Tt*) = 4.71; $[Tt_9]^{4-}$ and $[Tt_4]^{4-}$ anions in ratio 1:2), and A_4Tt_4 (vec(*Tt*) = 5; $[Tt_4]^{4-}$ anions). These compounds are generally included in an extended definition for Zintl phases, using Wade's rules for the electron count and structure of the polyanionic clusters.

The ternary phases **$Na_{12}NiSn_{17}$** (vec(*T*–*Tt*) = 4.71; $[Ni@Sn_9]^{4-}$ and $[Sn_4]^{4-}$ anions) and **$A_{14}ZnGe_{16}$** (vec(*T*–*Tt*) = 4.71; $[(Ge_4)Zn(Ge_4)]^{6-}$ and $[Ge_4]^{4-}$ anions) are closely related to the binary ones. The intermetalloid clusters $[Ni@Sn_9]^{4-}$ and $[(Ge_4)Zn(Ge_4)]^{6-}$ can still be described with respect to the homoatomic nine- or four-atom clusters, respectively. With the low *T* content they may be regarded as "*T*-doped *Tt* cluster species". $Na_{12}NiSn_{17}$ is among the first neat solid state phases with $\{T@Tt_9\}$ clusters. Before, these species were only known from solution.[1, 2] Electronic structure calculations for $A_{14}ZnGe_{16}$ reveal a band gap at the Fermi level, and support the description of the phases with discrete $[(Ge_4)Zn(Ge_4)]^{6-}$ and $[Ge_4]^{4-}$ anions and alkali metal cations.

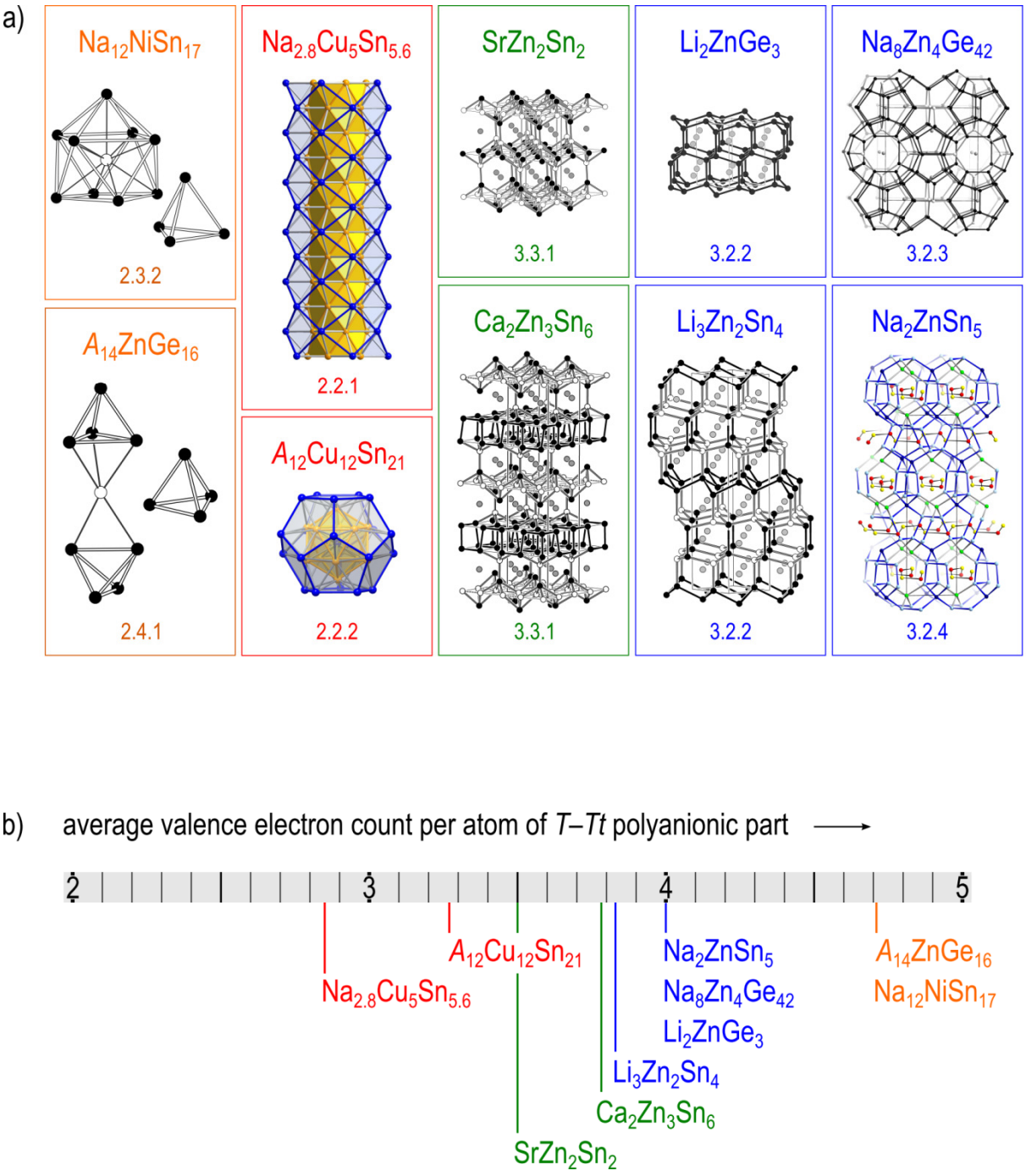

Figure 4.1. a) Graphical abstract for this thesis, referencing the subsections of chapters 2 and 3. b) Average valence electron count per atom of the *T*–*Tt* polyanionic substructures (referred to as vec(*T*–*Tt*) in the text) of the compounds that are described in this work.

Proceeding in the direction of lower average valence electron count per atom of the *T*–*Tt* polyanionic part (Figure 4.1b), the series of phases **Na_2ZnSn_5**, **$Na_8Zn_4Ge_{42}$** and **Li_2ZnGe_3** with vec(*T*–*Tt*) = 4 is next. These are classic electron precise Zintl phases. They show networks of four-bonded atoms that follow the 8–*N* rule, like the α-modifications of Ge and Sn (cubic diamond structure). The electron donation by the alkali metals is exactly compensated by the incorporation of the electron poorer group 12 metal *T* = Zn in the network (*A*:Zn = 2:1). In case of the Na phases $Na_8Zn_4Ge_{42}$ and Na_2ZnSn_5, more open network structures are realized with Na atoms as guests in cages or channels provided by the Zn–*Tt* frameworks. For a model for the stable *tI*-Na_2ZnSn_5 polymorph a band gap is calculated, as expected for a Zintl phase of this type. With the smallest alkali metal Li, a diamond-like network is retained for Li_2ZnGe_3. **$Li_3Zn_2Sn_4$** (vec(*T*–*Tt*) = 3.82) also adopts such a Li-stuffed diamond polytype like network structure, though it falls short of the expected electron count. Analyses with the electron localization function indicate that there might be important Li–Sn interactions.

The alkaline earth metal phases **$SrZn_2Sn_2$** (vec(*T*–*Tt*) = 3.5) and **$Ca_2Zn_3Sn_6$** (vec(*T*–*Tt*) = 3.78) with lower valence electron counts per atom of the *T*–*Tt* parts (< 4) are typical polar intermetallics. The Zn–Sn network structures of these phases also comprise atoms with coordination number five and cannot follow the 8–*N* rule. Including both two-center and multicenter bonding, the electron count of the phases can still be straightforwardly rationalized. Assuming, like in the Zintl concept, a full charge transfer from the electropositive *Ae* metals to the Zn–Sn parts, these attain the optimal electron count to build the polyanionic substructures. However, other than Wade's rules, such multicenter bonding is mostly not regarded as a natural extension of the Zintl concept, but rather as one of the aspects marking the – though diffuse – border between Zintl phases (as valence compounds) and polar intermetallics. Related to the less strong (multicenter) interactions in the polyanionic network and the different interactions with the cations no band gap occurs at the Fermi level and the polar intermetallics have metallic properties.

The novel *A*–Cu–Sn phases that are presented in this work have even lower average valence electron counts per atom of the *T*–*Tt* polyanionic parts. **$A_{12}Cu_{12}Sn_{21}$** (vec(*T*–*Tt*) = 3.27) and **$Na_{2.8}Cu_5Sn_{5.6}$** (vec(*T*–*Tt*) = 2.85) show discrete polyanionic $[Sn@Cu_{12}@Sn_{20}]^{12-}$ clusters and $^1_\infty\{Sn_{0.6}@Cu_5@Sn_5\}$ columns separated by *A* atoms. These species are unprecedented in the cluster chemistry of the group 14 elements. Their *T* = Cu content is beyond "doping", and

there are no simple rules applicable to rationalize their electron count. They can be seen as truly intermetalloid species – the $[Sn@Cu_{12}@Sn_{20}]^{12-}$ clusters with delocalized cluster bonding and the $^{1}_{\infty}\{Sn_{0.6}@Cu_5@Sn_5\}$ rods giving rise to one-dimensional metallic characteristics. However, also in this case, the polyanions obviously do have a preferred electron count. The crystal structure analyses and the electronic structure calculations both for the $A_{12}Cu_{12}Sn_{21}$ phases and $Na_{2.8}Cu_5Sn_{5.6}$ indicate that the alkali metal content of the phases is adjusted via partial occupancy of alkali metal sites so that the composition meets a band gap in the electronic structure. In case of $Na_{2.8}Cu_5Sn_{5.6}$ the band structure shows metallic characteristics parallel to the Cu–Sn rods and the opening of a band gap perpendicular to it. Thus, the *A*–Cu–Sn phases may be considered in analogy to the Zintl compounds as "salt-like" with alkali metal cations and intermetalloid Cu–Sn polyanions. This view of the structure and bonding of these new cluster phases suggests to start the discussion – as the synthesis – directly with a binary Cu–Sn alloy. In taking up the alkali metal scissor picture again, the formation of the ternary phases with Cu–Sn polyanions parallels that of binary Zintl phases with polyanions of p block (semi)metals, and the Cu–Sn polyanions may be regarded as reduced "small charged alloy particles" (in analogy to the description of homoatomic cluster anions as "small charged element particles"[3]). Such species are of interest both concerning questions of chemical bonding, as they have been addressed in this thesis, and also as potential precursors for novel binary Cu–Sn materials. The synthesis of meso- and nano-structured elemental materials from homoatomic Zintl anions,[4, 5] and the recently reported metastable binary Ni–Bi phase that was obtained by the reduction of the polycationic Ni–Bi rods in the $Bi_{5.6}Ni_5I$ subhalide,[6] suggests to anticipate similar findings when exploring the chemistry of the *A*–Cu–Sn compounds presented in this work. If the alkali metal matrices can be removed without destroying the Cu–Sn substructures, new metastable binary Cu–Sn phases might be formed by the "bronze wires and dots".

References

[1] S. Scharfe, F. Kraus, S. Stegmaier, A. Schier, T. F. Fässler, *Angew. Chem. Int. Ed.* **2011**, *50*, 3630; *Angew. Chem.* **2011**, *123*, 3712.

[2] M. M. Gillett-Kunnath, J. I. Paik, S. M. Jensen, J. D. Taylor, S. C. Sevov, *Inorg. Chem.* **2011**, *50*, 11695.

[3] L. Yong, S. D. Hoffmann, T. F. Fässler, *Z. Anorg. Allg. Chem.* **2005**, *631*, 1149.

[4] G. Armatas, M. Kanatzidis, in *Structure and Bonding, Vol. 140* (Ed.: T. F. Fässler), Springer Berlin / Heidelberg, **2011**, pp. 133.

[5] S. Dong, A. E. Riley, A. J. Cadby, E. K. Richman, S. D. Korlann, S. H. Tolbert, *Nature* **2006**, *441*, 1126.

[6] M. Kaiser, A. Isaeva, M. Ruck, *Angew. Chem. Int. Ed.* **2011**, *50*, 6178; *Angew. Chem.* **2011**, *123*, 6302.

5 Methods

This chapter gives an overview of experimental procedures, characterization techniques, equipment, computational methods and programs for electronic structure calculations that were employed in the course of this thesis. Detailed records on the synthesis and characterization of each compound that is presented in this work are included in the respective publication or manuscript, as are the details for the computational studies.

5.1 General Experimental Procedures

Most of the intermetallic phases that are presented in this thesis, as well as the employed alkali and alkaline earth metals, are not stable against air and moisture. An argon-filled glovebox (MB 20 G, MBRAUN) and other standard inert gas techniques were used for handling materials in argon-atmosphere.

5.2 Synthesis

5.2.1 Starting Materials

For the syntheses of the ternary *A*–*T*–*Tt* and *Ae*–Zn–Sn phases, the respective elements (*A* = Li, Na, K, Rb, Cs; *Ae* = Ca, Sr; *T* = Ni, Cu, Zn; *Tt* = Ge, Sn) were used as indicated in the corresponding publications and manuscripts. In case of the Na–Ni–Sn and *A*–Cu–Sn phases, binary Ni–Sn and Cu–Sn precursors were prepared by arc-melting Ni and Sn or Cu and Sn, respectively. The employed arc-melting system (Mini Arc Melting System MAM-1, JOHANNA OTTO), which is installed inside an argon-filled glovebox, has a water-cooled copper sample holder and a tungsten electrode fixed in a movable electrode holder. Cu or Ni wire, respectively, was melted with Sn granules in the arc furnace. To ensure homogenization, the reguli were turned upside down and melted several times.

5.2.2 Reaction Containers

Tantalum and niobium ampoules were used as reaction containers. These were prepared from pieces (about 3 to 5 cm length) of tantalum or niobium tubing (external diameter 10 mm, wall thickness 0.5 mm). The open ends of the tubes were sealed by arc-welding under reduced pressure in argon-atmosphere. For this, the tubes' ends were either crimped shut to prepare for a welding line, or tight fitting lids (blanked from tantalum or niobium sheets) were put on the tubes' ends. Prior to sample loading, one-side welded ampoules and additional lids were cleaned by washing (under ultrasonification) successively in diluted nitric acid, deionized water, and acetone, dried and stored in a drying oven at 120 °C. For the syntheses, ampoules were then transferred into an argon-filled glovebox and loaded with the starting materials (which were stored in the glovebox). Then the second end of the tubes was also sealed by arc-welding.

5.2.3 Furnaces

Most reactions were carried out using vertical resistance tube furnaces to apply defined temperature programs to the samples (furnaces Type LOBA, HTM REETZ, regulator of EUROTHERM Deutschland, type S thermocouple placed in the middle of the furnace to monitor the actual temperature). In these cases, the loaded ampoules were placed in silica tubes which were evacuated and flushed with argon several times, finally evacuated (approx. 10^{-3} mbar), sealed, and inserted in the tube furnaces.

For experiments using a high-frequency induction furnace (Type TIG 2.5/300, HÜTTINGER Elektronik), the loaded ampoules were placed in the water-cooled sample chamber of the induction furnace and heated under a continuous argon-flow.

5.3 Experimental Characterization

5.3.1 Powder X-ray Diffraction

In an argon-filled glovebox, samples of the reaction products were (if possible) finely ground in an agate mortar, optionally diluted with diamond powder, and filled in glass capillaries (silica for high temperature measurements, see manuscript 6.11) which were then sealed using a hot tungsten filament and capillary wax. To test the air stability of reaction products, samples were exposed to air, a piece of scotch tape was coated with a thin layer of the

powder, a second piece of scotch tape was used to cover the sample, and then this assembly was fixed in a flat sample holder.

Powder XRD data were collected with a STOE STADI P powder diffractometer equipped with an imaging plate and a linear position sensitive detector (IP-PSD and L-PSD) using Cu $K_{\alpha 1}$ radiation (λ = 1.54060 Å, curved Ge (111) monochromator). Samples in capillaries or flat sample holders were measured in Debye-Scherrer or transmission mode, respectively. All measurements were carried out at room temperature, with the exception of the high temperature experiments described in manuscript 6.11. For these, a capillary furnace high temperature attachment version 0.65.3 was employed and data were collected with the IP-PSD.

The STOE WINXPOW program package[1] was used for phase analysis. The powder patterns of the reaction products were compared with powder patterns of known compounds, using the Search/Match module of the WINXPOW software with the ICDD PDF-2 database (International Centre for Diffraction Data, Powder Diffraction File), or data from the ICSD (Inorganic Crystal Structure Database),[2] or the Pearson's Crystal Data[3] crystallographic database.

5.3.2 Single Crystal X-ray Diffraction and Crystal Structure Determination

Single crystals of air sensitive compounds were selected in an argon-filled glovebox equipped with a microscope. The crystals were mounted on glass fibers (mostly using grease, not using any sort of glue in case of high temperature measurements, see manuscript 6.11), and these were inserted in glass capillaries. Then the fibers were fixed in the capillaries and these were sealed using a hot tungsten filament and capillary wax. For low temperature measurements, crystals were alternatively mounted on glass fibers using perfluoropolyalkylether. In that case the glass fibers were already fixed in sample holder pins and suitable containers were used for the transfer (under argon) from the glovebox to the diffractometer. Single crystals of air stable compounds were selected under normal atmosphere using a microscope. In that case, crystals were glued on glass fibers e.g. using nail polish.

Single crystal XRD data were collected either with an OXFORD DIFFRACTION Xcalibur 3 (Sapphire 3 CCD detector), a BRUKER APEX II (KAPPA goniometer, APEX II CCD detector), or a STOE IPDS 2T (imaging plate) diffractometer system. All instruments use

Mo K_α radiation (λ = 0.71073 Å, graphite monochromator), the Xcalibur 3 has a sealed tube X-ray source, the APEX II and the IPDS 2T are operated with a rotating anode source (Nonius FR591). The Xcalibur 3 and the APEX II systems are equipped with OXFORD INSTRUMENTS Cryojet cooling systems (nitrogen jet), allowing to perform measurements at lower temperatures. In case of the IPDS 2T a HEATSTREAM high temperature attachment (heating medium nitrogen, vertical gas flow) can be employed for measurements at higher temperatures.

For data collection and processing the respective diffractometer software is used. The data processing software for the Xcalibur 3 is the OXFORD CrysAlis RED software[4] (including ABSPACK for absorption corrections; alternatively data can be exported to apply absorption corrections with the STOE X-RED[5]/X-SHAPE[6] software). For the APEX II it is the BRUKER SAINT software (absorption corrections with SADABS), and for the IPDS 2T it is the STOE X-AREA software[7] (numerical absorption corrections with X-RED[5]/X-SHAPE[6]). XPREP[8] was used for space group assignment and data merging (identical indices only). In most cases a structure solution (direct methods) was attained with XS,[9, 10] alternatively SUPERFLIP[11] (charge-flipping) implemented in the WinGX package[12] was employed. Structure refinements were carried out with XL[9, 13] (full-matrix least-squares on F_o^2). Atomic coordinates were standardized with STRUCTURE TIDY[14] implemented in PLATON[15]. Graphical representations of the crystal structures were prepared with DIAMOND.[16]

5.3.3 Scanning Electron Microscopy and Energy Dispersive X-ray Spectroscopy

For qualitative and semi-quantitative EDX analyses and to obtain SEM images A JEOL 5900LV scanning electron microscope system operating at 20 kV, which is equipped with an OXFORD INSTRUMENTS INCA energy dispersive X-ray microanalysis system, was employed. Samples for SEM and EDX measurements (e.g. crystals after XRD measurements) were fixed on carbon pads on cylindrical aluminum sample holders.

5.3.4 Differential Thermal Analysis

DTA measurements were performed with a NETZSCH DSC 404 C PEGASUS instrument equipped with a DTA sample carrier system with integrated radiation shield and type S thermocouple. Custom-built niobium ampoules were used as sample containers and an empty niobium ampoule of the same type was used as reference. A continuous argon-flow was employed during the measurements. The NETZSCH PROTEUS software[17] was used for data evaluation.

5.3.5 Magnetic Measurements

Samples for SQUID magnetometer measurements were enclosed in gelatin capsules that were fixed in the centers of plastic straws. A MPMS XL5 SQUID magnetometer (QUANTUM DESIGN) was used for the magnetic measurements. Zero-field cooling measurements were performed to test for superconducting behavior.

5.4 Computational Studies

5.4.1 Solid State Electronic Structure Calculations

DFT electronic structure calculations were carried out with the Stuttgart TB-LMTO-ASA program,[18] employing the tight-binding (TB) version of the linear muffin-tin orbital (LMTO) method in the atomic sphere approximation (ASA). The Barth-Hedin local exchange correlation potential[19] was used. Radii of the atomic spheres and interstitial empty spheres were determined by the procedures implemented in the TB-LMTO-ASA programs. The *k*-space integration was performed by the tetrahedron method.[20] The basis sets that were employed for the calculations are stated in the respective publications and manuscripts.

Discussions on the electronic structures of the compounds are based on analyzes of the total and partial density of states (DOS and PDOS), band structure, and fat band plots. Chemical bonding was further investigated using the crystal orbital Hamilton population (COHP) technique,[21] as well as topological analyses of the electron localization function (ELF).[22, 23] GNUPLOT[24] was used to obtain (P)DOS, band structure, fat band, and −(I)COHP plots. Graphical representations of the ELF were prepared with VESTA.[25]

5.4.2 Molecular Electronic Structure Calculations

Molecular orbital calculations were preformed with the GAUSSIAN[26] package of programs (for the employed versions and the corresponding full citations see the respective publications and manuscripts). Hybrid DFT calculations were performed with the B3LYP functional.[27, 28] The basis sets that were used for the calculations are indicated in the publications and manuscripts. To compensate for the highly negative charge of the cluster anions, continuum solvation models as implemented in GAUSSIAN were used, or alkali metal atoms or positive point charges were included in the calculations. Natural charges were calculated using Version 3.1 of the NBO program[29] as implemented in GAUSSIAN.

ELF calculations based on GAUSSIAN results were performed with the program DGRID (Version 4.6).[30] VESTA[25] was employed to prepare graphical representations of the ELF. GAUSSVIEW[31] was used to visualize molecular orbitals.

5.5 References

[1] *WinXPOW (Version 2.08)*, STOE & Cie GmbH, Darmstadt, **2003**.

[2] *FindIt, ICSD Database (Version 1.7.0)*, FIZ, Karlsruhe, Germany, **2010**.

[3] P. Villars, K. Cenzual, *Pearson's Crystal Data: Crystal Structure Database for Inorganic Compounds (on CD-ROM) (Release 2007/8)*, ASM International, Materials Park, Ohio, USA.

[4] *CrysAlis RED (Version 1.171.33.34d)*, Oxford Diffraction Ltd., **2009**.

[5] *X-RED32 (Version 1.26)*, STOE & Cie GmbH, Darmstadt, **2004**.

[6] *X-SHAPE (Version 2.05)*, STOE & Cie GmbH, Darmstadt, **2004**.

[7] *X-AREA (Version 1.26)*, STOE & Cie GmbH, Darmstadt, **2004**.

[8] *XPREP (Version 6.14)*, Bruker Nonius, **2003**.

[9] G. Sheldrick, *Acta Cryst. A* **2008**, *64*, 112.

[10] *XS - Crystal Structure Solution - SHELXTL (Version 6.12)*, Bruker AXS, **2001**.

[11] L. Palatinus, G. Chapuis, *J. Appl. Crystallogr.* **2007**, *40*, 786.

[12] L. Farrugia, *J. Appl. Cryst.* **1999**, *32*, 837.

[13] *XL - Crystal Structure Refinement - SHELXTL (Version 6.12)*, Bruker AXS, **2001**.

[14] L. M. Gelato, E. Parthe, *J. Appl. Cryst.* **1987**, *20*, 139.

[15] A. L. Spek, *Acta Cryst. A* **1990**, c34.

[16] K. Brandenburg, *Diamond (Version 3.2)*, Crystal Impact GbR, Bonn, Germany, **2012**.

[17] *NETZSCH Proteus Software for Thermal Analysis (Version 4.3.1)*, Germany, **2004**.

[18] O. Jepsen, A. Burkhardt, O. K. Andersen, *The Stuttgart TB-LMTO-ASA Program (Version 4.7)*, Max-Planck-Institut für Festkörperforschung, Stuttgart, **1998**.

[19] U. v. Barth, L. Hedin, *J. Phys. C: Solid State Phys.* **1972**, *5*, 1629.

[20] P. E. Blöchel, O. Jepsen, O. K. Andersen, *Phys. Rev. B* **1994**, *49*, 16223.

[21] R. Dronskowski, P. E. Blöchl, *J. Phys. Chem.* **1993**, *97*, 8617.

[22] A. D. Becke, K. E. Edgecombe, *J. Chem. Phys.* **1990**, *92*, 5397.

[23] A. Savin, R. Nesper, S. Wengert, T. F. Fässler, *Angew. Chem. Int. Ed. Engl.* **1997**, *36*, 1808; *Angew. Chem.* 109 (1997) 1892-1918.

[24] T. Williams, C. Kelley, *GNUPLOT (Version 4.4)*, **2011**.

[25] K. Momma, F. Izumi, *J. Appl. Cryst.* **2008**, *41*, 653.

[26] M. J. Frisch et al., *Gaussian*, Gaussian, Inc., Wallingford CT.

[27] A. D. Becke, *J. Chem. Phys.* **1993**, *98*, 5648.

[28] C. Lee, W. Yang, R. G. Parr, *Phys. Rev. B* **1988**, *37*, 785.

[29] E. D. Glendening, A. E. Reed, J. E. Carpenter, F. Weinhold, *NBO (Version 3.1)*.

[30] M. Kohout, *DGrid (Version 4.6)*, Radebeul, **2011**.

[31] R. Dennington II, T. Keith, J. Millam, K. Eppinnett, W. L. Hovell, R. Gilliland, *GaussView (Version 3.09)*, Semichem, Inc., Shawnee Mission, KS, **2003**.

6 Publications and Manuscripts

6.1 $Na_{2.8}Cu_5Sn_{5.6}$: A Crystalline Alloy Featuring Intermetalloid $^1_\infty\{Sn_{0.6}@Cu_5@Sn_5\}$ Double-Walled Nanorods with Pseudo-Five-Fold Symmetry

S. Stegmaier, T. F. Fässler,

Angew. Chem. Int. Ed. **2012**, *51*, 2647; *Angew. Chem.* **2012**, *124*, 2701.

6.2 A Bronze Matryoshka: The Discrete Intermetalloid Cluster $[Sn@Cu_{12}@Sn_{20}]^{12-}$ in the Ternary Phases $A_{12}Cu_{12}Sn_{21}$ (A = Na, K)

S. Stegmaier, T. F. Fässler,

J. Am. Chem. Soc. **2011**, *133*, 19758.

6.3 $[Cu@Sn_9]^{3-}$ and $[Cu@Pb_9]^{3-}$: Intermetalloid Clusters with Endohedral Cu Atoms in Spherical Environments

S. Scharfe, T. F. Fässler, S. Stegmaier, S. D. Hoffmann, K. Ruhland,
Chem. Eur. J. **2008**, *14*, 4479.

6.4 Step-by-Step Synthesis of the Endohedral Stannaspherene $[Ir@Sn_{12}]^{3-}$ via the Capped Cluster Anion $[Sn_9Ir(cod)]^{3-}$

J.-Q. Wang, S. Stegmaier, B. Wahl, T. F. Fässler,
Chem. Eur. J. **2010**, *16*, 1793.

6.5 $[Co@Ge_{10}]^{3-}$: An Intermetalloid Cluster with Archimedean Pentagonal Prismatic Structure

J.-Q. Wang, S. Stegmaier, T. F. Fässler,

Angew. Chem. Int. Ed. **2009**, *48*, 1998; *Angew. Chem.* **2009**, *121*, 2032.

6.6 *Chapter on Theoretical Investigations in the Review Article:*
Zintl Ions, Cage Compounds, and Intermetalloid Clusters of Group 14 and Group 15 Elements

S. Scharfe, F. Kraus, S. Stegmaier, A. Schier, T. F. Fässler,
Angew. Chem. Int. Ed. **2011**, *50*, 3630; *Angew. Chem.* **2011**, *123*, 3712.

6.7 Intermetalloid Ni-Filled Sn Clusters $[Ni@Sn_9]^{4-}$ and Tetrahedral $[Sn_4]^{4-}$ in the Solid State Phase $Na_{12}NiSn_{17}$

Saskia Stegmaier, Thomas. F. Fässler,

manuscript in preparation

Abstract

$Na_{12}NiSn_{17}$, the first ternary Na–Ni–Sn phase, contains $[Ni@Sn_9]^{4-}$ nine-vertex Sn clusters with endohedral Ni atoms and tetrahedral $[Sn_4]^{4-}$ Zintl anions. $Na_{12}NiSn_{17}$ was obtained from a reaction of a preformed Ni–Sn alloy with Na. The crystal structure was determined by means of single crystal X-ray diffraction methods, and it is described in space group $P2_1/c$ (No. 14) with $a = 23.734(1)$ Å, $b = 13.680(1)$ Å, $c = 44.620(2)$ Å, and $\beta = 91.53(1)°$. $Na_{12}NiSn_{17}$ is a ternary derivative to the series of $A_{12}Tt_{17}$ phases (A: alkali metal; Tt: group 14 (semi)metal). The arrangement of the $[Ni@Sn_9]^{4-}$ and $[Sn_4]^{4-}$ clusters, which are present in ratio 1:2, represents a hierarchical replacement variant of the hexagonal Laves phase $MgZn_2$.

Introduction

Until recently, structurally characterized compounds with intermetalloid[1] cluster anions of group 14 (semi)metals (Tt) and d block metals (T) of the type $\{T_m@Tt_n\}$, with filled Tt cage clusters, were only known from solution based chemistry.[2, 3] The $A_{12}Cu_{12}Sn_{21}$ phases (A = Na to Cs), which we presented lately, feature the first discrete endohedral T–Tt cluster anion in the solid state, namely the onion-skin-like $[Sn@Cu_{12}@Sn_{20}]^{12-}$.[4] Together with the $Na_{2.8}Cu_5Sn_{5.6}$ phase that contains polyanionic $\{Sn_{0.6}@Cu_5@Sn_5\}$ rods,[5] the $A_{12}Cu_{12}Sn_{21}$ phases have introduced discrete intermetalloid polyanionic cluster species with a high T metal content to the chemistry of the group 14 elements.

Herein we present $Na_{12}NiSn_{17}$, the first ternary Na–Ni–Sn phase, and one of the first[6] examples of neat solid state compounds that contain smaller $\{T@Tt_9\}$ cluster anions with a nine-vertex cage centered by a single endohedral d block metal atom.

Results and Discussion

$Na_{12}NiSn_{17}$ was obtained via a reaction of elemental Na with a pre-prepared Ni–Sn alloy. The title phase was structurally characterized by means of single crystal X-ray diffraction methods. $Na_{12}NiSn_{17}$ contains {Ni@Sn_9} nine-vertex Sn clusters with endohedral Ni atoms and tetrahedral {Sn_4} clusters in ratio 1:2. The ideal formula $Na_{12}NiSn_{17}$ represents an electron precise phase with 12 Na^+ cations, two $[Sn_4]^{4-}$ anions and one $[Ni@Sn_9]^{4-}$ cluster per formula unit. The $[Ni@Sn_9]^{4-}$ polyanion, which is known from solution based chemistry,[7] may formally be described as built up by incorporating a Ni^0 atom with d^{10} configuration into a $[Sn_9]^{4-}$ cage cluster.

According to the current state of the structure refinement, which is not yet regarded as a final result (see Experimental Section below), the empirical formula of the title phase is $Na_{11.94(3)}Ni_{0.93(1)}Sn_{17}$. For several partially occupied Na sites, as well as for the four crystallographically independent Ni sites, occupancy parameters were refined freely. As shown by the empirical formula, this led to a Na content close to the ideal value according to the formula $Na_{12}NiSn_{17}$. For the Ni sites occupancy factors of 0.93(1) to 0.94(1) resulted. This is close to full occupancy but indicates that there are also some empty {Sn_9} clusters present. Further studies will show whether $Na_{12}NiSn_{17}$ with unambiguously fully occupied Ni sites and thus only filled {Ni@Sn_9} clusters can be characterized. Note that the Ni content does not affect the (valence) electron count for the phase, since $[Ni@Sn_9]^{4-}$ and empty $[Sn_9]^{4-}$ anions bear the same charge. For clarity, the phase will be referred to as $Na_{12}NiSn_{17}$ at the current state.

The structure model for $Na_{12}NiSn_{17}$ (Z = 16) comprises seven ordered tetrahedral {Sn_4} clusters (A to G, see Table 2) and a split model for the eighth {Sn_4} which describes two possible orientations of the cluster that are occupied with ratio 0.76:0.24 (H, I). Two of the four crystallographically independent {Ni@Sn_9} clusters are ordered (J and K, Figure 1), the other two are subject to disorder. For one of them a reasonable split model could be introduced that describes two orientations of the cluster with a refined occupancy ratio of 0.70:0.30 (L, M, Figure 2). For the second disordered {Ni@Sn_9} cluster (N) no suitable split model was found, and the current state of the refinement is afflicted with large anisotropic displacement parameters for the Sn atoms of this cluster (Figure 4, see Experimental Section), and also the large residual electron density peaks are associated with this cluster. Generally, disorder is often found for compounds with empty {Tt_9} or filled {T@Tt_9} clusters.[8]

The Sn–Sn distances for the tetrahedral $[Sn_4]^{4-}$ clusters in $Na_{12}NiSn_{17}$ are in the range from 2.897(2) to 3.07(1) Å, in good agreement with the Sn–Sn distances known for $[Sn_4]^{4-}$ anions in binary *A*–Sn phases, e.g. $Rb_{12}Sn_{17}$ (2.891 to 2.942 Å).[9] The two ordered {Ni@Sn_9} clusters are shown in Figure 1. Cluster J (Figure 1a) shows a structure close to a monocapped square antiprism, which is the *nido* cluster structure that is expected, according to Wade's rules, for $[Sn_9]^{4-}$. The structure of cluster K (Figure 1b) can be described as a tricapped trigonal prism with two elongated heights. Generally, both empty and filled {Tt_9} and {$T@Tt_9$} clusters are found to be structurally quite flexible, and it is not uncommon that one cluster species adopts such differing structures,[8] which are actually closely related.[10] Ni–Sn distances between 2.563(2) and 2.755(2) Å are found for the two ordered clusters in $Na_{12}NiSn_{17}$. These compare well with the Ni–Sn distances reported for {Ni@Sn_9} clusters obtained from solution,[7] and lie in the range of the Ni–Sn distances in the binary intermetallic phase NiSn (2.386 to 2.818 Å).[11] The shorter Sn–Sn distances, excluding the edges of the capped square of cluster J and the prism heights of cluster K, lie between 2.951(2) and 3.267(2) Å. The longest Sn–Sn distance in the capped square of cluster J is 3.518 Å, the prism heights of cluster K are 3.324(2) Å, 3.905(2) Å, and 3.942(2) Å. As commonly observed, these Sn–Sn distances of the filled clusters are somewhat longer than those found for empty $[Sn_9]^{4-}$ clusters.[12] A detailed listing of structural parameters for known empty and Ni-centered nine-vertex Sn clusters has been provided in ref. [7].

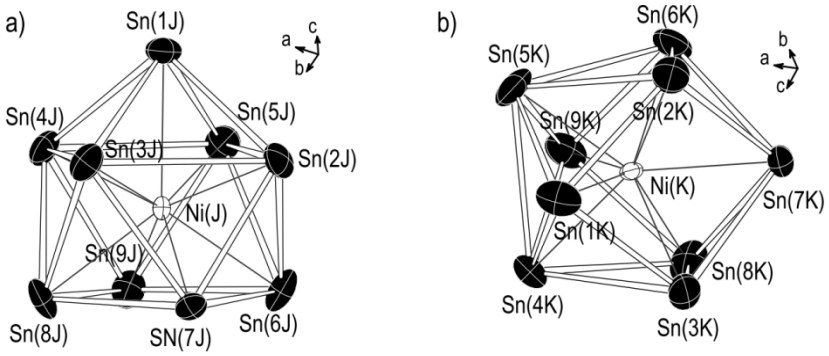

Figure 1. Ordered {Ni@Sn_9} clusters in $Na_{12}NiSn_{17}$. a) Ordered cluster J with a structure close to a monocapped square antiprism, with Sn(1J) as capping atom. b) Ordered cluster K, with the structure of a tricapped trigonal prism with two elongated heights, Sn(3K)–Sn(2K) and Sn(8K)–Sn(6K). Thermal ellipsoids shown at 70 % probability level.

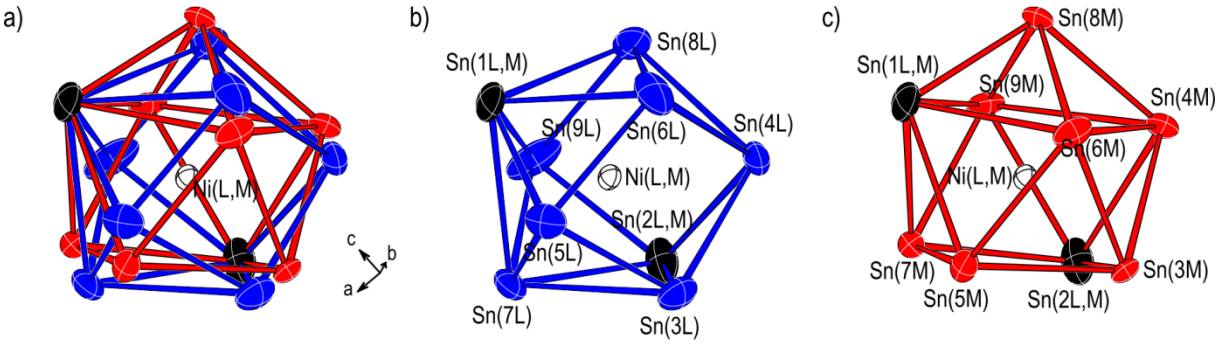

Figure 2. Split model (L, M) for one of the disordered clusters in $Na_{12}NiSn_{17}$. a) Both orientations overlayed. b) Orientation L (70 % occupancy). c) Orientation M (30 % occupancy). Thermal ellipsoids shown at 70 % probability level.

$Na_{12}NiSn_{17}$ represents a ternary derivative of the $A_{12}Tt_{17}$ phases, which feature empty $[Tt_9]^{4-}$ cages clusters and $[Tt_4]^{4-}$ anions.[8, 9, 13-15] As generally found for these compounds, the arrangement of the clusters can be described as a hierarchical replacement variant of a basic structure type. In case of $Na_{12}NiSn_{17}$, the $\{Ni@Sn_9\}$ clusters and twice as many $\{Sn_4\}$ tetrahedra are arranged in analogy to the Mg and Zn atoms, respectively, of the $MgZn_2$ hexagonal Laves phase structure (Figure 3). The central Ni atoms of the larger $\{Ni@Sn_9\}$ clusters occupy the nodes of a hexagonal diamond like network (orange in Figure 3). The smaller $\{Sn_4\}$ clusters are arranged alternately in 6.3.6.3. (Kagomé) nets and 3^6 nets (blue in Figure 3). The stacking sequence of the Kagomé nets is *AB*, the 3^6 nets are stacked primitive (*AA*), and this results in a net of face and vertex sharing supertetrahedra (blue in Figure 3b). Notably, no binary $A_{12}Tt_{17}$ phase with *A* = Na and *Tt* = Sn has yet been reported. Furthermore, the title phase is also the first *A*–Ni–Sn phase with one of the heavier alkali metals *A* = Na to Cs. ($LiNi_2Sn$ is known with *A* = Li.[16]) Recently, the $[Ni@Sn_9]^{4-}$ polyanion was obtained from solution via the extraction of a precursor that was obtained from a reaction of K, Ni and Sn in ratio K:Ni:Sn = 4:3:9.[7] For that precursor only a powder pattern was reported which shows elemental Sn as the main phase and some unindexed reflections.

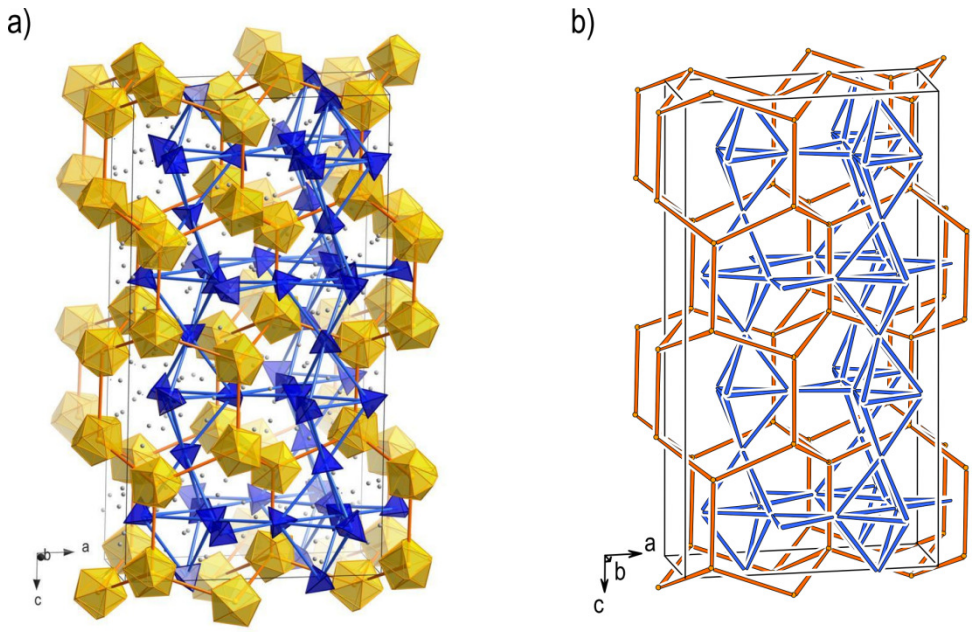

Figure 3. Representation of the crystal structure of $Na_{12}NiSn_{17}$. a) Arrangement of the $\{Ni@Sn_9\}$ clusters (orange) and $\{Sn_4\}$ clusters (blue). Na sites are shown as gray spheres. b) Schematic representation illustrating the relation to the $MgZn_2$ structure.

Conclusion

With the $[Ni@Sn_9]^{4-}$ cluster in $Na_{12}NiSn_{17}$, another intermetalloid *T*–*Tt* cluster has been characterized in a neat solid state compound. Together with the *A*–Cu–Sn phases with Cu–Sn cluster polyanions this shows that previously neglected ternary *A*–*T*–*Tt* systems with late d block metals *T* can bear a great potential for the synthesis of intermetalloid *T*–*Tt* cluster species.

Experimental Section

Synthesis. For the synthesis of the title compound, all materials were handled in argon atmosphere using and argon-filled glovebox and other standard inert gas techniques. Ni wire (99.98%, Alfa Aesar) and Sn granules (99.999 %, Chem Pur) were used as received, Na was purified by liquating.

First, a binary Ni–Sn precursor was pre-prepared from elemental Ni and Sn in ratio Ni:Sn = 1:2. For this, 0.744 g of Sn granules were melted together with 0.184 g of Ni wire in an arc furnace installed in an argon-filled glovebox. The regulus was turned upside down and melted four times to ensure homogenization. Then, 0.900 g of the as prepared Ni–Sn alloy and 0.070 g Na were sealed in a tantalum ampoule (overall ratio Na:Ni:Sn = 1:1:2). The ampoule was placed in a silica tube which was evacuated, sealed, and inserted in a vertical resistance tube furnace. The sample was heated to 880 °C at a rate of 2 K min^{-1}, held at this temperature for 48 hours, and then slowly cooled to room temperature at a rate of 0.1 K min^{-1}. An air-sensitive crystalline dark silver lustrous product was obtained from the reaction. The powder XRD pattern of the product shows that the title phase and Na_7Sn_{12} were obtained, and indicates the presence of elemental Ni.

Powder X-ray Diffraction. Powder XRD data were collected using a STOE STADI P powder diffractometer equipped with an imaging plate and a linear position sensitive detector (IP-PSD and L-PSD) using Cu $K_{\alpha1}$ radiation (λ = 1.54060 Å, curved Ge (111) monochromator). The STOE WINXPOW program package[17] was used for phase analysis.

Single Crystal X-ray Diffraction and Crystal Structure Determination. A single crystal of the title phase was selected in an argon-filled glovebox equipped with a microscope. The block shaped lustrous dark silver crystal was fixed on a glass fiber with perfluoropolyalkyl-ether and transferred (under argon) to an OXFORD Xcalibur 3 diffractometer system (Sapphire 3 CCD detector; Mo K_α radiation, λ = 0.71073 Å, graphite monochromator, sealed tube X-ray source), and positioned on the goniometer head in a 120 K cold nitrogen stream (OXFORD Instruments Cryojet cooling system). Before the full data collection, the crystal was first heated to 300 K and cooled again to 110 K. Data were then collected at 110 K with an exposure time of 90 seconds per frame, a frame width of 1°, and a detector distance of 50 mm. A total of 776 frames were collected in four ω scans (ω = −41° to 63°; κ = −79°; θ = 30°; φ = 0°, 90°, 180°, 270°) and one φ scan (φ = 0° to 360°; θ = 30°; ω = 0°; κ = 0°). The OXFORD CrysAlis RED software[18] was used for data processing, including an absorption correction with ABSPACK. The program XPREP[19] was used for space group determination

and data merging (identical indices only). The structure was solved in space group $P2_1/c$ (No. 14) with XS[20, 21] (direct methods). XL[20, 22] was used for structure refinement (full-matrix least-squares on F_o^2).

During the structure refinement several problems occurred. Some, but not all of them, could yet be satisfactorily resolved, and the structure model and the refinement results reported in this current version of the manuscript do not represent a final crystal structure determination for the title phase. In the following, these issues and the current state of the refinement are described. The most obvious problem is that two out of four crystallographically independent $\{Ni@Sn_9\}$ clusters are subject to disorder. For one of the disordered clusters a reasonable split model could be used (cluster L,M), for the other one (cluster N) this was not possible. At the current state of the refinement, this cluster is thus described with large thermal ellipsoids, and also the high residual electron density peaks are associated with this cluster. Note that such problems have been reported for many related compounds with empty and filled nine-vertex *Tt* clusters.[8] For one of the $\{Sn_4\}$ tetrahedra it was also necessary to introduce a split model (cluster H,I), but this case was unproblematic and the split model gives a reasonable description of two overlaying cluster orientations. The freely refined occupancy parameters for the Ni sites (0.93(1) to 0.95(1)) indicate that there are also some empty $\{Sn_9\}$ clusters in the structure. The location of the Na atoms is another issue. In the present structure model several partially occupied Na sites with freely refined occupancy factors are included (Na42 to Na56). Overall, the resulting Na content of the empirical formula $Na_{11.94(3)}Ni_{0.93(1)}Sn_{17}$ matches the ideal composition ($Na_{12}NiSn_{17}$) well. Note that the Ni content of the phase should not affect the Na content since Ni-filled $[Ni@Sn_9]^{4-}$ and empty $[Sn_9]^{4-}$ clusters have the same charge. Also the occupancy factors of pairs or groups of nearby partially occupied Na sites as well as nearby partially occupied Na and Sn sites are reasonable. For most of these partially occupied Na sites isotropic displacement parameters had to be used (except for Na42, Na46 and Na49), anisotropic displacement parameters were refined for the atoms on all other sites.

Further investigations will show whether these are intrinsic problems or more unequivocal results can be obtained with different data sets.

Selected crystallographic data and refinement details and results are given in Tables 1 and 2.

EDX Measurements. Qualitative EDX analyses were carried out using a JEOL 5900LV scanning electron microscope system operating at 20 kV which is equipped with an OXFORD INSTRUMENTS INCA energy dispersive X-ray microanalysis system. The measurement confirmed the presence of Na, Ni, and Sn and the absence of other elements heavier than Na.

Table 1. Selected crystallographic, data collection, and refinement data.

Empirical Formula	$\mathbf{Na_{11.94(3)}Ni_{0.93(1)}Sn_{17}}$
Formula weight, M / g mol^{-1}	2347.07
Space group	$P2_1/c$ (No. 14)
Z	16
Unit cell parameters	a = 23.734(1) Å b = 13.680(1) Å c = 44.620(2) Å β = 91.53(1)°
Unit cell volume, V / Å^3	14482(1)
Calculated density, ρ_{calc} / g cm^{-3}	4.31
Absorption coefficient (Mo K_α), μ / mm^{-1}	12.10
F(000)	16120
Crystal color, shape	dark silver lustrous, block
Max. crystal dimensions, mm	0.09, 0.06, 0.05
Temperature, T / K	110
Wavelength (Mo K_α), λ / Å	0.71073
Θ range	2.94 ° to 26.40°
Limiting indices	$-29 \le h \le 29$; $-17 \le k \le 17$; $-55 \le l \le 41$
Reflections / unique	101371 / 29617
Completeness	99.7 %
R_σ, R_{int}	0.165, 0.090
Refinement method	Full-matrix least-squares on F^2, with XL
Data / restraints / parameters	29617 / 0 / 1213
Residual map / e Å^{-3}	+7.156 and –7.619
Goodness-of-fit on F^2	0.821
R_1, wR_2 ($I > 2\sigma(I)$)	0.051, 0.089
R_1, wR_2 (all data)	0.119, 0.100

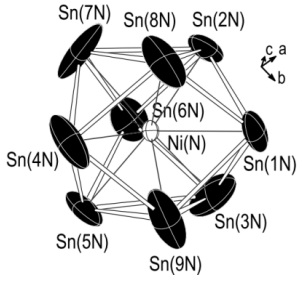

Figure 4. Disordered cluster N in $Na_{12}NiSn_{17}$. Thermal ellipsoids shown at 70 % probability level.

Table 2. Atomic coordinates, occupancy factors, and (equivalent) isotropic displacement parameters.

Cluster	Atom	Wyck.	Occ.≠1	*x*	*y*	*z*	U_{eq} / Å^2
J	Ni(J)	4*e*	0.94(1)	0.5910(1)	0.7426(2)	0.2831(1)	0.009(1)
K	Ni(K)	4*e*	0.93(1)	0.4097(1)	0.2465(2)	0.5345(1)	0.011(1)
L,M	Ni(L)	4*e*	0.93(1)	0.0917(1)	0.2637(2)	0.2855(1)	0.013(1)
N	Ni(N)	4*e*	0.93(1)	0.0843(1)	0.2598(2)	0.4702(1)	0.015(1)
A	Sn(1A)	4*e*		0.4433(1)	0.8026(1)	0.0926(1)	0.021(1)
	Sn(2A)	4*e*		0.5447(1)	0.1180(1)	0.3727(1)	0.023(1)
	Sn(3A)	4*e*		0.3523(1)	0.7355(1)	0.1330(1)	0.027(1)
	Sn(4A)	4*e*		0.4610(1)	0.8096(1)	0.1579(1)	0.022(1)
B	Sn(1B)	4*e*		0.1877(1)	0.0438(1)	0.0919(1)	0.028(1)
	Sn(2B)	4*e*		0.2221(1)	0.9638(1)	0.1513(1)	0.027(1)
	Sn(3B)	4*e*		0.1202(1)	0.0888(1)	0.1449(1)	0.024(1)
	Sn(4B)	4*e*		0.1201(1)	0.8928(1)	0.1195(1)	0.046(1)
C	Sn(1C)	4*e*		0.9901(1)	0.2352(1)	0.1126(1)	0.023(1)
	Sn(2C)	4*e*		0.1174(1)	0.8420(1)	0.3988(1)	0.020(1)
	Sn(3C)	4*e*		0.1181(1)	0.6378(1)	0.3770(1)	0.032(1)
	Sn(4C)	4*e*		0.0798(1)	0.7969(1)	0.3371(1)	0.029(1)
D	Sn(1D)	4*e*		0.3021(1)	0.6995(1)	0.2285(1)	0.024(1)
	Sn(2D)	4*e*		0.2368(1)	0.8815(1)	0.2323(1)	0.019(1)
	Sn(3D)	4*e*		0.2606(1)	0.7651(1)	0.2871(1)	0.016(1)
	Sn(4D)	4*e*		0.1826(1)	0.6864(1)	0.2394(1)	0.021(1)
E	Sn(1E)	4*e*		0.3869(1)	0.4606(1)	0.3456(1)	0.017(1)
	Sn(2E)	4*e*		0.2766(1)	0.5537(1)	0.3577(1)	0.019(1)
	Sn(3E)	4*e*		0.3224(1)	0.3992(1)	0.3980(1)	0.018(1)
	Sn(4E)	4*e*		0.3755(1)	0.5918(1)	0.3979(1)	0.020(1)
F	Sn(1F)	4*e*		0.3529(1)	0.9136(1)	0.3508(1)	0.019(1)
	Sn(2F)	4*e*		0.3071(1)	0.1088(1)	0.3595(1)	0.019(1)
	Sn(3F)	4*e*		0.3972(1)	0.0365(1)	0.4007(1)	0.019(1)
	Sn(4F)	4*e*		0.2825(1)	0.9551(1)	0.4033(1)	0.019(1)
G	Sn(1G)	4*e*		0.3144(1)	0.7577(1)	0.4784(1)	0.028(1)
	Sn(2G)	4*e*		0.2379(1)	0.8504(1)	0.5199(1)	0.051(1)
	Sn(3G)	4*e*		0.1974(1)	0.6870(1)	0.4827(1)	0.044(1)
	Sn(4G)	4*e*		0.2789(1)	0.6475(1)	0.5310(1)	0.036(1)
H,I	Sn(1H)	4*e*	0.759(2)	0.1027(1)	0.4703(2)	0.0943(1)	0.017(1)
	Sn(2H)	4*e*	0.759(2)	0.1981(1)	0.6027(1)	0.1048(1)	0.021(1)
	Sn(3H)	4*e*	0.759(2)	0.2037(1)	0.4015(1)	0.1278(1)	0.018(1)
	Sn(4H)	4*e*	0.759(2)	0.1279(1)	0.5443(2)	0.1560(1)	0.018(1)
	Sn(1I)	4*e*	0.241(2)	0.1284(2)	0.3870(4)	0.1535(1)	0.020(1)
	Sn(2I)	4*e*	0.241(2)	0.2241(2)	0.4884(4)	0.1282(1)	0.019(1)
	Sn(3I)	4*e*	0.241(2)	0.1318(2)	0.6017(5)	0.1557(1)	0.017(1)
	Sn(4I)	4*e*	0.241(2)	0.1136(4)	0.5097(5)	0.0961(2)	0.018(2)
J	Sn(1J)	4*e*		0.6198(1)	0.6225(1)	0.3307(1)	0.023(1)
	Sn(2J)	4*e*		0.5050(1)	0.6918(1)	0.3135(1)	0.026(1)
	Sn(3J)	4*e*		0.6194(1)	0.8393(1)	0.3308(1)	0.024(1)
	Sn(4J)	4*e*		0.6981(1)	0.7111(1)	0.2848(1)	0.024(1)
	Sn(5J)	4*e*		0.5956(1)	0.5630(1)	0.2665(1)	0.026(1)
	Sn(6J)	4*e*		0.5050(1)	0.7103(1)	0.2459(1)	0.026(1)

	Sn(7J)	4*e*		0.5216(1)	0.8919(1)	0.2858(1)	0.018(1)
	Sn(8J)	4*e*		0.6434(1)	0.9060(1)	0.2684(1)	0.026(1)
	Sn(9J)	4*e*		0.6274(1)	0.7350(1)	0.2274(1)	0.026(1)
K	Sn(1K)	4*e*		0.5020(1)	0.1354(1)	0.5258(1)	0.033(1)
	Sn(2K)	4*e*		0.4287(1)	0.2241(1)	0.4776(1)	0.031(1)
	Sn(3K)	4*e*		0.3882(1)	0.0658(1)	0.5466(1)	0.035(1)
	Sn(4K)	4*e*		0.4597(1)	0.2175(1)	0.5853(1)	0.027(1)
	Sn(5K)	4*e*		0.4972(1)	0.3550(1)	0.5278(1)	0.035(1)
	Sn(6K)	4*e*		0.3715(1)	0.3937(1)	0.5040(1)	0.037(1)
	Sn(7K)	4*e*		0.3136(1)	0.1971(1)	0.5063(1)	0.022(1)
	Sn(8K)	4*e*		0.3284(1)	0.2345(1)	0.5734(1)	0.039(1)
	Sn(9K)	4*e*		0.4060(1)	0.4074(1)	0.5689(1)	0.032(1)
N	Sn(1N)	4*e*		0.1782(1)	0.3652(1)	0.4635(1)	0.060(1)
	Sn(2N)	4*e*		0.1503(1)	0.2428(1)	0.5166(1)	0.046(1)
	Sn(3N)	4*e*		0.0678(1)	0.4397(1)	0.4864(1)	0.086(1)
	Sn(4N)	4*e*		0.0524(1)	0.1438(2)	0.4260(1)	0.076(1)
	Sn(5N)	4*e*		0.9784(1)	0.2930(1)	0.4575(1)	0.057(1)
	Sn(6N)	4*e*		0.0257(1)	0.2710(1)	0.5195(1)	0.057(1)
	Sn(7N)	4*e*		0.0692(1)	0.0859(1)	0.4909(1)	0.100(1)
	Sn(8N)	4*e*		0.1683(1)	0.1528(2)	0.4536(1)	0.081(1)
	Sn(9N)	4*e*		0.0754(1)	0.3592(2)	0.4219(1)	0.156(2)
L,M	Sn(1L,M)	4*e*		0.1334(1)	0.3075(1)	0.3372(1)	0.049(1)
	Sn(2L.M)	4*e*		0.0687(1)	0.1078(1)	0.2531(1)	0.033(1)
	Sn(3L)	4*e*	0.697(3)	0.0912(2)	0.3073(4)	0.2291(1)	0.016(1)
	Sn(3M)	4*e*	0.303(2)	0.1214(1)	0.3018(2)	0.2307(1)	0.030(1)
	Sn(4L)	4*e*	0.697(3)	1.0002(1)	0.2930(2)	0.2524(1)	0.028(1)
	Sn(4M)	4*e*	0.303(2)	0.9862(3)	0.2827(5)	0.2653(1)	0.026(2)
	Sn(5L)	4*e*	0.697(3)	0.1820(1)	0.3878(2)	0.2827(1)	0.027(1)
	Sn(5M)	4*e*	0.303(2)	0.1910(2)	0.3321(4)	0.2708(1)	0.024(1)
	Sn(6L)	4*e*	0.697(3)	0.0614(1)	0.4405(2)	0.2920(1)	0.038(1)
	Sn(6M)	4*e*	0.303(2)	0.0835(2)	0.4538(4)	0.2785(1)	0.024(1)
	Sn(7L)	4*e*	0.697(3)	0.1866(1)	0.1692(1)	0.2821(1)	0.025(1)
	Sn(7M)	4*e*	0.303(2)	0.1661(2)	0.1353(3)	0.2995(1)	0.022(1)
	Sn(8L)	4*e*	0.697(3)	0.0073(1)	0.2652(2)	0.3209(1)	0.045(1)
	Sn(8M)	4*e*	0.303(2)	0.0201(2)	0.3530(3)	0.3271(1)	0.017(1)
	Sn(9L)	4*e*	0.697(3)	0.0896(1)	0.1002(2)	0.3179(1)	0.040(1)
	Sn(9M)	4*e*	0.303(2)	0.0486(2)	0.1424(3)	0.3235(1)	0.021(1)
	Na(1)	4*e*		0.5068(3)	0.0875(5)	0.4399(1)	0.031(2)
	Na(2)	4*e*		0.3410(3)	0.8958(5)	0.1864(1)	0.022(2)
	Na(3)	4*e*		0.2244(4)	0.7270(6)	0.1654(2)	0.061(3)
	Na(4)	4*e*		0.3949(3)	0.8053(5)	0.4204(1)	0.024(2)
	Na(5)	4*e*		0.1620(3)	0.6157(5)	0.3105(1)	0.029(2)
	Na(6)	4*e*		0.3725(3)	0.6967(5)	0.3331(1)	0.025(2)
	Na(7)	4*e*		0.1201(3)	0.2455(6)	0.0873(2)	0.043(2)
	Na(8)	4*e*		0.2830(3)	0.3122(5)	0.3307(1)	0.030(2)
	Na(9)	4*e*		0.1919(3)	0.9179(5)	0.4558(1)	0.034(2)
	Na(10)	4*e*		0.1864(3)	0.0940(6)	0.2109(2)	0.044(2)
	Na(11)	4*e*		0.2996(3)	0.1946(5)	0.4302(1)	0.027(2)
	Na(12)	4*e*		0.1857(3)	0.4355(6)	0.3920(2)	0.039(2)

Na(13)	4*e*		0.1253(3)	0.8827(5)	0.2757(1)	0.034(2)
Na(14)	4*e*		0.2964(3)	0.5321(5)	0.2836(1)	0.027(2)
Na(15)	4*e*		0.9134(3)	0.1522(6)	0.0530(2)	0.044(2)
Na(16)	4*e*		0.2446(3)	0.7137(5)	0.4112(2)	0.032(2)
Na(17)	4*e*		0.2948(3)	0.5264(5)	0.4588(1)	0.034(2)
Na(18)	4*e*		0.4085(3)	0.6158(5)	0.1962(1)	0.025(2)
Na(19)	4*e*		0.9883(3)	0.4124(6)	0.0599(2)	0.042(2)
Na(20)	4*e*		0.0633(3)	0.5615(8)	0.2191(2)	0.068(3)
Na(21)	4*e*		0.4902(3)	0.9024(5)	0.3609(1)	0.024(2)
Na(22)	4*e*		0.5302(3)	0.9404(5)	0.2108(1)	0.033(2)
Na(23)	4*e*		0.2539(3)	0.1983(7)	0.1368(2)	0.059(3)
Na(24)	4*e*		0.2232(3)	0.4365(5)	0.0518(2)	0.036(2)
Na(25)	4*e*		0.0582(4)	0.7002(6)	0.1143(2)	0.058(3)
Na(26)	4*e*		0.4908(3)	0.0307(5)	0.1269(1)	0.025(2)
Na(27)	4*e*		0.9894(3)	0.4788(6)	0.1348(2)	0.044(2)
Na(28)	4*e*		0.5906(3)	0.3718(6)	0.4769(1)	0.039(2)
Na(29)	4*e*		0.2888(3)	0.0216(5)	0.2883(1)	0.027(2)
Na(30)	4*e*		0.4255(3)	0.2588(5)	0.3822(2)	0.032(2)
Na(31)	4*e*		0.2271(3)	0.4684(5)	0.2032(1)	0.034(2)
Na(32)	4*e*		0.4450(3)	0.4398(5)	0.4414(1)	0.032(2)
Na(33)	4*e*		0.3548(3)	0.9827(5)	0.4754(2)	0.041(2)
Na(34)	4*e*		0.6566(4)	0.1671(5)	0.4378(2)	0.062(3)
Na(35)	4*e*		0.1682(3)	0.0824(6)	0.3794(2)	0.049(2)
Na(36)	4*e*		0.3885(3)	0.8403(5)	0.2655(2)	0.032(2)
Na(37)	4*e*		0.1049(4)	0.8948(8)	0.5308(2)	0.074(3)
Na(38)	4*e*		0.1127(4)	0.8689(9)	0.1930(2)	0.086(4)
Na(39)	4*e*		0.2163(3)	0.8436(8)	0.3479(2)	0.070(3)
Na(40)	4*e*		0.4358(3)	0.1011(6)	0.3232(2)	0.039(2)
Na(41)	4*e*		0.6654(4)	0.9902(5)	0.3800(2)	0.050(2)
Na(42)	4*e*	0.80(2)	0.0904(4)	0.3163(6)	0.1590(2)	0.034(4)
Na(43)	4*e*	0.24(2)	1.0387(13)	0.2230(20)	0.1796(6)	0.037(13)
Na(44)	4*e*	0.33(4)	1.0061(10)	0.0960(20)	0.1798(6)	0.037(11)
Na(45)	4*e*	0.43(4)	1.0036(6)	0.1437(16)	0.1904(4)	0.022(7)
Na(46)	4*e*	0.69(3)	−0.0153(5)	0.9780(9)	0.1351(2)	0.052(5)
Na(47)	4*e*	0.30(2)	0.0085(9)	0.9983(15)	0.1025(4)	0.022(9)
Na(48)	4*e*	0.65(3)	0.9480(6)	0.0305(11)	0.9339(3)	0.069(7)
Na(49)	4*e*	0.58(3)	0.8628(5)	0.0903(10)	0.9638(3)	0.047(6)
Na(50)	4*e*	0.55(4)	0.2517(7)	0.0969(12)	0.0321(3)	0.024(6)
Na(51)	4*e*	0.37(4)	0.2292(13)	0.0600(20)	0.0274(5)	0.038(10)
Na(52)	4*e*	0.26(2)	0.2121(12)	0.7030(20)	0.0918(6)	0.037(12)
Na(53)	4*e*	0.32(2)	0.8299(8)	0.1920(14)	0.9370(4)	0.017(7)
Na(54)	4*e*	0.32(2)	0.2324(7)	0.8067(13)	0.0922(4)	0.014(7)
Na(55)	4*e*	0.44(4)	0.3308(10)	0.9670(20)	0.1067(5)	0.033(8)
Na(56)	4*e*	0.49(4)	0.3155(7)	0.9308(14)	0.0993(3)	0.013(6)

U_{eq} is defined as one third of the trace of the orthogonalized U_{ij} tensor.

References

[1] T. F. Fässler, S. D. Hoffmann, *Angew. Chem. Int. Ed.* **2004**, *43*, 6242; *Angew. Chem.* **2004**, *116*, 6400.

[2] J. D. Corbett, *Angew. Chem. Int. Ed.* **2000**, *39*, 670; *Angew. Chem.* **2000**, *112*, 682.

[3] S. C. Sevov, J. M. Goicoechea, *Organometallics* **2006**, *25*, 5678.

[4] S. Stegmaier, T. F. Fässler, *J. Am. Chem. Soc.* **2011**, *133*, 19758.

[5] S. Stegmaier, T. F. Fässler, *Angew. Chem. Int. Ed.* **2012**, *51*, 2647; *Angew. Chem.* **2012**, *124*, 2701.

[6] V. Hlukhyy, H. He, L.-A. Jantke, T. F. Fässler, *Chem. Eur. J.* **2012**, *18*, 12000.

[7] M. M. Gillett-Kunnath, J. I. Paik, S. M. Jensen, J. D. Taylor, S. C. Sevov, *Inorg. Chem.* **2011**, *50*, 11695.

[8] S. Scharfe, F. Kraus, S. Stegmaier, A. Schier, T. F. Fässler, *Angew. Chem. Int. Ed.* **2011**, *50*, 3630; *Angew. Chem.* **2011**, *123*, 3712.

[9] C. Hoch, M. Wendorff, C. Röhr, *J. Alloy. Compd.* **2003**, *361*, 206.

[10] T. F. Fässler, *Coord. Chem. Rev.* **2001**, *215*, 347.

[11] M. K. Bhargava, K. Schubert, *J. Less. Common Met.* **1973**, *33*, 181.

[12] C. Hoch, M. Wendorff, C. Röhr, *Acta Cryst. C* **2002**, *58*, i45.

[13] H. G. von Schnering, M. Baitinger, U. Bolle, W. Carrillo-Cabrera, J. Curda, Y. Grin, F. Heinemann, J. Llanos, K. Peters, A. Schmeding, M. Somer, *Z. Anorg. Allg. Chem.* **1997**, *623*, 1037.

[14] V. Quéneau, E. Todorov, S. C. Sevov, *J. Am. Chem. Soc.* **1998**, *120*, 3263.

[15] W. Carrillo-Cabrera, R. Cardoso Gil, M. Somer, Ö. Persil, H. G. von Schnering, *Z. Anorg. Allgem. Chem.* **2003**, *629*, 601.

[16] A. Mewis, H.-U. Schuster, *Z. Naturforsch. B* **1971**, *26*, 62.

[17] *WinXPOW (Version 2.08)*, STOE & Cie GmbH, Darmstadt, **2003**.

[18] *CrysAlis RED (Version 1.171.33.34d)*, Oxford Diffraction Ltd., **2009**.

[19] *XPREP (Version 6.14)*, Bruker Nonius, **2003**.

[20] G. Sheldrick, *Acta Cryst. A* **2008**, *64*, 112.

[21] *XS - Crystal Structure Solution - SHELXTL (Version 6.12)*, Bruker AXS, **2001**.

[22] *XL - Crystal Structure Refinement - SHELXTL (Version 6.12)*, Bruker AXS, **2001**.

6.8 The Soluble Zintl Phases $A_{14}ZnGe_{16}$ (A = K, Rb) Featuring $[(\eta^3\text{-}Ge_4)Zn(\eta^2\text{-}Ge_4)]^{6-}$ and $[Ge_4]^{4-}$ Clusters and the Isolation of $[(MesCu)_2(\eta^3,\eta^3\text{-}Ge_4)]^{4-}$ – the Missing Link in the Solution Chemistry of Tetrahedral Group 14 Element Zintl Clusters

S. Stegmaier,[‡] M. Waibel,[‡] A. Henze, L.-A. Jantke, A. J. Karttunen, T. F. Fässler, *J. Am. Chem. Soc.* **2012**, *134*, 14450.

[‡] These authors contributed equally.

6.9 Lithium-Stuffed Diamond Polytype Zn–*Tt* Structures (*Tt* = Sn, Ge): The Two Lithium-Zinc-Tetrelides $Li_3Zn_2Sn_4$ and Li_2ZnGe_3

S. Stegmaier, T. F. Fässler,
Inorg. Chem., http://dx.doi.org/10.1021/ic3011037.

6.10 The Intermetallic Type-I Clathrate $Na_8Zn_4Ge_{42}$

Saskia Stegmaier, Thomas F. Fässler,

manuscript for publication

Abstract

The new intermetallic type-I clathrate $Na_8Zn_4Ge_{42}$ was obtained by direct reactions of the elements and its crystal structure was determined by means of single crystal X-ray diffraction methods. The structure is described in space group *Pm*-3*n* (No. 223) with $a = 10.698(1)$ Å. Zn/Ge mixed occupancy is found for one network site (6*c*). $Na_8Zn_4Ge_{42}$ represents an electron precise Zintl phase with Na cations encaged in the cavities of a polyanionic host network of four-connected Zn and Ge atoms.

Introduction

Clathrates owe their name to host frameworks featuring cavities in which guests can be encaged. Among the representatives of host-guest systems with clathrate type structures there are such different materials as gas hydrates, clathrasils/zeolites, and intermetallic clathrates. The most common clathrate host structures, namely the type-I (*cP*46) and type-II (*cF*136), represent four-connected networks. Generally, networks with covalent bonds between tetrahedrally connected atoms are native to the structural chemistry of the group 14 elements C, Si, Ge, and Sn. The suitability of empty clathrate networks as structures of (metastable) allotropes of group 14 elements is substantiated by the (almost) guest free type-II clathrates Na_xSi_{136} ($x < 1$)[1, 2] and $\square_{24}Ge_{136}$[3, 4] (□: vacant position). In the case of the so-called "intermetallic" or "semiconducting" clathrates of Si, Ge, and Sn, the cavities are occupied by electropositive alkali metal (*A*), alkaline earth metal (*Ae*), or rare earth metal atoms. The phases are described as polar intermetallics or electron precise Zintl compounds with cations in the cages of a polyanionic framework structure. A formally charge balanced situation with a framework structure in accord with the 8–*N* rule can be reached either via vacancies or via

the partial substitution of group 14 (*Tt*: tetrel element) atoms by electron poorer group 13 (*Tr*: triel element) or late d block metal (*T*) atoms on network sites. Note that one vacancy is associated with four (3b-Tt^-) atoms on the neighboring positions (3b: three-bonded). Among the type-I clathrates, for example, binary $A_8Tt_{44}\square_2$ and $Ae_8Tt_{42}\square_4$ as well as ternary $A_8Tr_8Tt_{38}$ and $Ae_8Tr_{16}Tt_{30}$ are thus electron precise Zintl phases. The current interest in such intermetallic clathrates is mainly due to the promising thermoelectric properties of some representatives, e.g. for $Ba_8Ga_{16}Ge_{30}$ considerably high *ZT* (figure of merit) values have been reported.[5, 6] A conceptual approach to understand the potential of the intermetallic clathrates as thermoelectric materials is provided by the PGEC (phonon-glass and electron-crystal) concept.[7]

In this context, and in view of other four-connected network structures that have been found for Sn-rich ternary Na–Zn–Sn phases,[8, 9] we investigated the Ge-rich side of the Na–Zn–Ge system. Known type-I clathrates of Ge or Sn with alkali metal atoms as guests and group 12 element atoms (*T* = Zn, Cd, or Hg) on framework sites include $K_8Zn_xGe_{46-x}$,[10] $A_8Zn_xSn_{46-x}$ with *A* = Rb[11] and Cs,[11, 12] $Cs_8Cd_xSn_{46-x}$,[13] $A_8Hg_xGe_{46-x}$ with *A* = K and Rb,[14] as well as $A_8Hg_xSn_{46-x}$ with *A* = K, Rb and Cs.[15] Generally, these phases are described as electron precise Zintl compounds with the ideal composition $A_8T_4Tt_{42}$, with the exception of the Hg-substituted Ge clathrates which are reported to have an (approximate) composition of $A_8Hg_3Ge_{43}$. Another type-I clathrate with *Tt* = Ge and *T* = Zn (besides $K_8Zn_xGe_{46-x}$[10] mentioned above) is $Ba_8Zn_8Ge_{38}$.[16] With *A* = Na and *Tt* = Ge, $Na_8Tr_xGe_{46-x}$ phases with *Tr* = Al and Ga are known.[17] Notably, a binary $A_8Ge_{46-y}\square_y$ phase with *A* = Na has not been reported, and generally Na is considered not to fit well in the larger cages of a Ge type-I clathrate host framework.[18] Herein we present the new type-I clathrate $Na_8Zn_4Ge_{42}$.

Experimental Section

Synthesis. For the synthesis of the title compound, all materials were handled in argon atmosphere using an argon-filled glovebox and other standard inert gas techniques. Ge pieces (99.999 %, ChemPur) and Zn granules (Merck) were used as received, Na was purified by liquating. To apply defined temperature programs to samples sealed in niobium or tantalum ampoules, the ampoules were placed in silica tubes which were evacuated, sealed, and inserted in vertical resistance tube furnaces.

$Na_8Zn_4Ge_{42}$ was first obtained by a direct reaction of the elements in ratio Na:Zn:Ge = 2:1:5. 0.078 g of Na, 0.110 g of Zn, and 0.612 g of Ge were sealed in a tantalum ampoule. The sample was heated to 650 °C, held at this temperature for two days, then the oven was turned off, and the sample was removed from the oven after it had cooled to room temperature. Powder XRD analysis of the product of this reaction showed the presence of the type-I clathrate $Na_8Zn_4Ge_{42}$, α-Ge, and some unindexed reflections. The latter were not observed in the powder XRD pattern of a sample that was exposed to air and are thus attributed to at least one unidentified air sensitive phase. $Na_8Zn_4Ge_{42}$ is stable in air. After the characterization of $Na_8Zn_4Ge_{42}$ by means of single crystal XRD structure analysis, the title phase was also synthesized using stoichiometric amounts of the elements. However, no pure phase samples were obtained. For example, the product of a reaction for which 0.053 g of Na, 0.075 g of Zn, and 0.873 g of Ge were used, and a temperature program analogous to that described above but with isothermal dwelling for six days was employed, contained $Na_8Zn_4Ge_{42}$ as the main phase but also the air sensitive impurity mentioned above.

Powder X-ray Diffraction. For powder XRD analysis of the reaction products, samples were finely ground, optionally diluted with diamond powder, and sealed in glass capillaries in an argon-filled glovebox. To test the air stability of the reaction products, samples were exposed to air and measured in transmission mode. Powder XRD data were collected with a STOE STADI P powder diffractometer equipped with an imaging plate and a linear position sensitive detector (IP-PSD, and L-PSD) using Cu $K_{\alpha 1}$ radiation (λ = 1.54060 Å, curved Ge (111) monochromator). The STOE WINXPOW program package[19] was used for phase analysis.

Single Crystal X-ray Diffraction and Crystal Structure Determination. Block shaped dark silver lustrous crystals of $Na_8Zn_4Ge_{42}$ were selected under normal atmosphere using a microscope. A suitable single crystal was fixed on a glass fiber and mounted on the

goniometer head of a BRUKER APEX II diffractometer system (KAPPA goniometer, APEX II CCD detector). Single crystal XRD data were collected at 293 K using Mo K_α radiation ($\lambda = 0.71073$ Å, graphite monochromator, rotating anode source). The BRUKER SAINT software was used for data processing, including an absorption correction with SADABS. XPREP[20] was used for space group determination, XS[21, 22] for structure solution (direct methods) and XL[21, 23] for structure refinement (full-matrix least-squares on F_o^2). The structure was solved in space group *Pm*-3*n* (No. 223). Selected crystallographic data and refinement details are given in Tables 1, 2, and 3. Refinement cycles with a free variable for the occupancy parameter of the Na1 (2*a*) and Na2 (6*d*) site, respectively, showed that both are fully occupied. Zn/Ge mixed occupancy was tested in separate refinement cycles for all three network sites (6*c*, 16*i*, 24*k*). This showed that Zn only occupies the 6*c* site. The free refinement of the occupancy parameters for Zn and Ge on this site with the sum fixed to 1 led to an occupancy parameter of 0.31(5) for Ge. This result is close to the ideal Zn:Ge ratio of 2/3:1/3 for the 6*c* site which relates to the Zintl phase composition $Na_8Zn_4Ge_{42}$. In the final refinement steps the ratio was thus fixed to this ideal value. The same Zn:Ge ratio was determined from full single crystal XRD structure analyses using crystals of $Na_8Zn_4Ge_{42}$ that were obtained from reactions of the elements in different ratios.

EDX Measurements. EDX analyses of single crystals of $Na_8Zn_4Ge_{42}$ (unit cell determined by single crystal XRD previous to EDX analysis) were carried out using a JEOL 5900LV scanning electron microscope equipped with an OXFORD INSTRUMENTS INCA energy dispersive X-ray microanalysis system. The qualitative analysis showed the presence of Na, Zn, and Ge, and the absence of other elements heavier than Na.

Table 1. Selected crystallographic, data collection, and refinement data for $Na_8Zn_4Ge_{42}$.

Formula	**$Na_8Zn_4Ge_{42}$**
Formula weight, M / g mol^{-1}	3494.18
Space group	*Pm*-3*n* (No. 223)
Z	1
Unit cell parameter, a / Å	10.698(1)
Unit cell volume, V / Å^3	1224.4(1)
Calculated density, ρ_{calc} / g cm^{-3}	4.739
Absorption coefficient (Mo K_α), μ / mm^{-1}	27.30
F(000)	1552
Crystal colour, shape	dark silver lustrous, block
Temperature, T / K	293
Wavelength (Mo K_α), λ / Å	0.71073
Θ range	2.69° to 31.40°
Limiting indices	$-15 \le h \le 15$; $-15 \le k \le 15$; $-15 \le l \le 14$
Reflections / unique	12469 / 395
Completeness	100 %
R_σ, R_{int}	0.009, 0.030
Data / restraints / parameters	395 / 1 / 17
Extinction coefficient	0.0020(1)
Residual map / e Å^{-3}	+0.691 and −0.621
Goodness-of-fit on F^2	1.29
R_1, wR_2 ($I > 2\sigma(I)$)	0.011 / 0.025
R_1, wR_2 (all data)	0.011 / 0.025

Table 2. Atomic coordinates and equivalent isotropic displacement parameters for $Na_8Zn_4Ge_{42}$.

$Na_8Zn_4Ge_{42}$						
Atom	Wyck.	Occ.	*x*	*y*	*z*	U_{eq} / Å^2
Zn/Ge1	6*c*	2/3:1/3 [a)]	1/2	1/4	0	0.0114(1)
Ge2	16*i*		0.18299(1)	*x*	*x*	0.01002(8)
Ge3	24*k*		0	0.30920(2)	0.11683(2)	0.01049(8)
Na1	2*a*		0	0	0	0.0348(9)
Na2	6*d*		1/4	1/2	0	0.142(3)

U_{eq} is defined as one third of the trace of the orthogonalized U_{ij} tensor.

[a)] Occupancy factors fixed in final refinement steps, see Experimental Section.

Table 3. Anisotropic displacement parameters (U_{ij} / Å^2) for $Na_8Zn_4Ge_{42}$.

$Na_8Zn_4Ge_{42}$						
Atom	U_{11}	U_{22}	U_{33}	U_{23}	U_{13}	U_{12}
Zn/Ge1	0.0129(2)	0.0106(1)	U_{22}	0	0	0
Ge2	0.01002(8)	U_{11}	U_{11}	−0.00049(5)	U_{23}	U_{23}
Ge3	0.0108(1)	0.0111(1)	0.0096(1)	−0.00057(7)	0	0
Na1	0.0348(9)	U_{11}	U_{11}	0	0	0
Na2	0.098(5)	0.163(4)	U_{22}	0	0	0

Results and Discussion

$Na_8Zn_4Ge_{42}$ adds to the group of ternary $A_8T_xTt_{46-x}$ intermetallic typ-I clathrates (space group *Pm*-3*n*, No. 223) of the tetrel elements (*Tt*) Ge and Sn with group 12 element atoms (*T*) in the framework and alkali metal atoms (*A*) as guests (cf. Introduction). As such, the title phase shows a host framework structure of tetrahedrally four-bonded atoms on 6*c* (Zn/Ge1), 16*i* (Ge2), and 24*k* (Ge3) sites which features two types of cavities. The corresponding two guest sites (2*a* and 6*d*) in the cage centers are arranged in style of an A15 (Cr_3Si) type structure (cf. Figure 1b). The coordination polyhedra of the Na atoms, i.e. the cages, are pentagonal dodecahedra and tetrakaidecahedra for Na1 (on 2*a*) and Na2 (on 6*d*), respectively. The 20 vertices of a pentagonal dodecahedron (with twelve pentagonal faces) comprise eight Ge2 (16*i*) and twelve Ge3 (24*k*) positions, and a 24-vertex tetrakaidecahedron with twelve pentagonal and two hexagonal faces is built of four Zn/Ge1 (6*c*), eight Ge2 (16*i*) and twelve Ge3 (24*k*) positions (see Figure 2). The type-I clathrate structure can be described as a space filling arrangement of these polyhedra as shown in Figure 1a. Separate drawings of the arrangement of tetrakaidecahedra and pentagonal dodecahedra are depicted in Figure 1c and 1d, respectively. Columns of tetrakaidecahedra are aligned in style of a rod packing as schematically shown in Figure 1b (connecting lines between Na2 positions) and the pentagonal dodecahedra take the remaining space, thereby forming a bcc (body centered cubic) like array, see Figure 1d and Figure 1b (Na1 positions). A tetrakaidecahedron shares its two hexagonal faces with adjacent tetrakaidecahedra of the same column, eight pentagonal faces with other tetrakaidecahedra of columns that run perpendicularly, and four pentagonal faces with pentagonal dodecahedra.

The displacement parameters for the network atoms of $Na_8Zn_4Ge_{42}$ are small (see Table 3 and Figure 2), as it is generally observed for the intermetallic clathrates and typical for rigid frameworks of covalently bonded atoms. In contrast, the large displacement parameters for the Na atoms stand out, especially for Na2 (on 6*d*) in the larger cages (see also Table 3 and Figure 2). The displacement parameters of the guest atoms in intermetallic clathrates are associated with their “rattling” in the cages, and the differences between the parameters for the atoms in the 20- and 24-vertex cages is also a common feature of the type-I clathrates. For $Na_8Zn_4Ge_{42}$ the ratio of U_{eq}(Na2):U_{eq}(Na1) is approx. 4.1, comparable, for example, to the findings for the K atoms in $K_8Hg_4Sn_{42}$.[15] In series of $A_8T_xTt_{46-x}$ phases with same *T* and *Tt* but different *A* atoms, the phases with larger alkali metals generally show smaller displacement parameters of the *A* atoms, and also smaller differences between the parameters

for *A*1 and *A*2.[14, 15] Another characteristic concerning the displacement parameters is the isotropic behavior of Na1 (2*a*) in the pentagonal dodecahedra, in contrast to the pronounced anisotropy that is found for Na2 (6*d*) in the tetrakaidecahedra. This relates to the different shapes of the polyhedra (cf. Figure 2 and Na–Ge and Na–Zn/Ge interatomic distances given in Table 4). For $Na_8Zn_4Ge_{42}$ the ratio U_{22}(Na2):U_{11}(Na2) is approx. 1.7, again similar to the corresponding ratio for related phases.[14, 15]

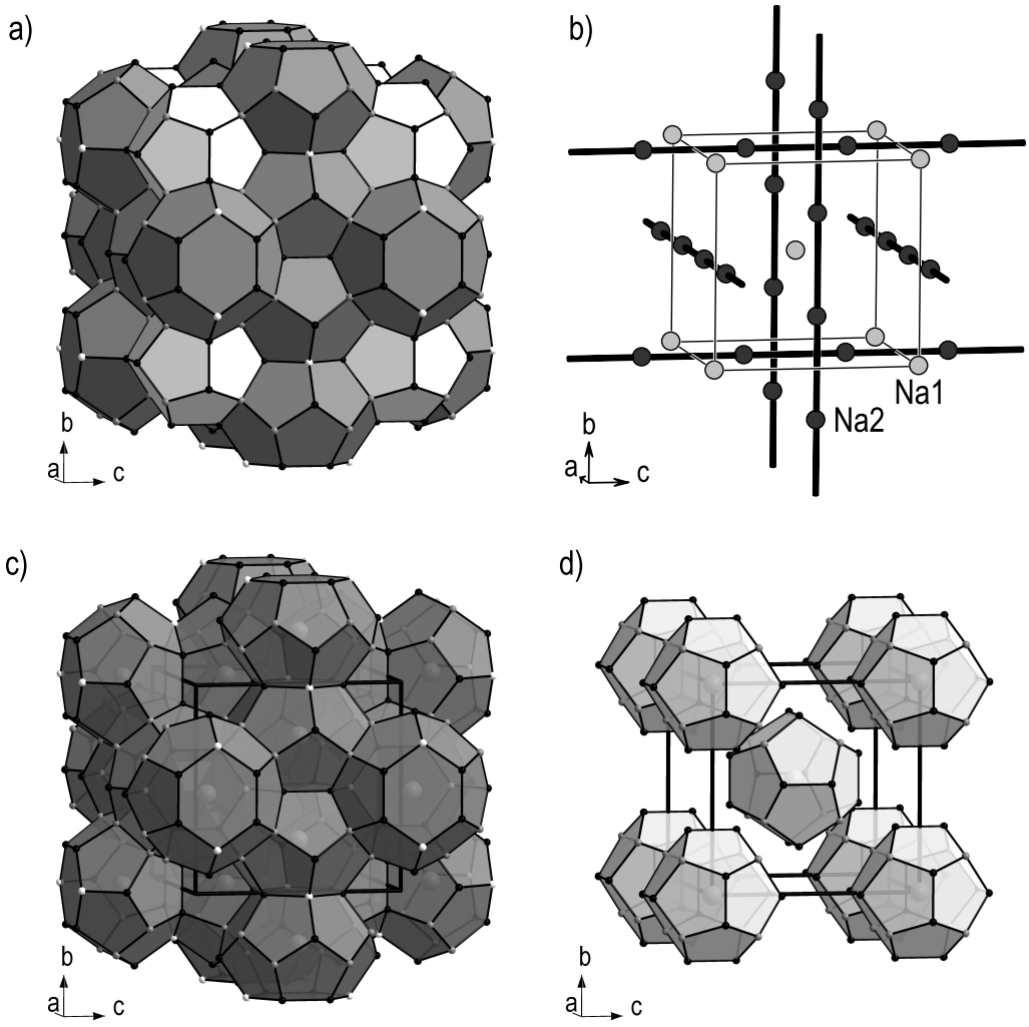

Figure 1. Crystal structure of the intermetallic type-I clathrate $Na_8Zn_4Ge_{42}$. a) Space filling arrangement of tetrakaidecahedra (dark gray) and pentagonal dodecahedra (light gray). b) A15 style arrangement of guest sites. The connecting lines between Na2 positions indicate the rod packing that describes the alignment of columns of tetrakaidecahedra which share hexagonal faces. c) Separate drawing of the arrangement of tetrakaidecahedra. d) Separate drawing of the bcc like array of pentagonal dodecahedra.

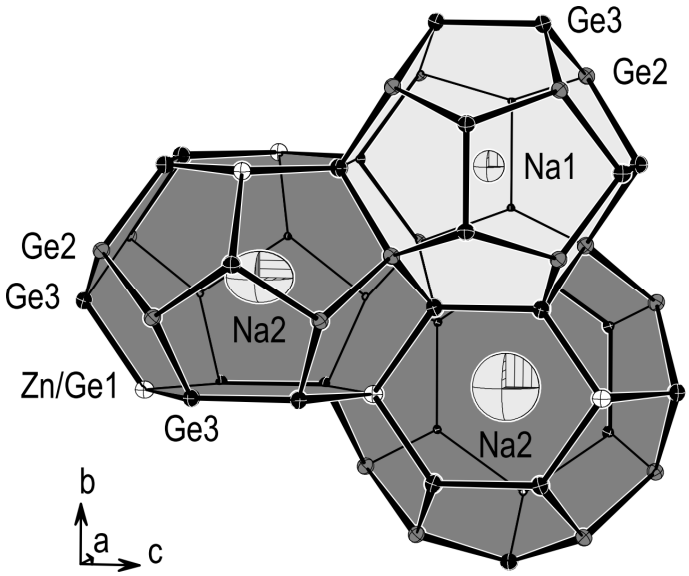

Figure 2. Representation of a section of the crystal structure of $Na_8Zn_4Ge_{42}$. Thermal ellipsoids with 70 % probability level.

Table 4. Interatomic distances for $Na_8Zn_4Ge_{42}$.

Atoms		Mult.	Distance / Å	Atoms		Mult.	Distance / Å
Zn/Ge1	–Ge3	4×	2.489(1)	Na1	–Ge2	8×	3.391(1)
	–Na2	4×	3.78(1)		–Ge3	12×	3.536(1)
Ge2	–Ge2	1×	2.483(1)	Na2	–Zn/Ge1	4×	3.78(1)
	–Ge3	3×	2.481(1)		–Ge2	8×	3.98(1)
	–Na1	1×	3.391(1)		–Ge3	8×	3.589(1)
	–Na2	3×	3.98(1)		–Ge3	4×	4.148(1)
Ge3	–Ge3	1×	2.500(1)				
	–Na1	1×	3.536(1)				
	–Na2	2×	3.589(1)				
	–Na2	1×	3.589(1)				

The interatomic distances in the Zn–Ge network are in the narrow range from 2.481(1) to 2.500(1) Å, that is only slightly longer than the interatomic distance in α-Ge (2.445 Å) or the sum of covalent radii for Zn and Ge (2.42 Å; according to ref. [24]). With the exception of the (Zn/Ge1–Ge3–Ge3) bond angle of 124.9° in the six-membered rings (hexagonal faces of the tetrakaidecahedra), all other bond angles in the framework are between 104.2° and 111.1°, close to the ideal tetrahedral angle of 109.5°.

As for related intermetallic clathrates, the exact composition of the title phase is also an issue to be discussed. In the structure refinement on the basis of single crystal XRD data, Zn/Ge mixed occupancy was found only for the 6*c* network site. The free refinement of the occupancy parameters for Zn and Ge on this site (with the sum fixed to 1) led to a Zn:Ge ratio close to 2/3:1/3 which results in the Zintl phase composition $Na_8Zn_4Ge_{42}$. Thus, the ratio was fixed to this ideal value in the final refinement steps. Of course, with atoms that have almost the same atomic number, like Zn and Ge, the results of such a refinement of mixed site occupancy are not beyond any doubt. The description of the title phase as $Na_8Zn_4Ge_{42}$ with Na cations and a polyanionic network of formally isoelectronic (4b-Zn^{2-}) and (4b-Ge^0) atoms (4b: four-bonded) is in accord with previous findings for related phases (cf. Introduction). The $A_8T_xTt_{46-x}$ type-I clathrates (space group *Pm*-3*n*, No. 223) with group 12 element atoms show *T*/*Tt* mixed occupancy exclusively on the 6*c* site, and with the exception of the *A*–Hg–Ge clathrates they are all described as electron precise Zintl compounds with formula $A_8T_4Tt_{42}$.

In this context, one may point to different possibilities to reach electron precise compositions for these ternary phases. Provided that the two guest sites are fully occupied by alkali metal atoms (which is generally found to be the case and can be determined reliably on the basis of XRD data), there is exactly one value for *x* that corresponds to an electron precise Zintl phase $A_8T_xTt_{46-x}$ with full occupancy of all framework sites ($x = 4$ for group 12 elements *T* = Zn, Cd, Hg). However, there is also the possibility that there are both *T* atoms and vacancies besides the *Tt* atoms in the framework. This can be described by the formula $A_8T_xTt_{46-x-y}\square_y$ and opens another way to reach a charge balanced situation which even includes the possibility of a homogeneity range. (Note that in case of the binary A_8Tt_{46-x} phases the vacancies also occur at the 6*c* site.) With group 12 element atoms all compositions $A_8T_xTt_{46-x-y}\square_y$ that meet the condition $2x+4y = 8$ (or $x = 4-2y$) qualify as Zintl phases with formally eight A^+ cations, *x* (4b-T^{2-}) and *y*×4 (3b-Tt^-) (since there are four (3b-Tt^-) per vacancy). The occurrence of a phase width has been studied, for example, for $Ba_8Zn_xGe_{46-x-y}\square_y$ and related phases.[16, 25]

Conclusion

$Na_8Zn_4Ge_{42}$ is another example of a ternary $A_8T_xTt_{46-x}$ intermetallic type-I clathrate and can be described as an electron precise Zintl phase with Na cations in the voids of a polyanionic host framework of four-bonded Zn and Ge atoms. The title phase thus shows that a Ge based type-I clathrate framework with encaged *A* atoms can also be realized with the light alkali metal Na. The only other known Ge based type-I clathrates with Na atoms as guests are the $Na_8Tr_xGe_{46-x}$ phases with *Tr* = Al and Ga,[17] and so $Na_8Zn_4Ge_{42}$ also evidences the close relation between the structural chemistry of alkali metal-zinc-tetrelides and that of related alkali metal-trielide-tetrelides.

References

[1] J. Gryko, P. F. McMillan, R. F. Marzke, G. K. Ramachandran, D. Patton, S. K. Deb, O. F. Sankey, *Phys. Rev. B* **2000**, *62*, R7707.

[2] A. Ammar, C. Cros, M. Pouchard, N. Jaussaud, J.-M. Bassat, G. Villeneuve, M. Duttine, M. Ménétrier, E. Reny, *Solid State Sciences* **2004**, *6*, 393.

[3] A. M. Guloy, R. Ramlau, Z. Tang, W. Schnelle, M. Baitinger, Y. Grin, *Nature* **2006**, *443*, 320.

[4] T. F. Fässler, *Angew. Chem. Int. Ed.* **2007**, *46*, 2572; *Angew. Chem.* **2007**, *119*, 2624.

[5] H. Kleinke, *Chem. Mater.* **2009**, *22*, 604.

[6] M. Christensen, S. Johnsen, B. B. Iversen, *Dalton Trans.* **2010**, *39*, 978.

[7] G. A. Slack, in *CRC Handbook of Thermoelectrics* (Ed.: D. M. Rowe), CRC Press, Boca Raton, FL, **1995**, p. 407– 440.

[8] S. Ponou, S.-J. Kim, T. F. Fässler, *J. Am. Chem. Soc.* **2009**, *131*, 10246.

[9] S.-J. Kim, Dissertation, Technische Universität München, **2007**.

[10] Q. Xie, Dissertation, Eidgenössische Technische Hochschule Zürich, **2004**.

[11] G. S. Nolas, J. L. Cohn, J. S. Dyck, C. Uher, J. Yang, *Phys. Rev. B* **2002**, *65*, 165201.

[12] G. S. Nolas, T. J. R. Weakley, J. L. Cohn, *Chem. Mater.* **1999**, *11*, 2470.

[13] A. P. Wilkinson, C. Lind, R. A. Young, S. D. Shastri, P. L. Lee, G. S. Nolas, *Chem. Mater.* **2002**, *14*, 1300.

[14] A. Kaltzoglou, S. Ponou, T. F. Fässler, *Eur. J. Inorg. Chem.* **2008**, 4507.

[15] A. Kaltzoglou, S. Ponou, T. F. Fässler, *Eur. J. Inorg. Chem.* **2008**, 538.

[16] B. Kuhl, A. Czybulka, H.-U. Schuster, *Z. Anorg. Allg. Chem.* **1995**, *621*, 1.

[17] W. Westerhaus, H.-U. Schuster, *Z. Naturforsch. B* **1977**, *32*, 1365.

[18] A. J. Karttunen, T. F. Fässler, M. Linnolahti, T. A. Pakkanen, *Inorg. Chem.* **2011**, *50*, 1733.

[19] *WinXPOW (Version 2.08)*, STOE & Cie GmbH, Darmstadt, **2003**.

[20] *XPREP (Version 6.14)*, Bruker Nonius, **2003**.

[21] G. Sheldrick, *Acta Cryst. A* **2008**, *64*, 112.

[22] *XS - Crystal Structure Solution - SHELXTL (Version 6.12)*, Bruker AXS, **2001**.

[23] *XL - Crystal Structure Refinement - SHELXTL (Version 6.12)*, Bruker AXS, **2001**.

[24] B. Cordero, V. Gómez, A. E. Platero-Prats, M. Revés, J. Echeverría, E. Cremades, F. Barragán, S. Alvarez, *Dalton Trans.* **2008**, 2832.

[25] N. Melnychenko-Koblyuk, A. Grytsiv, L. Fornasari, H. Kaldarar, H. Michor, F. Rohrbacher, M. Koza, E. Royanian, E. Bauer, P. Rogl, M. Rotter, H. Schmid, F. Marabelli, A. Devishvili, M. Doerr, G. Giester, *J. Phys.: Condens. Matter* **2007**, *19*, 216223.

6.11 Reorientation of Hexagonal Helical Channels in Tetrahedral Framework Structures – Phase Transitions of the Zintl Phase Na_2ZnSn_5 and its Relation to $Na_5Zn_{2+x}Sn_{10-x}$

Saskia Stegmaier, Sung-Jin Kim, Alexander Henze, Thomas F. Fässler,

manuscript for publication

Abstract

Two modifications of the new Zintl compound Na_2ZnSn_5 were synthesized by direct reactions of the elements. *hP*-Na_2ZnSn_5, which is metastable at standard conditions, is obtained by fast cooling of a melt of stoichiometric composition, slow cooling of such a melt or tempering of *hP*-Na_2ZnSn_5 (e.g. at 300 °C) leads to thermodynamically stable *tI*-Na_2ZnSn_5. While there is only one, Sn/Zn mixed occupied site for the framework atoms in the structure model for *hP*-Na_2ZnSn_5, Zn and Sn are fully ordered on three sites in case of *tI*-Na_2ZnSn_5.The structures of *hP*-Na_2ZnSn_5 and *tI*-Na_2ZnSn_5 are described in space group $P6_122$ (No. 178) with $a = 6.451(1)$ Å, $c = 6.237(1)$ Å, $V = 224.78(6)$ Å^3, and space group $I\text{-}42d$ (No. 122) with $a = 6.336(1)$ Å, $c = 22.382(1)$ Å, $V = 898.5(2)$ Å^3, respectively. Both phases show an open framework structure of four-bonded Zn and Sn atoms exhibiting hexagonal helical channels in which the Na atoms are situated with disorder. In the network of *hP*-Na_2ZnSn_5 the channels are oriented along the *c* direction, while in case of *tI*-Na_2ZnSn_5 channels run along the *a* and *b* directions. The phase transition from *hP*-Na_2ZnSn_5 to *tI*-Na_2ZnSn_5 which is accompanied by an ordering of the Zn and Sn atoms in the network was studied using high temperature powder and single crystal X-ray diffraction methods. Na_2ZnSn_5 is stable up to about 350 °C and does not melt congruently but decomposes to form $Na_5Zn_{2+x}Sn_{10-x}$. DFT band structure calculations (TB-LMTO-ASA) were performed with ordered model structures for *tI*-Na_2ZnSn_5 and *hP*-Na_2ZnSn_5, using an idealized model with ordered Na positions and a model with ordered Na as well as ordered Zn and Sn atom positions, respectively. The ordered structures were deduced from a description of a topological pathway for the structural transition from *hP*-Na_2ZnSn_5 to *tI*-Na_2ZnSn_5. With the model structures, a band gap at the Fermi level is found for *tI*-Na_2ZnSn_5, while only a pseudogap appears at the Fermi level for the ordered variant of *hP*-Na_2ZnSn_5.

Introduction

Several allotropes of the tetrel elements C, Si, Ge, and Sn represent four-connected networks, reflecting the disposition of the group 14 element atoms to engage in four bonds to reach an electron octet, favorably in a tetrahedral arrangement. First there is the archetypal cubic diamond structure which is also adopted by the α-modifications of Si, Ge, and Sn. Then, there are other diamond polytype structures known for C, Si, and Ge allotropes. Furthermore, different network structures which feature only four-bonded atoms, but also involve bond angles that deviate from the ideal tetrahedral angle, have been described for Si and Ge. Examples include the structure models for *allo*-Ge and *m-allo*-Ge,[1,2] and the less dense cage structures of the (almost) guest free type-II clathrates Na_xSi_{136} ($x < 1$)[3,4] and $\square_{24}Ge_{136}$[5,6,7].

Zintl phases of the tetrel elements (*Tt*) with alkali metal (*A*), alkaline earth metal, or rare earth metal cations can show polyanionic structure parts with exclusively four-connected atoms if electron poorer group 13 (*Tr*: triel element) or late d block metal (*T*) atoms join the tetrel atoms to build *Tr*–*Tt* or *T*–*Tt* polyanions, respectively. Due to the need of new materials in the field of rechargeable batteries, there is a focus on phases that contain Li or Na ions as guests in the voids of a host network.[8,9] Furthermore, phases with open network structures that exhibit one-dimensional channels are of special interest since they might serve as possible ion conductors. Among the ternary *A*–*Tr*–Sn and *A*–*T*–Sn phases with four-connected *Tr*–Sn or *T*–Sn networks, there are Li phases which show diamond polytype like polyanionic networks, while open clathrate structures are realized with K, Rb, and Cs. With intermediate sized Na, there are some phases with different network structures of four-bonded atoms which have, other than the diamond and clathrate networks, no counterpart among group 14 element allotropes. The latter include the closely related Na–*Tr*–Sn compounds $NaGaSn_2$,[10] $NaInSn_2$,[11] and $NaGaSn_5$,[12] as well as the two isotypic $Na_5T_{2+x}Sn_{10-x}$ ($x \approx 0.5$) phases with T = Zn and Hg.[13] The three Na–*Tr*–Sn compounds show analogous *Tr*–Sn four-connected open framework structures that offer hexagonal helical channels in which the Na atoms reside, the $Na_5T_{2+x}Sn_{10-x}$ phases feature a new type of *T*–Sn four-connected network with realgar-like structural motifs.

Here we now present Na_2ZnSn_5, another Sn-rich Na–Zn–Sn compound, and its relation to $Na_5Zn_{2+x}Sn_{10-x}$. Two modifications of the new Zintl compound have been characterized: *hP*-Na_2ZnSn_5 and *tI*-Na_2ZnSn_5. The Zn–Sn network of *hP*-Na_2ZnSn_5 is analogous to the *Tr*–Sn structure parts of $NaGaSn_2$,[10] $NaInSn_2$,[11] and $NaGaSn_5$.[12] *tI*-Na_2ZnSn_5 exhibits a closely related Zn–Sn four-connected open framework with a different channel structure. The

structural phase transition from *hP*-Na_2ZnSn_5 to *tI*-Na_2ZnSn_5 is accompanied by a Sn/Zn atom disorder-order transition, and the topological description of the process bares facets of the fascinating possibilities for four-bonded Zn–Sn networks in intermetallics.

Experimental Section

hP-Na_2ZnSn_5 and *tI*-Na_2ZnSn_5 were first obtained during exploratory syntheses in the Na–Zn–Sn system. After characterization of both phases by single crystal XRD analyses, reaction conditions that allow the controlled synthesis of either one of the two modifications were determined in a series of experiments as described below.

The reagents and samples were handled in argon atmosphere using an argon-filled glovebox and other standard inert gas techniques. Na was purified by liquating, Zn granula (Merck) were used as received or purified by distillation, and Sn granules (99.999 % ChemPur) were used as received.

Differential Thermal Analysis. In order to find suitable conditions for the synthesis of pure phase samples of the title phases, the reaction of the elements in ratio Na:Zn:Sn = 2:1:5 was studied by means of a DTA experiment. For this, 0.013 g of Na, 0.018 g of Zn, and 0.163 g of Sn were loaded into a custom-built niobium ampoule which was then closed by crimping in an argon-filled glovebox before being transferred to a NETZSCH DSC 404 C PEGASUS instrument equipped with a DTA sample carrier system with integrated radiation shield and type S thermocouple. An empty niobium ampoule of the same type as the sample container was used as reference. A continuous argon flow (50 mL/min) was employed during the measurement. Two heating/cooling cycles were monitored with a heating/cooling rate of 1 K/min and an upper target temperature of 700 °C (Figure 1).

In the course of heating the mixture in the first cycle the melting of Na and Sn and several exothermic effects are visible. Upon cooling (blue lines in Figure 1), a sharp exothermal effect ① at 368 °C (peak) indicates the crystallization of the product phase from the melt, and the product of the reaction is an almost pure phase sample of *hP*-Na_2ZnSn_5. Two distinct endothermal effects, ② at 343 °C (onset) and ③ at 384 °C (onset; peak at 392 °C), were recorded during heating in the second cycle (dashed red line in Figure 1). This shows that Na_2ZnSn_5 does not melt congruently. Based on the shape of the second peak ③ and the fact

that no further thermal effects were observed up to 700 °C, it can be concluded that the sample is all in the liquid state at temperatures higher than the transition temperature marked by the second peak ③. As it will be discussed below, effect ② observed at 343 °C (onset) corresponds to a transition that involves the (peritectic) decompositon of Na_2ZnSn_5 and the formation of $Na_5Zn_{2-x}Sn_{10-x}$ and elemental Sn. The small effects observed at about 215 °C are most likely caused by small amounts of elemental Sn. (In the DTA experiment with the reaction mixture these effects are expectedly detected at lower temperature than the melting point of pure Sn, which is 232 °C.) The cooling curves of both cycles are virtually identical.

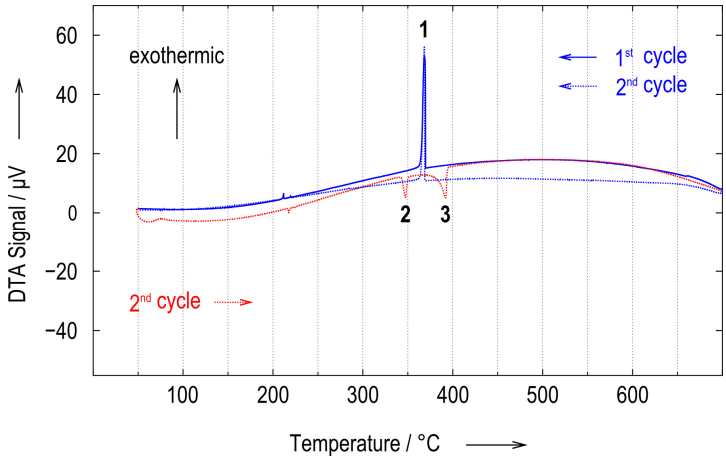

Figure 1. DTA curves obtained in an experiment starting with the elements Na, Zn, Sn in ratio 2:1:5. Red and blue lines represent the heating and cooling, respectively. Solid and dashed lines represent the first and second cycle, respectively.

Syntheses. Niobium or tantalum ampoules were loaded with the starting materials in an argon-filled glovebox, sealed by arc-welding in argon atmosphere and then placed in silica tubes which were evacuated, sealed, and inserted in vertical resistance tube furnaces that were used to apply defined temperature programs to the samples. The reaction products were characterized by means of powder XRD analyses. In order to study the events occurring upon heating a sample of *hP*-Na_2ZnSn_5, as in the second cycle of the DTA measurement, four samples were treated as follows: With heating/cooling rates of 1 K/min, mixtures of Na, Zn, and Sn in ratio 2:1:5 (total sample loadings of approx. 1.5 g) were heated to 700 °C, cooled to 50 °C (as in the first cycle of the DTA measurement) and subsequently heated to target temperatures of approx. 300 °C (below ②), 360 °C (between ② and ③), 380 °C (between ②

and ③), and 450 °C (above ③), respectively. At the respective target temperatures the samples were tempered for about a week and then they were quenched by dropping the ampoules into liquid nitrogen.

hP-*Na_2ZnSn_5*. *hP*-Na_2ZnSn_5 was obtained from the experiment with isothermal dwelling at 450 °C. The quenching of the sample from 450 °C (above ③) represents the cooling of a melt of composition Na:Zn:Sn = 2:1:5 at a very fast rate. Further, experiments with the same temperature program as used for the DTA measurement (heating/cooling rate of 1 K/min and an upper target temperature of 700 °C), confirmed that these reaction conditions also reproducibly lead to the formation of *hP*-Na_2ZnSn_5, regardless whether one or more heating/cooling cycles were applied.

***tI*-Na_2ZnSn_5 *and Phase Transition from* hP-Na_2ZnSn_5 *to* tI-Na_2ZnSn_5.** The product of the experiment with isothermal dwelling at 300 °C (below ②) was *tI*-Na_2ZnSn_5. That is, tempering of *hP*-Na_2ZnSn_5 (which shows a Sn/Zn disorder in the Zn–Sn substructure) at a temperature below the endothermal effect ② leads to the formation of *tI*-Na_2ZnSn_5 (with Zn and Sn fully ordered in the Zn–Sn substructure). These findings were confirmed by an experiment starting with a sample of *hP*-Na_2ZnSn_5 that was characterized by powder XRD analysis prior to being pressed to a pellet, heated to approx. 300 °C, annealed at this temperature and finally quenched (by dropping the ampoule into liquid nitrogen). Notably, this polymorphic phase transition from *hP*-Na_2ZnSn_5 to *tI*-Na_2ZnSn_5 was not observed in the DTA experiment. *tI*-Na_2ZnSn_5 was also obtained by heating a 2:1:5 mixture of Na, Zn, and Sn to 450 °C followed by very slow cooling at a rate of 0.1 K/min.

$Na_5Zn_{2+x}Sn_{10-x}$. In the samples obtained from the experiments with dwelling temperatures of approx. 360 °C and 380 °C (between the two endothermal effects ② and ③), $Na_5Zn_{2+x}Sn_{10-x}$ and β-Sn were identified as the main phases. Thus the effect ② can be associated to a transition that involves the (peritectic) decomposition of Na_2ZnSn_5 and the formation of $Na_5Zn_{2-x}Sn_{10-x}$ with a lower Sn content. This result was confirmed by an experiment starting with a sample of *hP*-Na_2ZnSn_5 (characterized by powder XRD analysis), that was pressed to a pellet, then heated to approx. 360 °C, annealed at this temperature and finally quenched (by dropping the ampoule into liquid nitrogen).

Powder X-ray Diffraction, Including Temperature Dependent Experiments. For powder XRD measurements, samples of the reaction products were finely ground, optionally diluted with diamond powder, and sealed in glass capillaries (silica for high temperature

measurements) in an argon-filled glovebox. Powder XRD data were collected with a STOE STADI P powder diffractometer equipped with an imaging plate and a linear position sensitive detector (IP-PSD and L-PSD) using Cu $K_{\alpha 1}$ radiation (λ = 1.54060 Å, curved Ge (111) monochromator). For temperature dependent (high temperature) powder XRD experiments a capillary furnace high temperature attachment version 0.65.3 was employed and data were collected with the imaging plate detector (IP-PSD). The STOE WINXPOW program package[14] was used for data evaluation. The lattice parameters of *hP*-Na_2ZnSn_5 and *tI*-Na_2ZnSn_5 (see e.g. Table 1) were obtained by Rietveld refinements of data sets collected at room temperature with the L-PSD. The FULLPROF SUITE software[15-17] was employed for the Rietveld analyses.

***Heating* hP-*Na_2ZnSn_5*: *Phase Transition from* hP-*Na_2ZnSn_5* *to* tI-*Na_2ZnSn_5*.** *hP*-Na_2ZnSn_5 was heated and XRD measurements with the temperature held constant during data collection were carried out at steps of 25 K from 25 °C to 150 °C, and at steps of 10 K from 150 °C to 340 °C. The phase transition from *hP*-Na_2ZnSn_5 to *tI*-Na_2ZnSn_5 was observed at approx. 250 °C (Figure 4a).

Heating tI-Na_2ZnSn_5. *tI*-Na_2ZnSn_5 was heated and XRD measurements with the temperature held constant during data collection were taken at 25°C, 150 °C, 200 °C, 250 °C, 280 °C, and at steps of 5 K in the range from 290 °C to 380 °C. *tI*-Na_2ZnSn_5 was observed to be stable up to about 350 °C (Figure 4b).

Single Crystal X-ray Diffraction and Crystal Structure Determinations. Suitable single crystals of *hP*-Na_2ZnSn_5 and *tI*-Na_2ZnSn_5 were selected in an argon-filled glovebox equipped with a microscope. The crystals were fixed on glass fibers with perfluoropolyalkylether. For *hP*-Na_2ZnSn_5, single crystal XRD data were collected at 110 K (OXFORD Instruments Cryojet cooling system, nitrogen jet) with a BRUKER APEX II diffractometer system (KAPPA goniometer, APEX II CCD detector) using Mo K_α radiation (λ = 0.71073 Å, graphite monochromator, rotating anode source). ω and φ scans (18 runs, total of 3268 images) were performed with an exposure time of 15 seconds and increments of 1° per frame, the detector distance was set to 35 mm. The BRUKER SAINT software was used for data processing, including an absorption correction with SADABS. For *tI*-Na_2ZnSn_5, single crystal XRD data were collected at 150 K (Oxford Instruments Cryojet cooling system, nitrogen jet) with an Oxford Xcalibur 3 diffractometer with a Sapphire 3 CCD detector using Mo K_α radiation (λ = 0.71073 Å, graphite monochromator). With an exposure time of 20 seconds, a frame width of 1° and a detector distance of 50 mm, a total of 776 frames were collected in

four ω scans (ω = −41° to 63°; κ = −79°; θ = 30°; φ = 0°, 90°, 180°, 270°) and one φ scan (φ = 0° to 360°; θ = 30°; ω = 0°; κ = 0°). The Oxford CrysAlis RED software[18] was used for data processing. A numerical absorption correction was applied with the STOE X-RED[19]/X-SHAPE[20] software. For both *hP*-Na_2ZnSn_5 and *tI*-Na_2ZnSn_5, XPREP[21] was used for space group determination and data merging (identical indices only), the programs XS[22,23] and XL[23,24] were used for structure solution (direct methods) and structure refinement (full-matrix least-squares on F_o^2), respectively. Atomic coordinates were standardized with the program STRUCTURE TIDY[25] implemented in PLATON[26].

The structure of *hP*-Na_2ZnSn_5 was solved in space group $P6_122$ (No. 178). In the final refinement a Flack parameter of 0.2(5) was calculated. Thus, the absolute structure or the volume fraction of an inversion twin could not be determined reliably, and the structure could alternatively be described in the enantiomorphic space group $P6_522$ (No. 179). The structure model provides only one site (6*b*) for the Zn and Sn atoms, which is consequently mixed occupied. Since the phase was found to represent a modification of Na_2ZnSn_5 (see below), the Sn:Zn ratio was fixed to 5:1 (5/6:1/6) in the refinement. With only one Sn/Zn mixed occupied site for the atoms of the anionic substructure, and one partially occupied site (6*b*) for the Na atoms, the Sn:Zn ratio could not be determined reliably only from the single crystal XRD data. Free refinement of the occupancy factor for the Na position led to a value of 0.35(2), and the parameter was fixed to 1/3 in the final refinement steps, meeting the overall composition of Na_2ZnSn_5.

The structure of *tI*-Na_2ZnSn_5 was solved in space group *I*-42*d* (No. 122). A Flack parameter of 0.03(15) was calculated in the final refinement. The structure model for *tI*-Na_2ZnSn_5 shows full ordering of Zn and Sn on three sites (Zn on 4*a*, Sn1 on 16*e*, and Sn2 on 4*b*), and involves a partially occupied Na position (on 16*e*). The freely refined value for the occupancy factor of the Na site is 0.47(2), in agreement with the value of 1/2 that results in the overall composition Na:Zn:Sn = 2:1:5. In the final refinement steps the parameter was fixed to 0.5.

EDX Measurements. EDX analyses of single crystals of *hP*-Na_2ZnSn_5 and *tI*-Na_2ZnSn_5 (unit cell determined by single crystal XRD previous to EDX analysis) were carried out using a JEOL 5900LV scanning electron microscope equipped with an OXFORD INSTRUMENTS INCA energy dispersive X-ray microanalysis system. The qualitative analyses showed the presence of Na, Zn, and Sn, and the absence of other elements heavier than Na.

Temperature Dependent Single Crystal XRD Measurements. With a STOE IPDS 2T imaging plate diffractometer using Mo K_α radiation (λ = 0.71073 Å, graphite monochromator, rotating anode source) that was equipped with a HEATSTREAM high temperature attachment (heating medium N_2, vertical gas flow), temperature dependent single crystal XRD measurements were performed at higher temperatures. Suitable single crystals of *hP*-Na_2ZnSn_5 were selected in an argon-filled glovebox equipped with a microscope. The crystals were sealed in glass capillaries in which they were fixed with glass fibers (not using any sort of glue). During heating crystals of *hP*-Na_2ZnSn_5 on the diffractometer, a transition could be observed. The analysis of a data set collected after the phase transition led to the conclusion that a Drilling of *tI*-Na_2ZnSn_5 had formed. (Details on the data collection and refinement results are given in the Supporting Information.) Measurements with a crystal that had undergone the transition and was subsequently cooled to 20 °C again confirmed that the transition is not reversible.

Electronic Structure Calculations. DFT calculations were carried out with the Stuttgart TB-LMTO-ASA program,[27] employing the tight-binding (TB) version of the linear muffin-tin orbital (LMTO) method in the atomic sphere approximation (ASA). The Barth-Hedin local exchange correlation potential[28] was used. Radii of the atomic spheres and interstitial empty spheres were determined by the procedures implemented in the TB-LMTO-ASA programs. The *k*-space integration was performed by the tetrahedron method.[29] Na 3s/(3p)/(3d), Zn 4s/4p/3d and Sn 5s/5p/(5d)/(4f) states were included in the calculations (downfolded in parentheses). VESTA[30] was used to prepare graphical representations of the ELF.

The calculations were performed for ordered model structures that were deduced from a description of a topological pathway of the structural transition from *hP*-Na_2ZnSn_5 to *tI*-Na_2ZnSn_5 (see Figure 5 and Supporting Information Figure S-1, Table S-1, and Table S-2). The structural parameters of the model structures are based on the experimentally determined unit cell parameters and atomic coordinates. For *tI*-Na_2ZnSn_5, the model structure ($P2_1$ (No. 4); a = 6.336 Å, b = 22.382 Å, c = 6.336 Å) with ordered Na positions is taken for a valid description. Concerning the employed model structure for *hP*-Na_2ZnSn_5 ($P2_1$ (No. 4); a = 22.347 Å, b = 6.237 Å, c = 6.451 Å) with ordered Zn and Sn atom positions and ordered Na positions, it must be noted that it involves e.g. the Sn/Zn–Sn/Zn site distances, instead of unequal Zn–Sn and Sn–Sn distances (as would be expected for an optimized ordered structure). 1040 or 1056 irreducible *k*-points were used for the calculations for the model for *tI*-Na_2ZnSn_5 or *hP*-Na_2ZnSn_5, respectively.

Table 1. Selected crystallographic, data collection, and refinement data for *hP*-Na_2ZnSn_5 and *tI*-Na_2ZnSn_5.

Formula[a] and bravais lattice type	***hP*-Na_2ZnSn_5**	***tI*-Na_2ZnSn_5**
Formula weight, M / g·mol^{-1}	704.80	704.80
Space group	$P6_122$ (No. 178)	$I\bar{4}2d$ (No. 122)
Z	1	4
Unit cell parameters[b] / Å	a = 6.451(1) c = 6.237(1)	a = 6.336(1) c = 22.382(1)
Unit cell volume, V / Å^3	224.78(6)	898.5(2)
Calculated density, ρ_{calc} / g·cm^{-3}	5.207	5.210
Absorption coefficient (Mo K_α), μ / mm^{-1}	16.30	16.31
F(000)	302	1208
Crystal colour, shape	silvery, block	silvery, block
Temperature for single crystal data collection, T / K	110	150
Wavelength (Mo K_α), λ / Å	0.71073	0.71073
Diffractometer	BRUKER APEX II (CCD detector, KAPPA goniometer)	OXFORD Xcalibur 3 (Sapphire 3 CCD detector)
Θ range	3.65° to 30.42°	3.34° to 26.00°
Limiting indices	$-9 \le h \le 9$; $-8 \le k \le 7$; $-8 \le l \le 8$	$-7 \le h \le 7$; $-7 \le k \le 7$; $-27 \le l \le 27$
Reflections / unique	2321 / 230	2919 / 449
Completeness	100 %	100 %
R_σ, R_{int}	0.014, 0.032	0.027, 0.045
Refinement method	Full-matrix least-squares on F^2, with XL	Full-matrix least-squares on F^2, with XL
Data / restraints / parameters	230 / 2 / 14	449 / 1 / 24
Extinction coefficient	0.015(2)	-
Flack parameter	0.2(5)	0.03(15)
Residual map / e Å^{-3}	+0.858 and −0.528	+1.963 and −0.865
Goodness-of-fit on F^2	1.336	1.057
R_1, wR_2 ($I > 2\sigma(I)$)	0.016, 0.038	0.032, 0.077
R_1, wR_2 (all data)	0.016, 0.038	0.036, 0.078

[a] See the Experimental Section for details on the refinement with partially occupied Na sites, and also Sn/Zn mixed occupancy in case of *hP*-Na_2ZnSn_5. [b] Unit cell parameters determined by Rietveld analyses of powder XRD data obtained at room temperature.

Table 2. Atomic coordinates and equivalent isotropic displacement parameters for *hP*-Na_2ZnSn_5 and *tI*-Na_2ZnSn_5. U_{eq} is defined as one third of the trace of the orthogonalized U_{ij} tensor.

***hP*-Na_2ZnSn_5**						
Atom	Wyck.	Occ.	*x*	*y*	*z*	U_{eq} / Å^2
Sn/Zn	6*b*	Sn:Zn = 5/6:1/6[a)]	0. 7643(1)	0. 5286(1)	1/4	0.016(1)
Na	6*b*	1/3[a)]	0. 103(1)	0. 205(2)	1/4	0.052(3)

***tI*-Na_2ZnSn_5**						
Atom	Wyck.	Occ .≠ 1	*x*	*y*	*z*	U_{eq} / Å^2
Sn1	16*e*		0.1572(1)	0.1679(1)	0.3154(1)	0.018(1)
Sn2	4*b*		0	0	1/2	0.018(1)
Zn	4*a*		0	0	0	0.019(2)
Na	16*e*	1/2[a)]	0. 150(2)	0.198(2)	0.145(1)	0.038(3)

[a)] Occupancy factors fixed in final refinement steps, see Experimental Section.

Table 3. Anisotropic displacement parameters (U_{ij} / Å^2) for *hP*-Na_2ZnSn_5 *tI*-Na_2ZnSn_5.

***hP*-Na_2ZnSn_5**						
Atom	U_{11}	U_{22}	U_{33}	U_{23}	U_{13}	U_{12}
Sn/Zn	0.013(1)	0.015(1)	0.020(1)	0	−0.004(1)	0.007(1)
Na	0.056(5)	0.028(4)	0.062(6)	0	−0.053(5)	0.014(2)

***tI*-Na_2ZnSn_5**						
Atom	U_{11}	U_{22}	U_{33}	U_{23}	U_{13}	U_{12}
Sn1	0.020(1)	0.022(1)	0.013(1)	0.003(1)	0.000(1)	−0.001(1)
Sn2	0.022(1)	0.022(1)	0.009(1)	0	0	0
Zn	0.022(1)	0.022(1)	0.013(1)	0	0	0
Na	0.029(5)	0.033(7)	0.050(8)	−0.016(5)	−0.008(5)	0.007(6)

Results

Single crystals of *hP*-Na_2ZnSn_5 and *tI*-Na_2ZnSn_5 were first obtained during exploratory syntheses on the Sn-rich side of the Na–Zn–Sn system. While the Na:Zn:Sn ratio can be deduced from single crystal XRD data for *tI*-Na_2ZnSn_5, the composition of *hP*-Na_2ZnSn_5 could not be determined reliably by this means, since the structure model not only involves a partial occupancy of the Na site but also the anionic structure part is formed by only one site, which is mixed occupied with Zn and Sn atoms (cf. Experimental Section). However controlled syntheses of either *hP*-Na_2ZnSn_5 or *tI*-Na_2ZnSn_5 by reactions of mixtures of the elements in ratio Na:Zn:Sn = 2:1:5, as well as *in situ* investigation of the phase transformation from *hP*-Na_2ZnSn_5 to *tI*-Na_2ZnSn_5 by means of temperature dependent powder and single crystal XRD measurements unequivocally proof that the two phases represent two modifications of Na_2ZnSn_5.

Description of the Crystal Structures

hP-Na_2ZnSn_5 and *tI*-Na_2ZnSn_5 show open network structures of four-bonded Zn and Sn atoms with hexagonal helical channels in which the Na atoms are situated with disorder.

The structure of *hP*-Na_2ZnSn_5 (Figure 2) is described with hexagonal symmetry in space group $P6_122$ (No. 178) with lattice parameters $a = 6.451(1)$ Å and $c = 6.237(1)$ Å. In Figure 2b, the Zn–Sn network of *hP*-Na_2ZnSn_5 is depicted emphasizing hexagonal helical chains running parallel to the *c* direction. These chains are aligned in style of a hexagonal rod packing and interconnected so that channels with walls made of five-membered rings result (Figure 2c). The description in space group $P6_122$ (No. 178) involves the right-handed helices, while the corresponding structure with left-handed helices is associated with the enantiomorphic space group $P6_522$ (No. 179). The structure is realized with only one crystallographic site (6*b*), which is consequently mixed occupied with Sn and Zn atoms. Each network atom exclusively belongs to one helical chain and is involved in two intra-chain bonds (*d*(Sn/Zn–Sn/Zn): 2.831(1) Å) and two bonds to atoms of two adjacent helical chains (*d*(Sn/Zn–Sn/Zn): 2.810(1) Å). The bond angles are 125° between three atoms of the same chain (1×), 109° between atoms of three different helical chains (1×), and 106° between two atoms of one and one atom of another chain (4×). There is also only one, partially occupied, Na site (6*b*). This generates hexagonal helical chains of Na positions inside the channels formed by the Zn and Sn atoms (Figure 2c). The chains of Na positions and the Sn/Zn chains are shifted with respect to each other by half a helix turn, resulting in a double-helix type

arrangement (Figure 2c). The occupancy factor for the Na site is 1/3 (cf. Experimental Section), and the assumption that every third Na position of a helical chain is occupied involves reasonable Na–Na distances of 3.87 Å (see Figure 2d,e). Distances (< 4 Å) between Na sites and Sn/Zn positions range from 3.09 Å to 3.78 Å.

An alternative description of the Zn–Sn structure part highlights puckered layers of five-membered rings (Figure 2d,e,f) as they also occur in $NaSn_5$.[31] A set of layers extending parallel *ac* is marked in Figure 2d,e. The layers are stacked in sequence *AA'* (stacking direction perpendicular to *ac*) and interconnected so that the hexagonal helical channels result between the layers. With the stacking direction perpendicular to *ac* the stacking sequence is *AA'* (Figures 2d,e). Of course, due to the three-fold symmetry axes parallel to the *c* direction, there are three equivalent layer sets for the Zn–Sn network structure of *hP*-Na_2ZnSn_5 (see Figure 6).

The structure of *tI*-Na_2ZnSn_5 (Figure 3), which is described in space group *I*-42*d* (No. 122) with lattice parameters $a = 6.336(1)$ Å and $c = 22.382(1)$ Å, is closely related to that of *hP*-Na_2ZnSn_5. In case of *tI*-Na_2ZnSn_5, puckered layers of five-membered rings extend parallel *ab* with stacking sequence *AA'A''A'''* along the *c* direction (Figure 3d). As a consequence of this different stacking sequence if compared to *hP*-Na_2ZnSn_5, the channels in the structure of *tI*-Na_2ZnSn_5 are aligned in layers of parallel channels that run alternately along *a* and *b*. Helical Zn–Sn chains running perpendicularly share Zn atoms at nodal points as shown in Figure 3b. While all network positions of the *hP*-Na_2ZnSn_5 structure are equivalent, Zn and Sn atoms are fully ordered on three sites in case of *tI*-Na_2ZnSn_5: Sn1 atoms (on 16*e*) are part of one helical chain. Zn atoms (on 4*a*), as already mentioned, belong to two helical chains (Figure 3b). Sn2 atoms (on 4*b*) are not part of any helical chain. The helical chains have a distorted hexagonal structure involving unequal bond length and angles, and different distances from the helix axis for the Zn and the Sn1 atoms. The helices along *a* are left-handed, those along *b* are right-handed (Figure 3b). Within one helical chain, the Zn–Sn1 and Sn1–Sn1 distances are 2.750(1) Å and 2.914(2) Å, respectively, and the bond angles are 115.7° (Sn1–Zn–Sn1), and 129.3° (Sn1–Sn1–Zn). The Sn1–Sn1 distances between Sn1 atoms of neighboring helical chains are 2.915(2) Å. The shortest Sn–Sn distances, 2.827(1) Å, are found for the Sn1–Sn2 contacts. Most of the bond angles which are not associated with three atoms of the same helical chain are in the range from 104.5° to 108.1°. The exceptions are a small angle of 99.4° (Sn2–Sn1–Sn1) with the Sn2 atom and two Sn1 atoms of the same helical chain, and a larger angle of 117.6° (Sn1–Sn2–Sn1, 2×) with the Sn2 atom and two Sn1 atoms of two helical chains running in the same direction.

For the Na atoms which occupy the channels of the Zn–Sn framework of *tI*-Na_2ZnSn_5 there is also only one, partially occupied, site (16*e*) and the occupancy factor of 1/2 results in the composition Na:Zn:Sn = 2:1:5. The location of the Na positions in the Zn–Sn channels is shown in Figure 3a,c,d. An occupancy pattern with every second position along the line occupied involves reasonable Na–Na distances of 3.81 Å. The Na–Zn and Na–Sn distances < 4 Å are in the range from 3.09 Å to 3.82 Å.

Figure 2. (*Next page.*) Representation of the structure of *hP*-Na_2ZnSn_5. a) Four-connected Zn–Sn framework with helical channels filled with Na atoms. b) Zn–Sn framework structure, hexagonal helical chains of Sn and Zn atoms running along the *c* direction emphasized. c) Na positions located in one of the hexagonal channels. d) Parallel projection in the direction of the hexagonal channels, puckered layers of Zn and Sn atoms extending parallel *ac* are highlighted (gray background). Due to the symmetry of the crystal structure there are three equivalent sets of layers related via three-fold rotations (see also Figure 6). e) Side view of the hexagonal helical channels and Na positions, puckered layers of Zn and Sn atoms highlighted (gray background). f) Top view of one of the puckered layers of five-membered rings highlighted in d) and e).
Sn/Zn mixed occupied positions are represented with dark teal color. The occupancy factor of the Na site is 1/3, and Na positions in a channel are shown alternately with red, orange, and yellow, so that every third position in a channel is shown with the same color. Connecting lines between neighboring Na positions in a) and b) highlight the helical chains of Na positions; in d) and e) same colored positions are interconnected to indicate the sets of Na positions with reasonable Na–Na distances within a channel (cf. Figure 5).

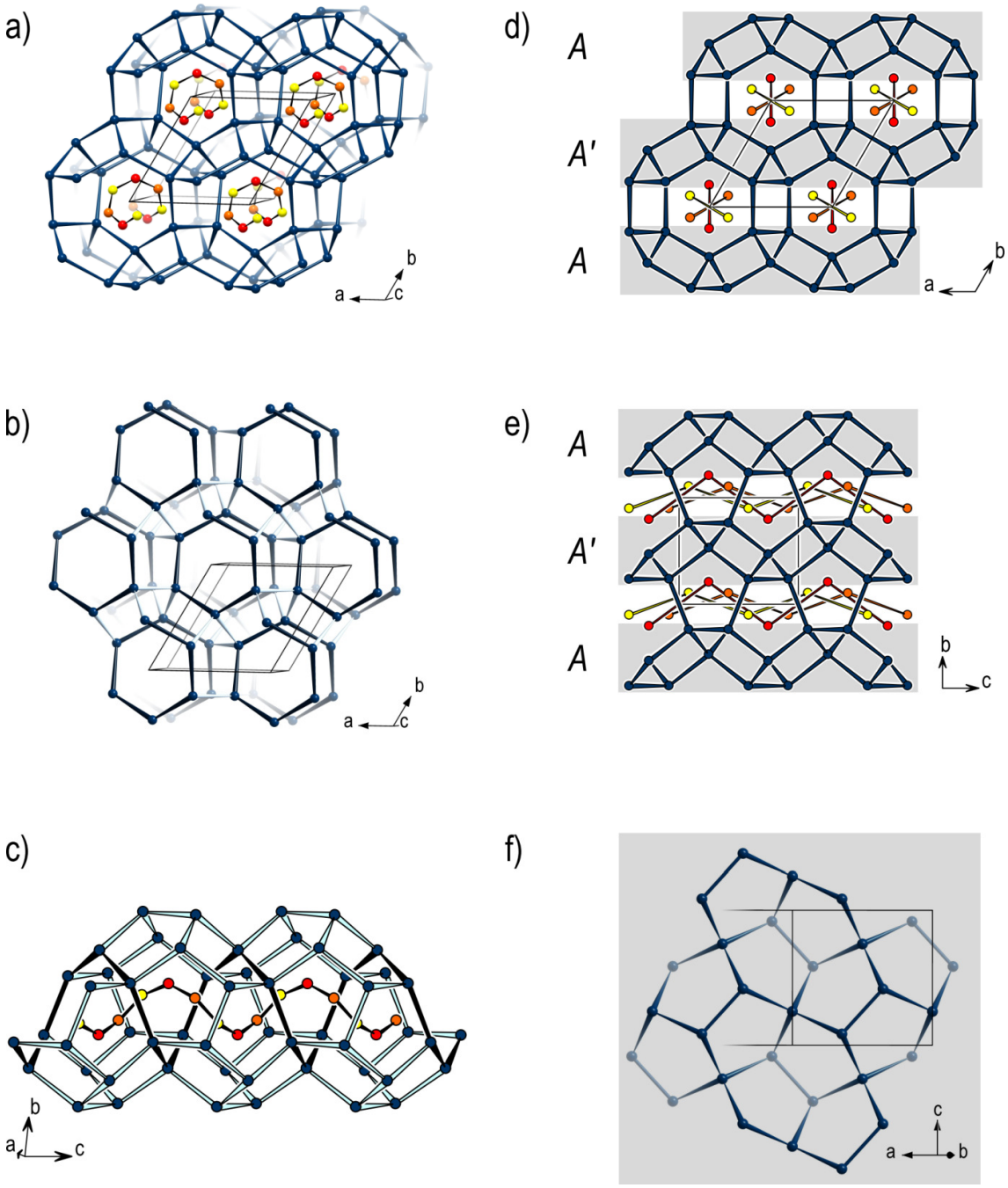

Figure 2. (*Detailed figure caption on previous page.*) Representation of the structure of *hP*-Na_2ZnSn_5.

Figure 3. (*Next page.*) Representation of the structure of *tI*-Na_2ZnSn_5. a) Four-connected Zn–Sn framework with helical channels filled with Na atoms. b) (Distorted) hexagonal helical chains and channels of Zn and Sn atoms. c) Na positions located in one of the channels. d) Projection along *b*, puckered layers of Zn and Sn atoms highlighted (gray background). e) Top view of puckered layer of five-membered rings highlighted in d).
Zn atoms are represented with green, Sn1 and Sn2 with light and dark blue color, respectively. The occupancy factor of the Na site is 1/2, and Na positions in a channel are shown alternately with red and yellow, so that every second position in a channel is shown with the same color. Connecting lines between neighboring Na positions in a) and c) highlight the chains of Na positions; in d) same colored positions are interconnected to indicate the sets of Na positions with reasonable Na–Na distances within a channel (cf. Figure 5).

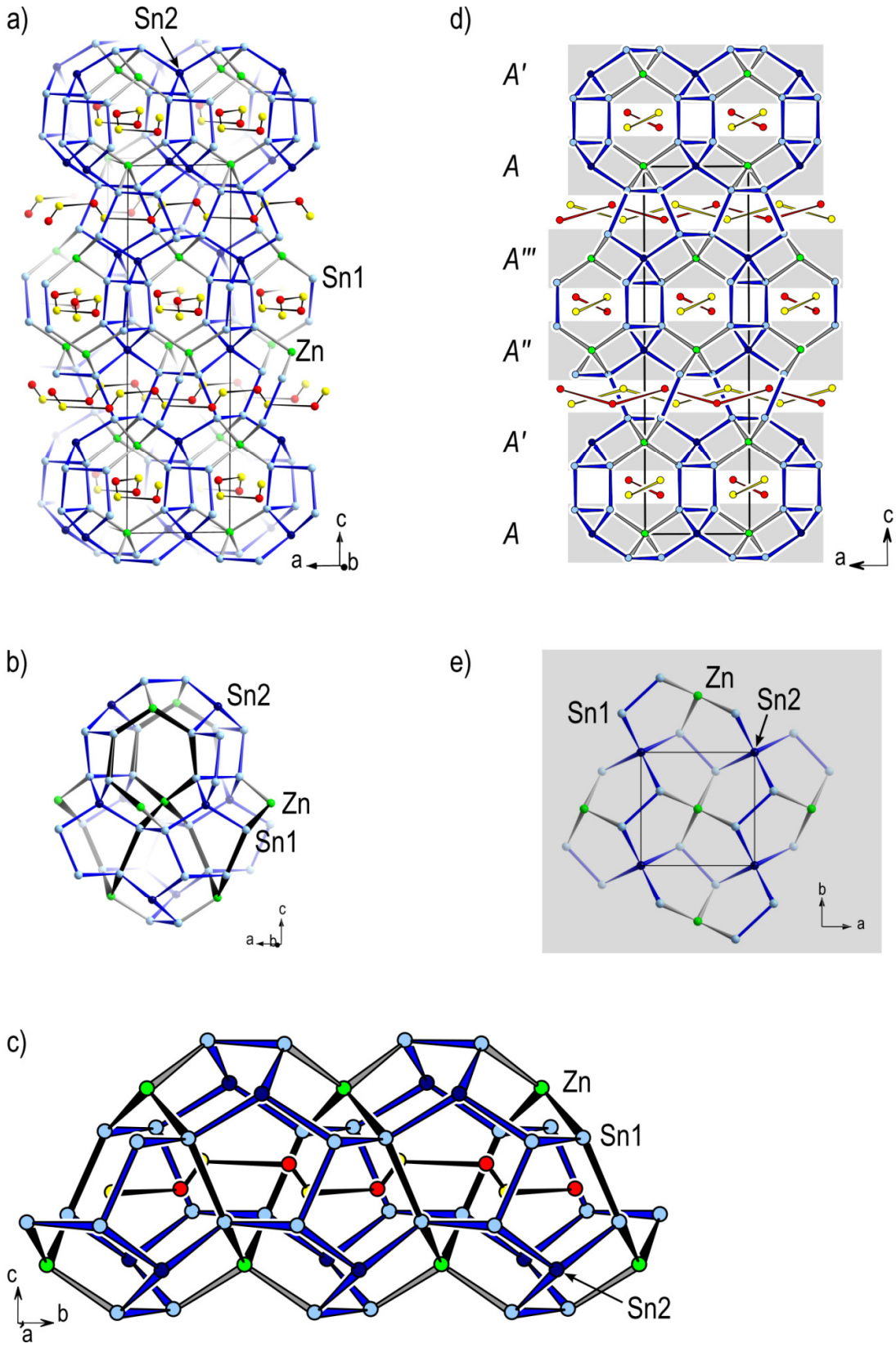

Figure 3. (*Detailed figure caption on previous page.*) Representation of the structure of *tI*-Na_2ZnSn_5.

Syntheses and Phase Transitions

hP-Na_2ZnSn_5 and *tI*-Na_2ZnSn_5 were both obtained from reactions of mixtures of Na, Zn, and Sn in ratio 2:1:5—as described in detail in the Experimental Section. *hP*-Na_2ZnSn_5 forms if a melt of stoichiometric composition is cooled fast (by quenching or with a cooling rate of 1 K/min). In contrast, *tI*-Na_2ZnSn_5 is obtained if a very slow cooling rate (0.1 K/min) is used. These findings indicate that *hP*-Na_2ZnSn_5 is kinetically favored, while *tI*-Na_2ZnSn_5 is the thermodynamically stable modification at standard conditions. This interpretation is in accord with the observation that *tI*-Na_2ZnSn_5 forms if a sample of *hP*-Na_2ZnSn_5 is annealed at 300 °C, a temperature below the first thermal effect that is found in the DTA heating curve recorded for a cycle starting with *hP*-Na_2ZnSn_5 (see Figure 1). Though the polymorphic phase transition was not observed by differential thermal analysis, two exothermal effects are apparent in this heating curve, revealing that Na_2ZnSn_5 does not melt congruently. The first effect (②; onset 343 °C) was attributed to a transition that involves the (peritectic) decomposition of Na_2ZnSn_5 and the formation of $Na_5Zn_{2-x}Sn_{10-x}$ with a lower Sn content. At temperatures above the second effect (③; onset 384 °C) the sample is all in the liquid state.

The conclusions that can be drawn from the syntheses and thermal analysis are confirmed by the results of temperature dependent powder XRD experiments in the temperature range from 25 °C to 380 °C. Upon heating *hP*-Na_2ZnSn_5, only the reflections of *hP*-Na_2ZnSn_5 occur up to a temperature of 220 °C (Figure 4a). At 240 °C both *hP*-Na_2ZnSn_5 and *tI*-Na_2ZnSn_5 are present and in the temperature range from 260 °C to 340 °C only the reflections of *tI*-Na_2ZnSn_5 were observed. During heating of a single crystal of *hP*-Na_2ZnSn_5 the transition was observed as well – under formation of a Drilling of *tI*-Na_2ZnSn_5. Subsequently cooling a crystal that had undergone the transition to 20 °C confirmed that the transition is not reversible. Heating *tI*-Na_2ZnSn_5 shows, in accordance with the results of the DTA experiment (②; onset 343 °C), that the phase is stable up to about 350 °C (Figure 4b). At higher temperatures the powder XRD patterns show the decomposition of the compound. As described above, tempering experiments in sealed metal ampoules showed that the decomposition of Na_2ZnSn_5 yields $Na_5Zn_{2+x}Sn_{10-x}$. With the *in situ* high temperature powder XRD experiments, the formation of $Na_5Zn_{2+x}Sn_{10-x}$ could, however, not be observed directly.

The experimental results establish the two title phases as modifications of the ternary compound Na_2ZnSn_5. The findings indicate that *tI*-Na_2ZnSn_5 is the thermodynamically stable polymorph while *hP*-Na_2ZnSn_5 is a metastable phase at standard conditions.

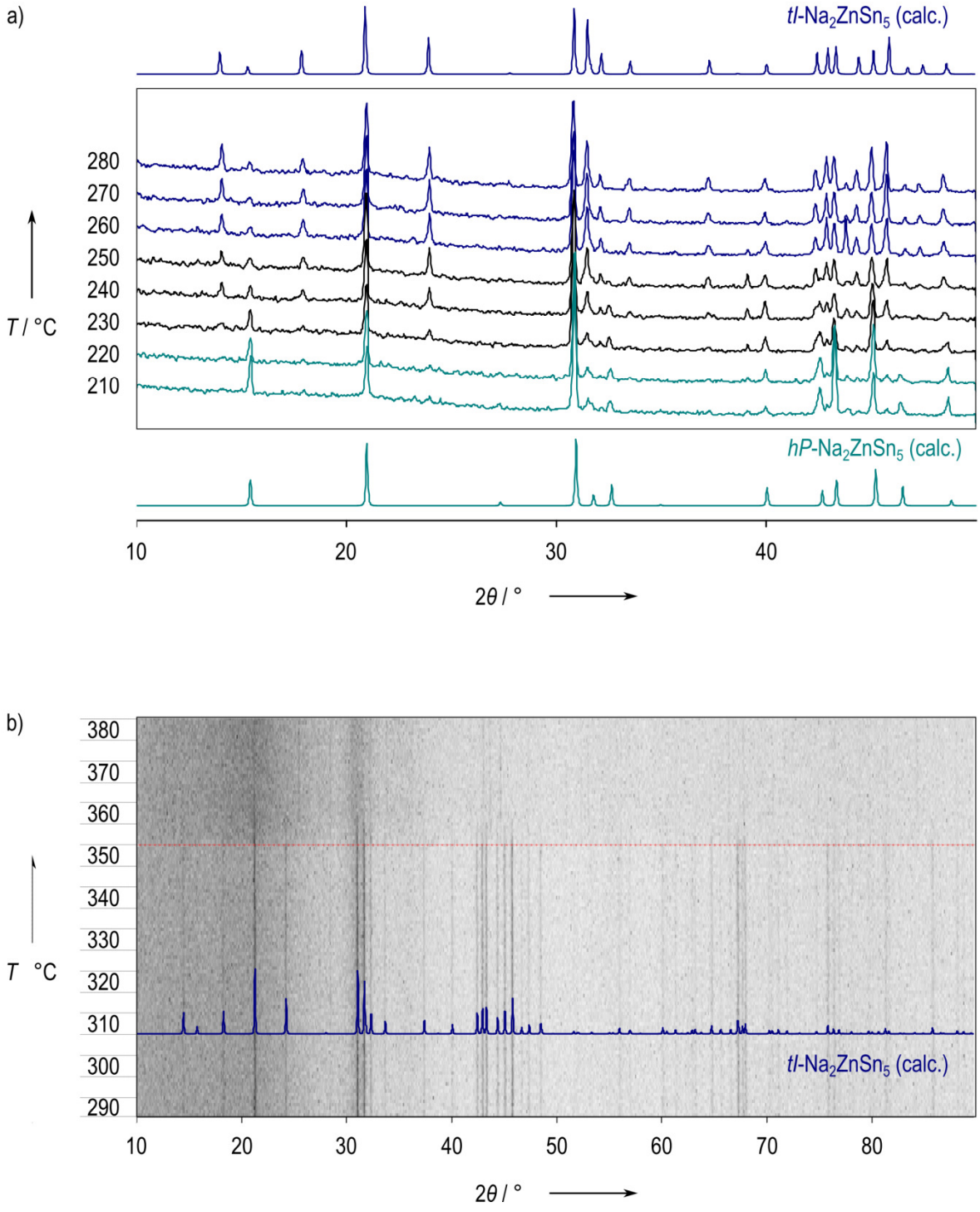

Figure 4. Powder XRD patterns obtained from temperature dependent measurements (heating) of samples of the Na_2ZnSn_5 polymorphs. a) Heating of a sample of *hP*-Na_2ZnSn_5. The phase transition from *hP*-Na_2ZnSn_5 to *tI*-Na_2ZnSn_5 is observed at about 250 °C. b) Heating of a sample of *tI*-Na_2ZnSn_5. The phase is found to be stable up to about 350 °C and decomposes above.

A Topological Pathway for the Structural Transition from* hP-*Na_2ZnSn_5* *to* tI-*Na_2ZnSn_5

The transition from the *hP*-Na_2ZnSn_5 structure to the *tI*-Na_2ZnSn_5 structure involves a transformation of the Zn–Sn network, accompanied by an ordering of Zn and Sn atoms on different network sites, and a rearrangement of the Na positions.

A model for the structural transition is illustrated in Figure 5. Fully ordered model structures for *hP*-Na_2ZnSn_5 (Figure 5a) and *tI*-Na_2ZnSn_5 (Figure 5c) are used for this topological description. See Tables S-1,2 in the Supporting Information for structure parameters and atomic coordinates for the model structures, and Figure S-1 for the group-subgroup relations between the structure models derived from the XRD crystal structure analyses and the model structures.

For *hP*-Na_2ZnSn_5, a suitable model with fully ordered Na, Zn and Sn positions can be described using a superstructure as shown in Figure 5a ($P2_1$; a = 22.347 Å, b = 6.237 Å, c = 6.451 Å). Dashed blue lines in Figure 5 indicate which Sn–Sn bonds will be broken (Figure 5a,d,g) or formed (Figure 5b,e,h) during the transformation of the Zn–Sn network and (dashed) red lines indicate the (re)orientation of the chains of Na atoms. Two out of four puckered layers of pentagons and their neighboring Na atoms are affected by these changes (Figure 5d,e,f), one layer is shown in top view in Figure 5g,h,i.

This topological description of the structural phase transition nicely illustrates the close relationship between the two network structures. But of course, the actual mechanism is not known, and no conclusions concerning e.g. the type of the phase transition (such as first or second order) can be drawn from these considerations.

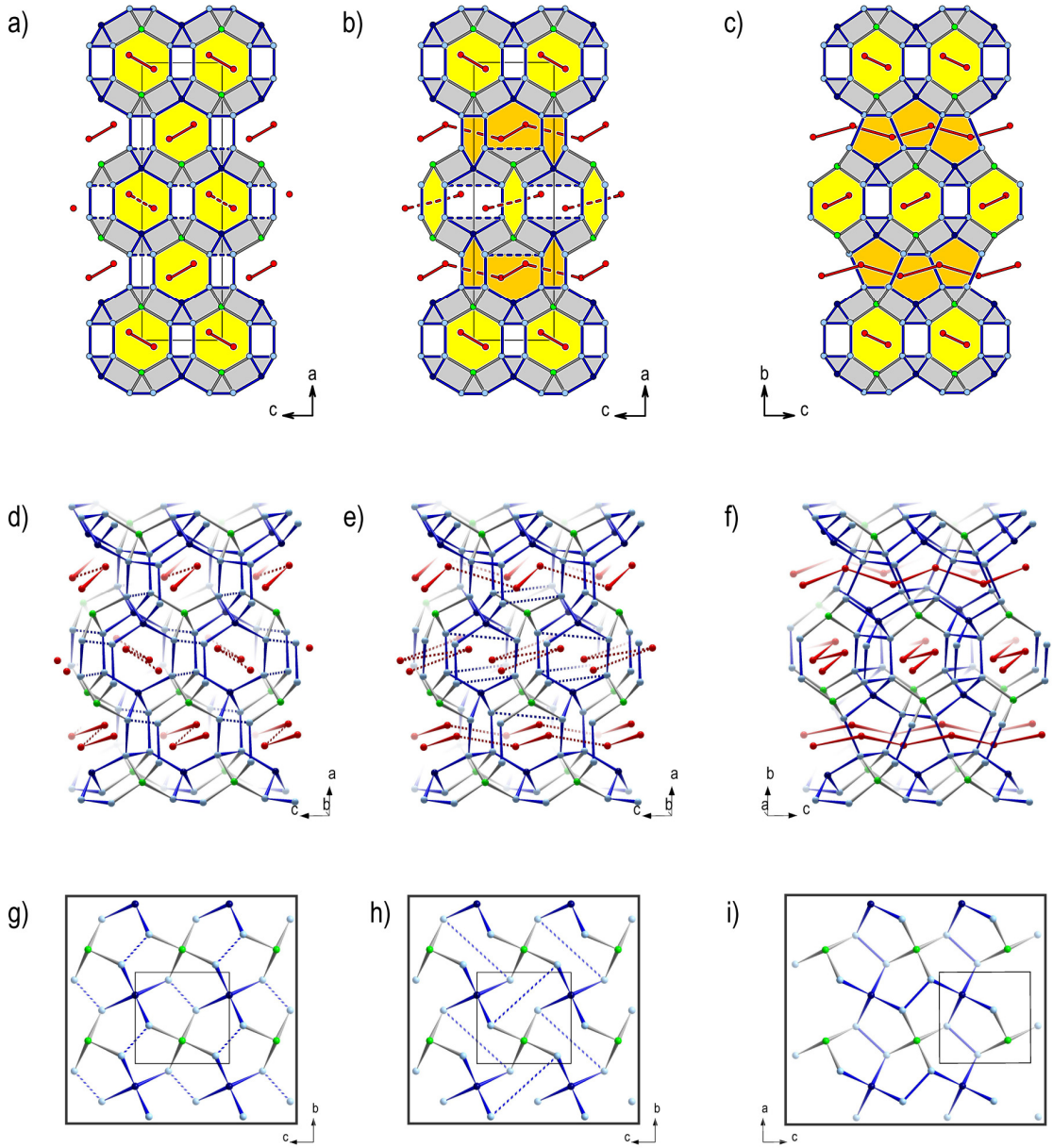

Figure 5. A pathway for the structural transition from *hP*-Na_2ZnSn_5 to *tI*-Na_2ZnSn_5 (left to right). a) to c) Overview. d) to f) Focusing on the part of the structure that is affected by the changes. g) to i) Illustrating the changes in a puckered layer of five-membered rings, top view. In a,b,d,e,g, and h atom positions of a fully ordered superstructure model for *hP*-Na_2ZnSn_5 are shown. In c,f, and i the model for *tI*-Na_2ZnSn_5 with ordered Na sites is depicted. Dashed blue lines in a,d, and g indicate bond scission in the network, in b,e, and h dashed blue lines indicate bond formation during the transition of the network structure. Dashed red lines between Na atoms indicate which Na atoms will no longer be (a,d) or end up (b,e) in the same channel (as shown in c,f). Na, Zn, and Sn atoms are represented as red, green and (light or dark) blue spheres, respectively. Further explanations are given in the text.

Due to the symmetry of the crystal structure of *hP*-Na_2ZnSn_5, the transformation described above can alternatively occur for one of the layer sets oriented in 120° directions (Figure 6). The three equivalent possibilities correspond to the observation that heating a single crystal of *hP*-Na_2ZnSn_5 leads to the formation of a drilling of *tI*-Na_2ZnSn_5.

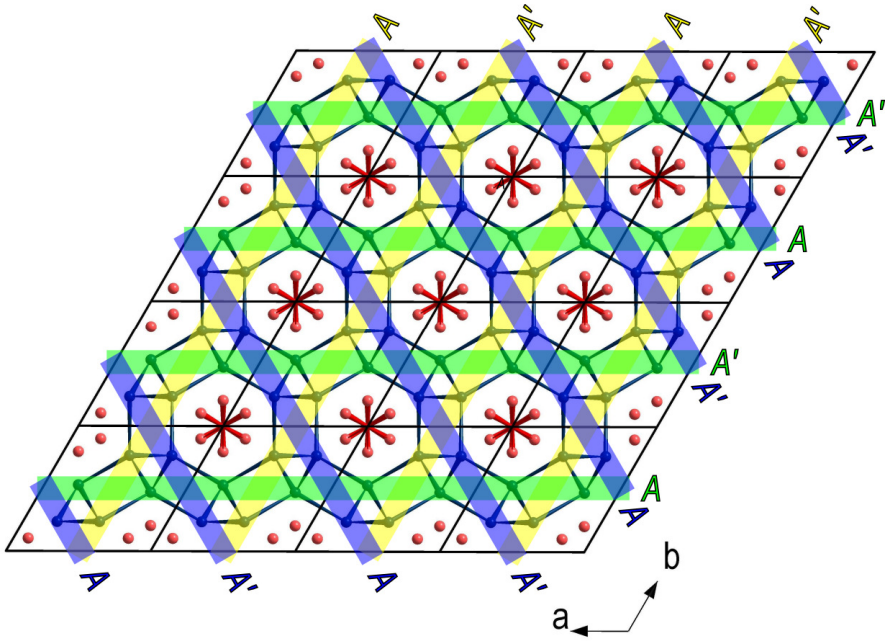

Figure 6. Stacking of puckered layers of five-membered rings in the structure of *hP*-Na_2ZnSn_5. The three possible choices for the stacking direction are shown. Rearrangement of bonds as shown in Figure 5 in each of the layer directions (blue, yellow, green) explains the formation of a drilling during the phase transition from *hP*-Na_2ZnSn_5 to *tI*-Na_2ZnSn_5, as it has been observed experimentally.

Structural Relations Between the Na_2ZnSn_5 Modifications and $Na_5Zn_{2+x}Sn_{10-x}$

The observation that the decomposition of Na_2ZnSn_5 yields $Na_5Zn_{2+x}Sn_{10-x}$ calls for a further analysis of the structural relations between different network structures with exclusively four-connected atoms such as the Zn–Sn networks of the two Na_2ZnSn_5 modifications and $Na_5Zn_{2+x}Sn_{10-x}$. A section of the cubic diamond structure as shown in Figure 7b,c will be used as basic unit for the discussion of these relations. (Notably, the tetragonal high pressure modification of LiGe[32] actually features such (isolated) layers of four- and two-connected Ge atoms.)

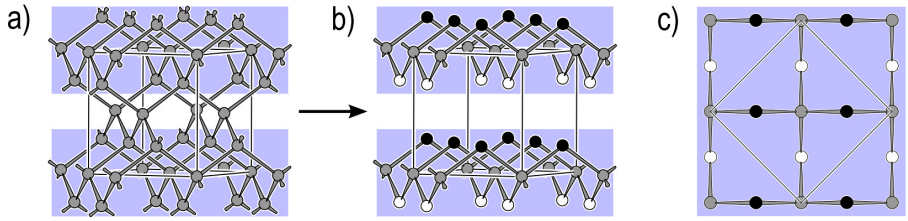

Figure 7. a) A representation of the cubic diamond structure. b) Layers of four- and two-connected atoms as cut out of the cubic diamond structure. c) Top view of such a layer. Broken-off bonds not shown.

The relation between this section of the cubic diamond (α-Sn) structure, the puckered layers of five-membered rings in the Zn–Sn substructure of the Na_2ZnSn_5 polymorphs, and the layers of the Zn–Sn part of $Na_5Zn_{2+x}Sn_{10-x}$ with realgar-like units is sketched in Figure 8. Of course, since the compounds differ in composition, this is merely a structural relation between the layer types that build up the different networks. Starting with the two-dimensional section of the α-Sn structure (cubic diamond), various layer structures can be obtained according to different bond formation patterns. Bond formation in analogy to the basket wave rectangular tiling and relaxation of the atoms to allow approximately equal bond lengths leads to a layer structure that corresponds to the Cairo-type (pentagonal) tiling as it is found for the two modifications of Na_2ZnSn_5 and $NaSn_5$ (Figure 8, left side). For a defined domain of the layer there are two distinct basket wave bonding patterns as shown in Figure 9a. (The resulting infinite layers are of course equivalent.) The interchange between these two patterns corresponds to the structural changes during the interconversion between the network structures of *hP*-Na_2ZnSn_5 and *tI*-Na_2ZnSn_5 as shown in Figure 5. The rearrangement

resembles the diamond-square-diamond mechanism (illustrated in Figure 9b) known for the transformation of polyhedral structures such as those of carboranes.[33,34] Bond formation according to another pattern, involving the formation of the same number of bonds, but with alternating formation of no bond, one bond and two bonds within the squares of the square tiling, leads to a layer with realgar-like structural motifs as observed for $Na_5Zn_{2+x}Sn_{10-x}$ (Figure 8, right side).

Figure 8 also shows the relations between the dimensions of the repeating units of the different layer types, as well as the unit cell dimensions of α-Sn (cubic diamond structure), *hP*- and *tI*-Na_2ZnSn_5, and $Na_5Zn_{2+x}Sn_{10-x}$. The actual structural parameters for the compounds, given in Table 4, fit well with the scheme. For the cell parameters parallel to the layers it is found that those of α-Sn, *hP*- and *tI*-Na_2ZnSn_5 differ only slightly and those for $Na_5Zn_{2+x}Sn_{10-x}$ are approximately double in length. This confirms the description of the Zn–Sn structure parts of the tin-rich Na–Zn–Sn phases as covalently bonded four-connected network structures. For the Na_2ZnSn_5 modifications and $Na_5Zn_{2+x}Sn_{10-x}$, Table 4 also lists the lattice parameters for the stacking directions and the corresponding number of layers, and this also reveals the close relationship between the networks build up of stacked and interconnected layers. For *hP*-Na_2ZnSn_5 the stacking takes 5.59 Å per layer, the value for *tI*-Na_2ZnSn_5 is quasi identical (5.60 Å), and the corresponding value for the layer stacking of $Na_5Zn_{2+x}Sn_{10-x}$ is 5.40 Å and thus only slightly smaller.

Table 4. Selected structural data for α-Sn, *hP*-Na_2ZnSn_5, *tI*-Na_2ZnSn_5, and $Na_5Zn_{2+x}Sn_{10-x}$.

	space group	lattice parameters parallel to		layers per repeating unit	height of stacking per layer[a]
		layers	stacking direction		
α-Sn	*Fd*-3*m* (No. 227)	a = 6.49 Å			
hP-Na_2ZnSn_5	$P6_122$ (No. 178)	orthohexagonal setting: a' = 6.237 Å; b' = 6.451 Å;	c' = 11.173 Å	2	c/2= 5.59 Å
tI-Na_2ZnSn_5	*I*-42*d* (No. 122)	a = 6.336 Å;	c = 22.382 Å	4	c/4 = 5.60 Å
$Na_5Zn_{2+x}Sn_{10-x}$	*Pbcn* (No. 60)	a = 12.772 Å; c = 12.777 Å;	b = 10.804 Å	2	b/2 = 5.40 Å

[a] Lattice parameter parallel to stacking direction divided by number of layers per repeating unit.

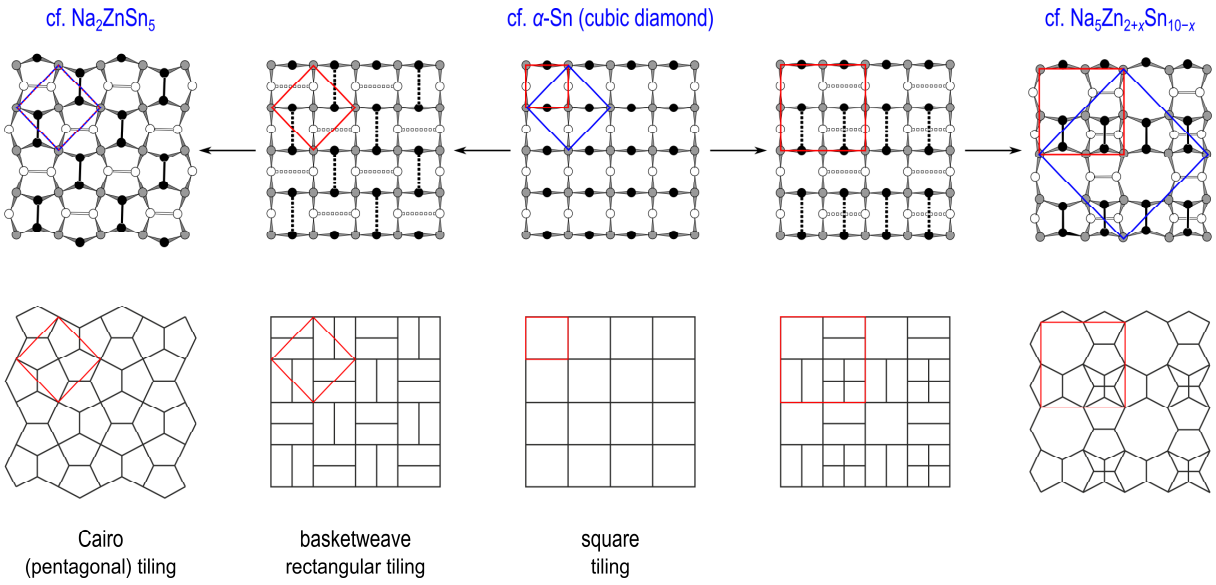

Figure 8. Relation between a two-dimensional section of the cubic diamond structure (see Figure 7c) and the layers in the Zn–Sn structure parts of the Na_2ZnSn_5 polymorphs and $Na_5Zn_{2+x}Sn_{10-x}$. In the upper part of the Figure schematic representations of the layers are shown in projection along the stacking directions, in the bottom part the related tessellations of the plane are depicted. Red squares show the repeating units of the layers and tessellations, respectively, blue squares indicate the unit cell dimensions of α-Sn, *hP*- and *tI*-Na_2ZnSn_5, and $Na_5Zn_{2+x}Sn_{10-x}$.

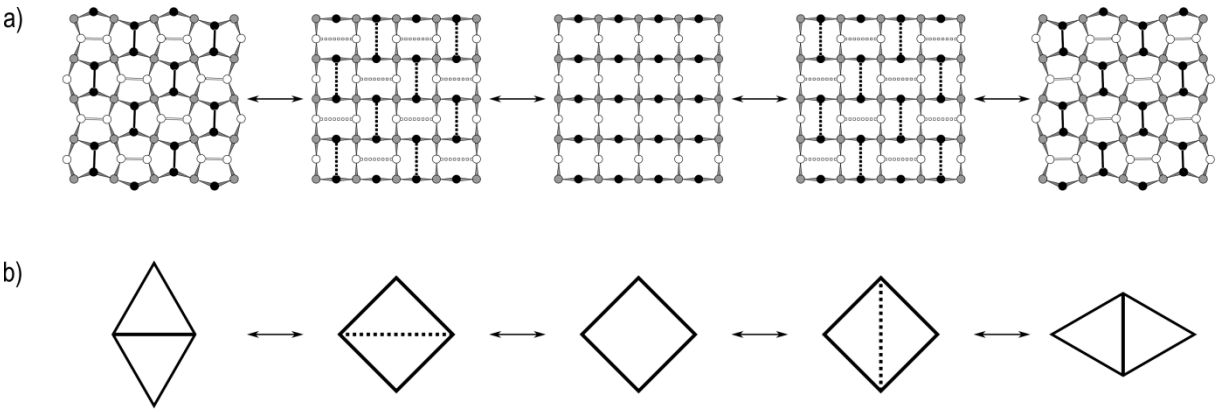

Figure 9. a) Schematic representations of the rearrangements in a puckered layer of five-membered rings as shown in Figure 5g,h, and i. b) Diamond-square-diamond mechanism.

Discussion

The Zn–Sn framework structure of *hP*-Na_2ZnSn_5 is analogous to the *Tr*–Sn (*Tr* = Ga, In) structure parts of $NaInSn_2$,[11] $NaGaSn_2$,[10] and $NaGaSn_5$[12]. Selected structural data for these phases, which are all electron precise Zintl compounds (with ratios of Na:Zn = 2:1 or Na:*Tr* = 1:1), are included in the Supporting Information Table S-3. Though different space groups are involved (for the group-subgroup relations see Figure S-2 in the Supporting Information), the structure models are all very similar. In all cases, there are exclusively mixed occupied sites for the network atoms, and for all but $NaInSn_2$ also disorder of the Na atoms is described (with split and/or partially occupied Na sites). The main difference between the structure models lies in the location of the Na positions within the channels of the polyanionic network (which comes along with the symmetry elements of the different space groups). Apart from $NaGaSn_5$, the phases show a ratio of Na to network atoms of 1:3. (Note that in the report on $NaGaSn_2$[10] it is stated that attempts to synthesize $NaGaSn_5$ were unsuccessful.) The phase transformation of *hP*-Na_2ZnSn_5 to *tI*-Na_2ZnSn_5 unequivocally reveals the composition of the phase with Sn/Zn disorder and shows the validation of the Zintl concept. The findings suggest to speculate that atom ordering and polymorphic transitions may also occur for the other phases of this structure family.

Electronic Structure

TB-LMTO-ASA band structure calculations for *tI*-Na_2ZnSn_5 (model with ordered Na sites) show a band gap (of approximately 0.5 eV) at the Fermi level, as expected for a Zintl phase. Total DOS (density of states) plots as well as atom type and orbital type resolved partial density of states (PDOS) plots for *tI*-Na_2ZnSn_5 (model with ordered Na sites) are shown in Figure 10. Sn-p and Zn-p states prevail just below the Fermi Level. The PDOS analysis supports the description of the Zn–Sn network of Na_2ZnSn_5 as an s-p bonded framework, Zn acts as a "pseudo main group metal". The Zn-*d* states can be regarded as "pseudo core states", giving rise to the main DOS peak at approx. −8 eV. Note that Na states also make important contributions to the total DOS.

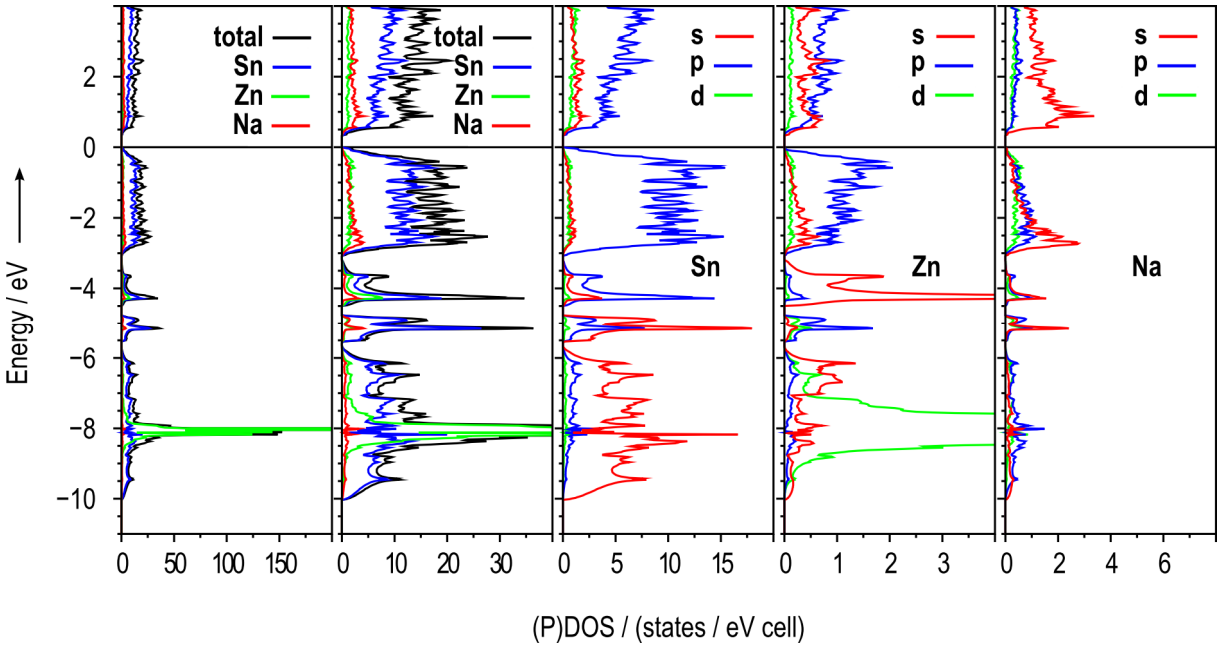

Figure 10. Total and partial density of states curves for *tI*-Na_2ZnSn_5 (model with ordered Na sites). Fermi level (E_F) at 0 eV. Notice, different scales are used for the representation of the PDOS curves for Sn, Zn, and Na, taking into account the composition of Na_2ZnSn_5.

References

(1) Grüttner, A.; Nesper, R.; von Schnering, H. G. *Angew. Chem. Int. Ed. Engl.* **1982**, *21*, 912.

(2) Kiefer, F.; Karttunen, A. J.; Döblinger, M.; Fässler, T. F. *Chemistry of Materials* **2011**, *23*, 4578.

(3) Gryko, J.; McMillan, P. F.; Marzke, R. F.; Ramachandran, G. K.; Patton, D.; Deb, S. K.; Sankey, O. F. *Phys. Rev. B* **2000**, *62*, R7707.

(4) Ammar, A.; Cros, C.; Pouchard, M.; Jaussaud, N.; Bassat, J.-M.; Villeneuve, G.; Duttine, M.; Ménétrier, M.; Reny, E. *Solid State Sciences* **2004**, *6*, 393.

(5) Guloy, A. M.; Ramlau, R.; Tang, Z.; Schnelle, W.; Baitinger, M.; Grin, Y. *Nature* **2006**, *443*, 320.

(6) Fässler, T. F. *Angew. Chem. Int. Ed.* **2007**, *46*, 2572; *Angew. Chem.* **2007**, *119*, 2624.

(7) For a recent overview of Ge modifications that have been obtained from high pressure experiments, also including more examples for network structures with four-bonded atoms, see for example: Schwarz, U.; Wosylus, A.; Böhme, B.; Baitinger, M.; Hanfland, M.; Grin, Y. *Angew. Chem. Int. Ed.* **2008**, *47*, 6790.

(8) Pöttgen, R.; Dinges, T.; Eckert, H.; Sreeraj, P.; Wiemhöfer, H.-D. *Z. Phys. Chem* **2010**, *224*, 1475.

(9) *Handbook of Battery Materials*; 2nd ed.; Claus, D.; Besenhard, J. O., Eds.; Wiley-VCH: Weinheim, 2011.

(10) Vaughey, J. T.; Corbett, J. D. *J. Am. Chem. Soc.* **1996**, *118*, 12098.

(11) Blase, W.; Cordier, G.; Kniep, R.; Schmidt, R. *Z. Naturforsch. B* **1989**, *44*, 505.

(12) Blase, W.; Cordier, G. *Z. Naturforsch. B* **1988**, *43*, 1017.

(13) Ponou, S.; Kim, S.-J.; Fässler, T. F. *J. Am. Chem. Soc.* **2009**, *131*, 10246.

(14) *WinXPOW (Version 2.08)*, STOE & Cie GmbH, Darmstadt, **2003**.

(15) *FullProf Suite*, Rodriguez-Carvajal, J.

(16) *FullProf.2k (Version 4.80)*, Rodriguez-Carvajal, J., **2010**.

(17) *WinPLOTR*, T. Roisnel; Rodriguez-Carvajal, J., **2010**.

(18) *CrysAlis RED (Version 1.171.33.34d)*, Oxford Diffraction Ltd., **2009**.

(19) *X-RED32 (Version 1.26)*, STOE & Cie GmbH, Darmstadt, **2004**.

(20) *X-SHAPE (Version 2.05)*, STOE & Cie GmbH, Darmstadt, **2004**.

(21) *XPREP (Version 6.14)*, Bruker Nonius, **2003**.

(22) *XS - Crystal Structure Solution - SHELXTL (Version 6.12)*, Bruker AXS, **2001**.

(23) Sheldrick, G. *Acta Cryst. A* **2008**, *64*, 112.

(24) *XL - Crystal Structure Refinement - SHELXTL (Version 6.12)*, Bruker AXS, **2001**.

(25) Gelato, L. M.; Parthe, E. *J. Appl. Cryst.* **1987**, *20*, 139.

(26) Spek, A. L. *Acta Cryst. A* **1990**, c34.

(27) *The Stuttgart TB-LMTO-ASA Program (Version 4.7)*, O. Jepsen; A. Burkhardt; Andersen, O. K., Max-Planck-Institut für Festkörperforschung, Stuttgart, **1998**.

(28) Barth, U. v.; Hedin, L. *J. Phys. C: Solid State Phys.* **1972**, *5*, 1629.

(29) Blöchel, P. E.; Jepsen, O.; Andersen, O. K. *Phys. Rev. B* **1994**, *49*, 16223.

(30) Momma, K.; Izumi, F. *J. Appl. Cryst.* **2008**, *41*, 653.

(31) Fässler, T. F.; Kronseder, C. *Angew. Chem. Int. Ed.* **1998**, *37*, 1571; *Angew. Chem.* **1999**, *110*, 1641.

(32) Evers, J.; Oehlinger, G.; Sextl, G.; Becker, H.-O. *Angew. Chem. Int. Ed. Engl.* **1987**, *26*, 76.

(33) Fässler, T. F. *Coord. Chem. Rev.* **2001**, *215*, 347.

(34) Lipscomb, W. N. **1966**, *153*, 373.

Supporting Information

for

Reorientation of Hexagonal Helical Channels in Tetrahedral Framework Structures – Phase Transitions of the Zintl Phase Na_2ZnSn_5 and its Relation to $Na_5Zn_{2+x}Sn_{10-x}$

Saskia Stegmaier, Sung-Jin Kim, Alexander Henze, Thomas F. Fässler,

manuscript for publication

Contents

Ordered Models Structures for* hP-*Na_2ZnSn_5* *and* tI-*Na_2ZnSn_5

Figure S-1. Group-subgroup relations between the structure models derived from the XRD crystal structure analyses and the ordered model structures used for the electronic structure calculations.

Table S-1. Structural data for the model structure with ordered Na, Zn and Sn sites based on the structure model for *hP*-Na_2ZnSn_5.

Table S-2. Structural data for the model, with ordered Na sites, for *tI*-Na_2ZnSn_5.

Structural Relations

Table S-3. Selected structural data reported for Na_2ZnSn_5, $NaInSn_2$, $NaGaSn_2$, and $NaGaSn_5$ with analogous polyanionic network structures.

Temperature Dependent Single Crystal XRD Measurement

Table S-4. Selected crystallographic, data collection, and refinement data.

Table S-5. Atomic coordinates and equivalent isotropic displacement parameters.

Table S-6. Anisotropic displacement parameters.

References

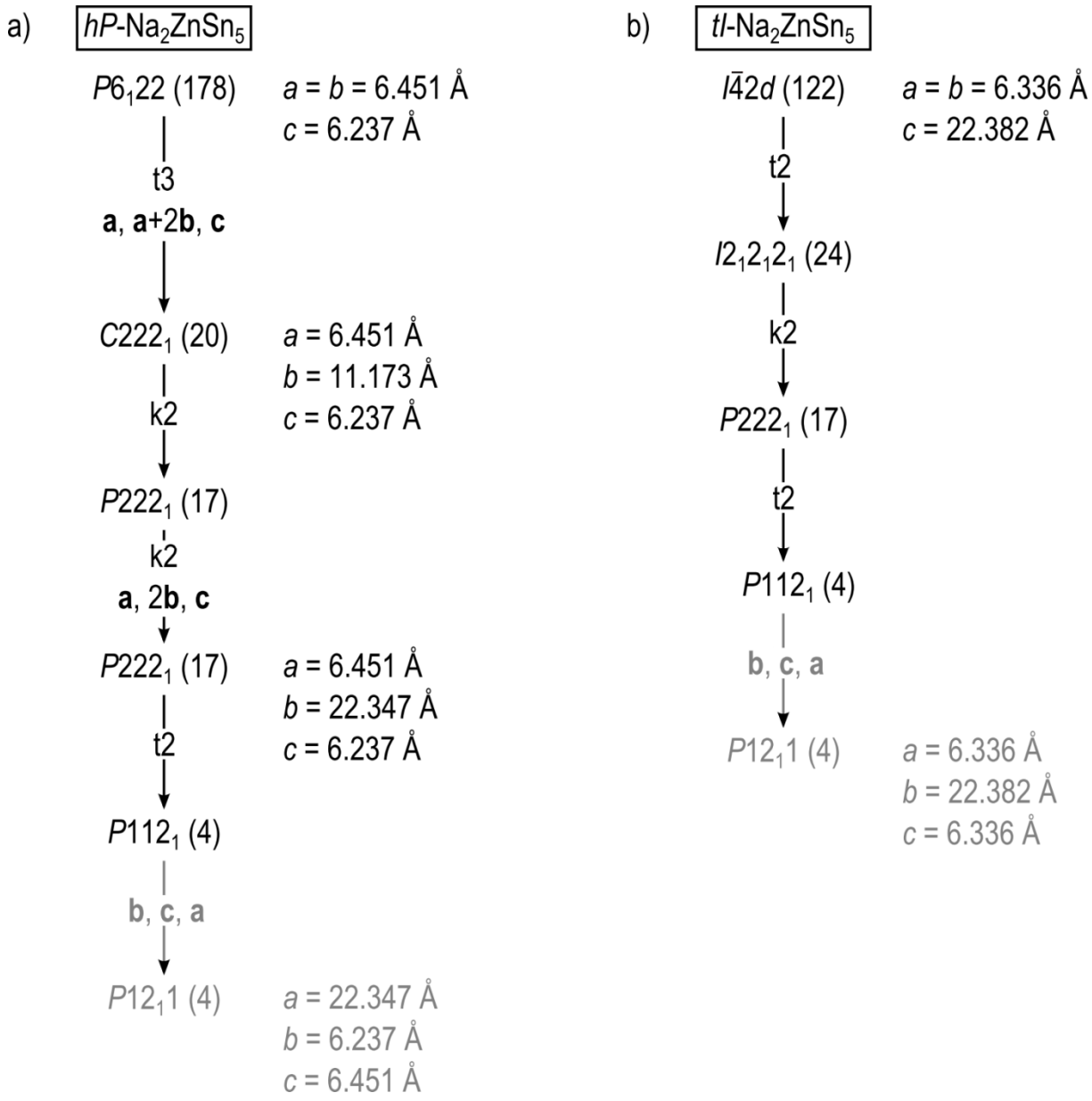

Figure S-1. Group-subgroup relations between the structure models derived from the XRD crystal structure analyses and the ordered model structures depicted in Figure 5 (manuscript), which were also used for the electronic structure calculations. The last steps (gray arrows and font) are only changes of the settings which are required to obtain suitable input structures for the TB-LMTO-ASA calculations.

Table S-1. Structural data for the model structure with ordered Na, Zn and Sn sites based on the structure model for *hP*-Na_2ZnSn_5. A set of Na sites has been chosen in analogy to the $NaInSn_2$[1] structure, and Zn and Sn atoms are positioned in preparation for the transition to the structure of *tI*-Na_2ZnSn_5 as shown in Figure 5.

Model based on *hP*-Na_2ZnSn_5	
Formula	Na_2ZnSn_5
Space group	$P12_11$ (No. 4)
Z	4
Unit cell parameters [a)]	a = 22.347 Å, b = 6.237 Å; c = 6.451 Å β = 90°

[a)] β = 90.001° for calculation so that the program recognizes the structure as monoclinic.

Atom	Wyck.	*x*	*y*	*z*
Sn	2*a*	0.3822	0.2500	0.0000
Sn	2*a*	0.1322	0.2500	0.5000
Sn	2*a*	0.0589	0.5833	0.3535
Sn	2*a*	0.0589	0.9167	0.6465
Sn	2*a*	0.5589	0.5833	0.3535
Sn	2*a*	0.5589	0.9167	0.6465
Sn	2*a*	0.3089	0.5833	0.8535
Sn	2*a*	0.3089	0.9167	0.1465
Sn	2*a*	0.8089	0.5833	0.8535
Sn	2*a*	0.8089	0.9167	0.1465
Zn	2*a*	0.8822	0.2500	0.0000
Zn	2*a*	0.6322	0.2500	0.5000
Na	2*a*	0.2244	0.9167	0.6537
Na	2*a*	0.7244	0.9167	0.6537
Na	2*a*	0.4744	0.5833	0.8463
Na	2*a*	0.9744	0.5833	0.8463

Table S-2. Structural data for the model, with ordered Na sites, for *tI*-Na_2ZnSn_5.

Model for *tI*-Na_2ZnSn_5	
Formula	Na_2ZnSn_5
Space group	$P12_11$ (No. 4)
Z	4
Unit cell parameters[a)]	a = 6.336 Å; b = 22.382 Å; c = 6.336 Å β = 90°

[a)] β = 90.001° for calculation so that the program recognizes the structure as monoclinic.

Atom	Wyck.	*x*	*y*	*z*
Sn	2*a*	0.4179	0.6904	0.4072
Sn	2*a*	0.4179	0.8096	0.5928
Sn	2*a*	0.9179	0.3096	0.0928
Sn	2*a*	0.9179	0.1904	0.9072
Sn	2*a*	0.0928	0.0596	0.4179
Sn	2*a*	0.0928	0.4404	0.5821
Sn	2*a*	0.5928	0.9404	0.0821
Sn	2*a*	0.5928	0.5596	0.9179
Sn	2*a*	0.2500	0.8750	0.2500
Sn	2*a*	0.2500	0.6250	0.7500
Zn	2*a*	0.2500	0.3750	0.2500
Zn	2*a*	0.2500	0.1250	0.7500
Na	2*a*	0.4479	0.9798	0.5997
Na	2*a*	0.9479	0.0202	0.9003
Na	2*a*	0.0997	0.2298	0.4479
Na	2*a*	0.5997	0.7702	0.0521

Table S-3. Selected structural data reported for Na_2ZnSn_5, $NaInSn_2$, $NaGaSn_2$, and $NaGaSn_5$ with analogous polyanionic network structures.

formula	space group	statement concerning the absolute configuration	lattice parameters	orthohexagonal lattice parameters[a] or relations[b]	ref.
Na_2ZnSn_5	$P6_122$ (No. 178)	not determined (enantiomorphic space group: $P6_522$ (No. 179))	a = 6.451(1) Å c = 6.237(1) Å	$a' = c$ = 6.237 Å $b' = a$ = 6.451 Å $c' = a\sqrt{3}$ = 11.173 Å	this work
$NaInSn_2$	$P2_12_12_1$ (No. 19)	no statement given (Sohncke group)	a = 6.279(4) Å b = 6.543(2) Å c = 11.396(2) Å	$c/\sqrt{3}$ = 6.579 Å	[1]
$NaGaSn_2$	$C222_1$ (No. 20)	slightly higher R values for other enantiomer (Sohncke group)	c = 6.162(2) Å a = 6.309(3) Å b = 10.986(4) Å	$b/\sqrt{3}$ = 6.343 Å	[2]
$NaGaSn_5$	$P3_112$ (No. 151)	not determined (enantiomorphic space group: $P3_212$ (No. 153))	a= 6.328(4) Å c = 6.170(3) Å	$a' = c$ = 6.170 Å $b' = a$ = 6.328 Å $c' = a\sqrt{3}$ = 10.960 Å	[3]

[a] For the hexagonal or trigonal structures orthohexagonal lattice parameters are given for comparison.

[b] For the orthorhombic structures the given relation reveals the deviation from hexagonal metrics.

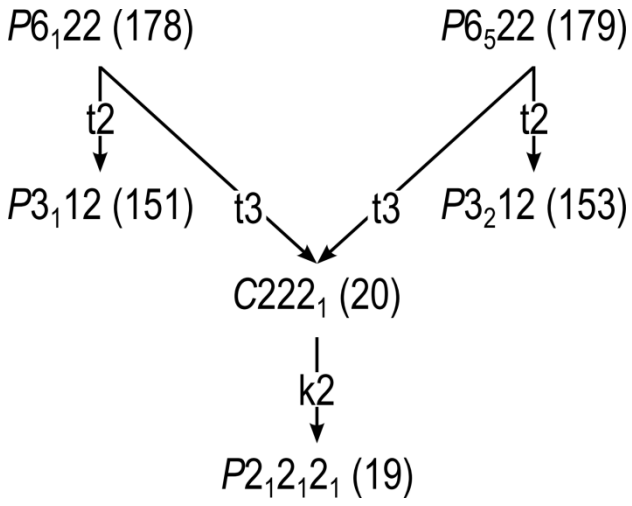

Figure S-2. Group-subgroup relations between the space groups that appear in Table 4. $P6_122$ (No. 178) and $P6_522$ (No. 179) as well as $P3_112$ (No.151) and $P3_212$ (No. 153) are enantiomorphic space groups.

Temperature Dependent Single Crystal XRD Measurement

During heating a single crystal of *hP*-Na_2ZnSn_5 on the STOE IPDS 2T diffractometer (details see Experimental Section in the manuscript) diffraction patterns were monitored and a transition was observed. After the phase transition a data set was collected at a sample temperature of approx. 220 °C. The analysis of the data showed that a Drilling of *tI*-Na_2ZnSn_5 had formed. The orientation matrices of the individuals were determined with the STOE X-AREA software.[4] A HKLF5 file was generated for the refinement with XL.[5,6]

Table S-4. Selected crystallographic, data collection, and refinement data for *tI*-Na_2ZnSn_5 – high temperature single crystal XRD measurement after phase transition from *hP*-Na_2ZnSn_5 to *tI*-Na_2ZnSn_5 (Drilling).

Formula and bravais lattice type	***tI*-Na_2ZnSn_5**
Formula weight, M / g·mol^{-1}	704.80
Space group	*I*-42*d* (No. 122)
Z	4
Unit cell parameters / Å	a = 6.367(1) c = 22.514(5)
Unit cell volume, V / Å^3	912.6(3)
Calculated density, ρ_{calc} / g·cm^{-3}	5.130
Absorption coefficient (Mo K_α), μ / mm^{-1}	16.061
F(000)	1208
Crystal colour, shape	silvery, block
Temperature for single crystal data collection, T	approx. 220 °C
Wavelength (Mo K_α), λ / Å	0.71073
Diffractometer	STOE IPDS 2T (imaging plate)
Θ range	3.62 ° to 26.01°
Limiting indices	$-7 \le h \le 7$; $-7 \le k \le 7$; $-27 \le l \le 27$
Completeness	96.7 %
Data / restraints / parameters	12293 / 0 / 26
BASF 1, BASF 2	0.258(1), 0.229(1)
Extinction coefficient	0.014(1)
Residual map / e Å^{-3}	+3.86 and −1.19
R_1, wR_2 ($I > 2\sigma(I)$)	0.104, 0.244
R_1, wR_2 (all data)	0.109, 0.247

Table S-5. Atomic coordinates and equivalent isotropic displacement parameters for *tI*-Na_2ZnSn_5 – high temperature single crystal XRD measurement after phase transition from *hP*-Na_2ZnSn_5 to *tI*-Na_2ZnSn_5 (Drilling).

***tI*-Na_2ZnSn_5**						
Atom	Wyck.	Occ.≠ 1	*x*	*y*	*z*	U_{eq} / Å^2
Sn1	16*e*		0.1576(1)	0.1678(1)	0.3153(1)	0.024(1)
Sn2	4*b*		0	0	1/2	0.024(1)
Zn	4*a*		0	0	0	0.031(2)
Na	16*e*	1/2[a)]	0. 153(1)	0.212(3)	0.143(1)	0.089(3)

U_{eq} is defined as one third of the trace of the orthogonalized U_{ij} tensor.

[a)] Occupancy factor fixed in final refinement steps.

Table S-6. Anisotropic displacement parameters (U_{ij} / Å^2) for *tI*-Na_2ZnSn_5 – high temperature single crystal XRD measurement after phase transition from *hP*-Na_2ZnSn_5 to *tI*-Na_2ZnSn_5 (Drilling).

***tI*-Na_2ZnSn_5**						
Atom	U_{11}	U_{22}	U_{33}	U_{23}	U_{13}	U_{12}
Sn1	0.024(1)	0.024(1)	0.024(1)	0.002(1)	0.000(1)	0.003(1)
Sn2	0.024(1)	0.024(1)	0.022(1)	0	0	0
Zn	0.030(1)	0.030(1)	0.031(1)	0	0	0
Na	0.049(5)	0.10(1)	0.12 (2)	−0.07(1)	−0.008(5)	0.033(6)

References

(1) Blase, W.; Cordier, G.; Kniep, R.; Schmidt, R. *Z. Naturforsch. B* **1989**, *44*, 505.

(2) Vaughey, J. T.; Corbett, J. D. *J. Am. Chem. Soc.* **1996**, *118*, 12098.

(3) Blase, W.; Cordier, G. *Z. Naturforsch. B* **1988**, *43*, 1017.

(4) *X-AREA (Version 1.26)*, STOE & Cie GmbH, Darmstadt, **2004**.

(5) Sheldrick, G. *Acta Cryst. A* **2008**, *64*, 112.

(6) *XL - Crystal Structure Refinement - SHELXTL (Version 6.12)*, Bruker AXS, **2001**.

6.12 Topological Relationships of Four-Connected Networks Based on Structures of Sn-Rich Na–Zn–Sn Phases

Saskia Stegmaier, Thomas F. Fässler,

manuscript for publication

Abstract

A construction scheme for a series of four-connected networks is derived from an analysis of the structural relations between the Zn–Sn network structures of four-bonded atoms that are found for the Sn-rich Na–Zn–Sn phases *hP*- and *tI*-Na_2ZnSn_5 and $Na_5Zn_{2+x}Sn_{10-x}$.

For this a layer of four- and two-connected atoms which can be derived as a cutout of the cubic diamond structure serves as the basic module. Via intralayer bond formation between the two-connected atoms, modified layers of four- and three-connected atoms can be obtained. Among these are puckered layers of five-membered rings and layers with realgar-like units as known from the structures of the two Na_2ZnSn_5 modifications and $Na_5Zn_{2+x}Sn_{10-x}$, respectively. To build up three-dimensional networks of exclusively four-connected atoms, the layers are stacked so that interlayer bonds between the intralayer three-connected atoms can be formed. There are two stacking modes available for this, one is realized in the structures of the Na_2ZnSn_5 polymorphs, the other one in the structure of $Na_5Zn_{2+x}Sn_{10-x}$.

This construction scheme with the series of layers and the two stacking modes allows anticipating a family of four-connected networks that may be considered not only as polyanionic substructures in polar intermetallics or Zintl phases, but also as possible new allotrope structures of the group 14 elements C, Si, Ge, and Sn.

Introduction

The group 14 elements C, Si, Ge, and Sn engage in structures with covalent bonds between tetrahedral coordinated atoms. Four-connected networks are thus native to their structural chemistry. Network types of exclusively four-bonded atoms that are represented by at least one allotrope structure of C, Si, Ge, or Sn include the series of diamond polytype structures, clathrate structures, and the so-called *allo*-Ge structure models.

For the diamond polytype networks a puckered layer of six-membered rings in chair conformation (with all atoms involved in three intralayer bonds) can be seen as the basic structural module. To build up the network structures, such layers are stacked and interconnected so that all atoms are four-bonded and six-membered rings either in chair or in boat conformation occur between adjacent layers. The different polytypes represent variants with different stacking sequences. The archetypal cubic diamond structure is also adopted by the α-modifications of Si, Ge, and Sn, and few other diamond polytype structures are known for C, Si, and Ge allotropes. These and more have been subject to theoretical studies, e.g. in [1] 2H, 3C, 4H, and 6H polytype structures have been considered for C, Si and Ge.

Clathrates owe their name to framework structures featuring cavities in which guests can be encaged. With a set of polyhedral cages as building blocks, most of the basic and intergrowth clathrate frameworks may be described as space-filling arrangements comprising one to four different cage types.[a] The (almost) guest free type-II clathrates Na_xSi_{136} ($x < 1$) [2, 3] and $\square_{24}Ge_{136}$ [4] (□: vacant position in cage) substantiate the suitability of (empty) clathrate networks as allotrope structures for the group 14 elements. An extensive theoretical study on clathrate structures for C, Si, Ge, and Sn has been published recently.[5],[b] Hypothetical carbon modifications derived from zeolite frameworks (including the clathrate type-I and type-II structures) have also been considered in [6].

Structure models for so-called *allo*-Ge constitute another series of four-connected networks.[7-10] According to the synthesis of *allo*-Ge by oxidative delithiation of Li_7Ge_{12},[7, 10] the basic structural module for these networks is a layer featuring four-, three-, and two-connected atoms as present in the structure of Li_7Ge_{12} (where adjacent layers are separated by Li atoms). Networks are again built up by stacking layers and forming interlayer bonds, furthermore, some of the intralayer connections are affected. Different stacking and interconnection

[a] Note that this does not hold for all network structures that are numbered among the clathrates, and that there are also some examples for clathrate frameworks that do not exclusively comprise four-connected atoms.

[b] See also [5] for an overview on previous theoretical studies on this subject.

patterns are possible and there are also variations concerning some of the intralayer bonds. Similarly, a number of contemplable four-connected networks have been constructed (as so-called *allo*-Si structure models) starting with a layer of four-, three-, and two-connected atoms that is known from the structure of $NaLi_3Si_6$ (where adjacent layers are separated by Na and Li atoms). Structures based on the layers of Li_7Ge_{12} have been considered in theoretical studies for Ge[8-10] and Si,[8, 9] and also the structures derived from the layers of $NaLi_3Si_6$[11] have been considered for both Si and Ge.[9]

Four-connected networks with tetrel element atoms are also found for a number of ternary silicides, germanides and stannides. These are either Zintl compounds or closely related polar intermetallic phases with alkali metal, alkaline earth metal, or rare earth metal cations as guests in the voids of polyanionic networks. A charge balanced situation, with a four-connected network structure that abides to the 8–*N* rule, can be reached in ternary compounds with electron poorer group 13 or late d block metal atoms alongside the group 14 element atoms in the network. Among such ternary tetrelides, there are phases with cation-stuffed diamond polytype structures and intermetallic clathrates, and beyond that, also some phases featuring four-connected networks that are not known for elemental modifications.

The two isotypic $Na_5T_{2+x}Sn_{10-x}$ phases ($x \approx 0.5$; T = Zn, Hg)[12] show a novel T–Sn network with realgar-like structural motifs. *tI*-Na_2ZnSn_5 [see manuscript 6.11] exhibits an open framework with (non-intersecting) helical channels in two perpendicular directions which is closely related to the framework with helical channels in only one direction that is presented by $NaGaSn_2$,[13] $NaInSn_2$,[14] $NaGaSn_5$,[15] and *hP*-Na_2ZnSn_5 [see manuscript 6.11]. In case of these experimentally known ternary phases the channels are occupied by Na atoms. In theoretical studies, the (empty) framework structure with helical channels in one direction[c] has also been considered as a possible allotrope structure for C,[16, 17] Si,[9, 16-18] Ge,[9, 16] and Sn.[16] Notably, the structure was not only deduced from $NaGaSn_5$ (in [9]), but also rediscovered via random search approaches for C[16] and Si.[16, 18] It was found to be comparable in energy to type-I clathrate (if considered) and type-II clathrate structures,[9, 16, 18] and lower in energy than any of the considered (Si and Ge) *allo*-structures.[9, 18] (The cubic diamond structure is always established to be energetically most favorable.) So, this type of open framework structure seems to be quite a promising candidate for new group 14 element allotrope structures.

[c] The network was recognized (in [15]) as related to a hypothetical zeolite structure enumerated 271 and identified as chemically feasible in: M. D. Foster, O. Delgado Friedrichs, R. G. Bell, F. A. Almeida Paz, J. Klinowski, *J. Am. Chem. Soc.* **2004**, *126*, 9769.

A brief account on the structural relations between the Zn–Sn networks of these phases has already been given in the report on *hP*- and *tI*-Na_2ZnSn_5 and their relation to $Na_5Zn_{2+x}Sn_{10-x}$ [manuscript 6.11]. Here we now expand on some general features of these network structures and present a construction scheme for a series of related four-connected networks that might be considered as possible new allotrope structures of the group 14 elements C, Si, Ge, and Sn.

A Construction Scheme for Networks of Four-Connected Atoms

Layers

The basic module for the construction scheme that will be drawn up in the following is a layer of four- and two-connected atoms[d] (Figure 1b,c) which can be cut out of the cubic diamond structure as shown in Figure 1a,b [cf. manuscript 6.11].

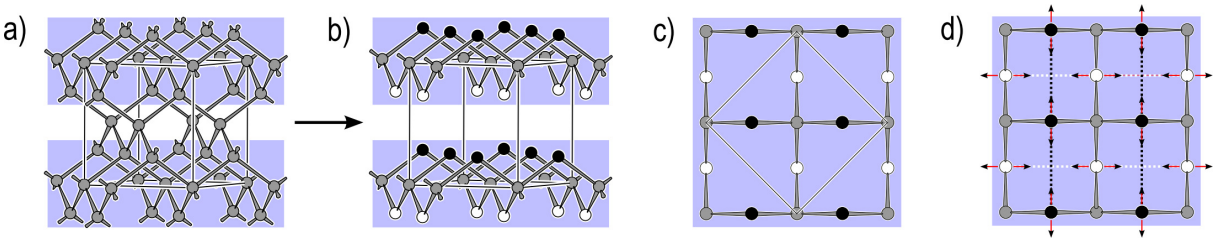

Figure 1.[cf. manuscript 6.11] a) A representation of the cubic diamond structure. b) Layers of four- and two-connected atoms cut out of the cubic diamond structure. Atoms are represented as black, gray, and white spheres to indicate their positioning within such a layer: Gray spheres are used for intralayer four-connected atoms, black and white spheres for intralayer two-connected atoms on the two different sites of the plane in which the four-connected atoms are situated. c) Top view of such a layer. Broken-off bonds not shown. d) For each two-connected atom there are two potential intralayer bonding partners.

[d] The structure of the tetragonal high pressure modification of LiGe (HP-LiGe) actually features such layers of four- and two-connected Ge atoms (separated by Li atoms), see: J. Evers, G. Oehlinger, G. Sextl, H.-O. Becker, *Angew. Chem. Int. Ed. Engl.* **1987**, *26*, 76.

A series of layers of four- and three-connected atoms can be created via the formation of bonds between the two-connected atoms of this basic layer. In doing so, there are initially two potential bonding partners for each of them, as indicated in Figure 1d. Each bond formation introduces two five-membered rings in envelope conformation. An eight-membered ring fragment of the basic layer can thus end up as two edge sharing five-membered rings (Figure 2a,b), a realgar-like unit (Figure 2c), or a reshaped eight-membered ring (Figure 2d).

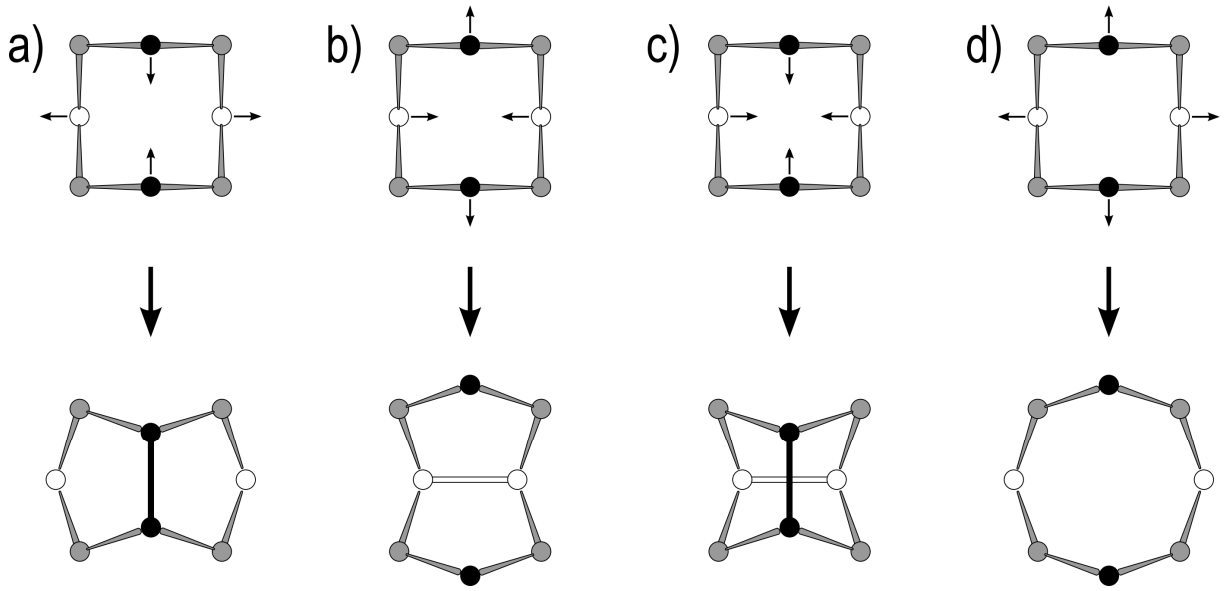

Figure 2. Displacement in eight-membered ring fragments of the basic layer (cf. Figure 1d), and (after bond formation) resulting structural motifs of the layers of four- and three-connected atoms. Broken-off bonds are not shown. Representation in top view. To indicate the positioning of the atoms in the projection direction, they are represented as black, gray, and white spheres as introduced in Figure 1. a) and b) One bond is formed in the fragment and two edge sharing five-membered rings result. c) Two bonds are formed in one fragment, leading to a realgar-like unit. d) No bond is formed in the fragment and a reshaped eight-membered ring remains.

Some thoughts on intralayer bonding patterns are illustrated in Figure 3, a description and explanations for the labels etc. are given in the figure caption. High symmetry designs for layers of four- and three-connected atoms are sketched in Figure 3f-j. The series of Figures 3a,f,k shows the construction of puckered layers of five-membered rings as they occur e.g. in *hP*- and *tI*-Na_2ZnSn_5 as well as in $NaSn_5$.[19] Layers as found in $Na_5Zn_{2+x}Sn_{10-x}$[12] can

be obtained according to Figures 3a,j,l. The details of the structural changes that are required for the transformation of the basic module to a finished layer of four- and three-connected atoms are fairly involved, including the alteration of the bond angles etc. Schematically, the four-connected atoms may be seen to act as anchors during the conversion while all other atoms engage in a new bond and undergo quite a displacement.

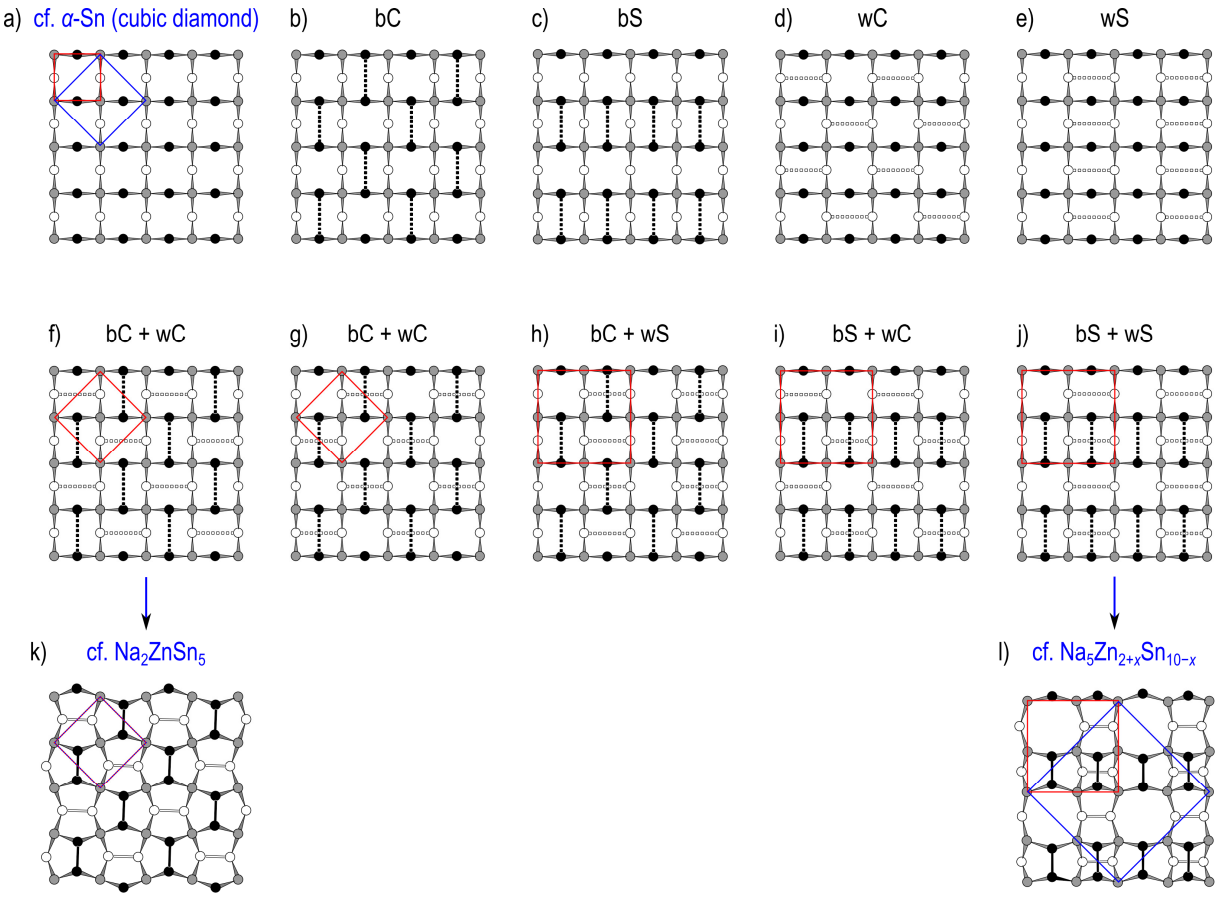

Figure 3. Construction of layers of four- and three-connected atoms. Representations in top view. To indicate the positioning of the atoms in the projection direction, they are represented as black, gray, and white spheres (cf. Figure 1). Red lines show the repeating units of the layers, blue lines indicate the relative unit cell dimensions of α-Sn, *hP*- and *tI*-Na_2ZnSn_5, and $Na_5Zn_{2+x}Sn_{10-x}$. a) Basic layer of four- and two-connected atoms (cf. Figure 1). b)-e) Basic chess board (b and d) and stripes (c and e) patterns for bond formation between atoms represented as black spheres (b and c) and between atoms shown as white spheres (d and e). Labels: "C" for chess board, "S" for "stripes", "b" for "black", and "w" for "white". f) to j) High symmetry layer designs that arise from combinations of the patterns shown in b) to e). k) Puckered layer of five-membered rings as found in *hP*- and *tI*-Na_2ZnSn_5. l) Layer with realgar-like units as known from $Na_5Zn_{2+x}Sn_{10-x}$.

Note that among the experimentally determined crystal structures, the tetragonal structure of *tI*-Na_2ZnSn_5 actually shows layers with undistorted square arrangements of intralayer four-connected atoms. In case of *hP*-Na_2ZnSn_5 there is just a small deviation, while for the layers of $Na_5Zn_{2+x}Sn_{10-x}$ (see Figure 3l), which feature all the structural motifs shown in Figure 2, the positioning of the four-connected atoms differs discernibly from a square pattern.

Stacking

Four-connected networks can be built up by stacking of the layers accompanied by the formation of interlayer bonds. Either the layers of four- and three-connected atoms are used for this, or the construction is started at this point with the basic layers and intralayer bond formation is taken care off afterwards. Interlayer bonds will obviously be formed between atoms that come close to each other in the stacking. In the representations of two adjacent layers *A* (red) and *A'* (blue) in Figure 4, these are the atoms shown as dark red and light blue spheres – see the figure caption for a detailed explanation of the color-coding etc. As depicted in Figures 4a and 4b for basic layers there are two arrangements in which these atoms come to lie on top of each other. (As viewed in projection along the stacking direction:) Adjacent stacked layers *A* and *A'* are either offset by half a diagonal of the square repeating unit of the basic layer (Figure 4a), or they appear rotated with respect to each other by 90° (Figure 4b).[e]

The network structures of *hP*- and *tI*-Na_2ZnSn_5 can be assembled via offset stacking of puckered layers of five-membered rings (Figure 3k) as illustrated for two layers in Figure 4c. The offset between the two layers equals half a basis vector of the layer – which corresponds to half a diagonal of the basic layer's repeating unit (as can be seen by comparison of the unit cell dimensions indicated in Figures 4a,c). The other stacking mode can be recognized in the network structure of $Na_5Zn_{2+x}Sn_{10-x}$. Layers of the type depicted in Figure 3l are stacked as shown in Figure 4d, with realgar-like units and eight-membered rings on top of each other.[f]

[e] An arrangement as sketched in Figure 4b has been described among a collection of some hypothetical structures based on the layer of four- and two-connected atoms known from tetragonal HP-LiGe (see footnote [d]) in: P. Sherwood, R. Hoffmann, *J. Am. Chem. Soc.* **1990**, *112*, 2881. Various stacking and interconnection patterns for the layers were considered therein, but no conversion of the layers themselves as it is described in the present manuscript.

[f] $Na_5Zn_{2+x}Sn_{10-x}$ is actually reported to adopt an orthorhombic structure with larger unit cell dimensions[11] (see blue lines in Figure 3l) – this is associated with the occupancy pattern (Zn and Sn atoms) in the network structure.

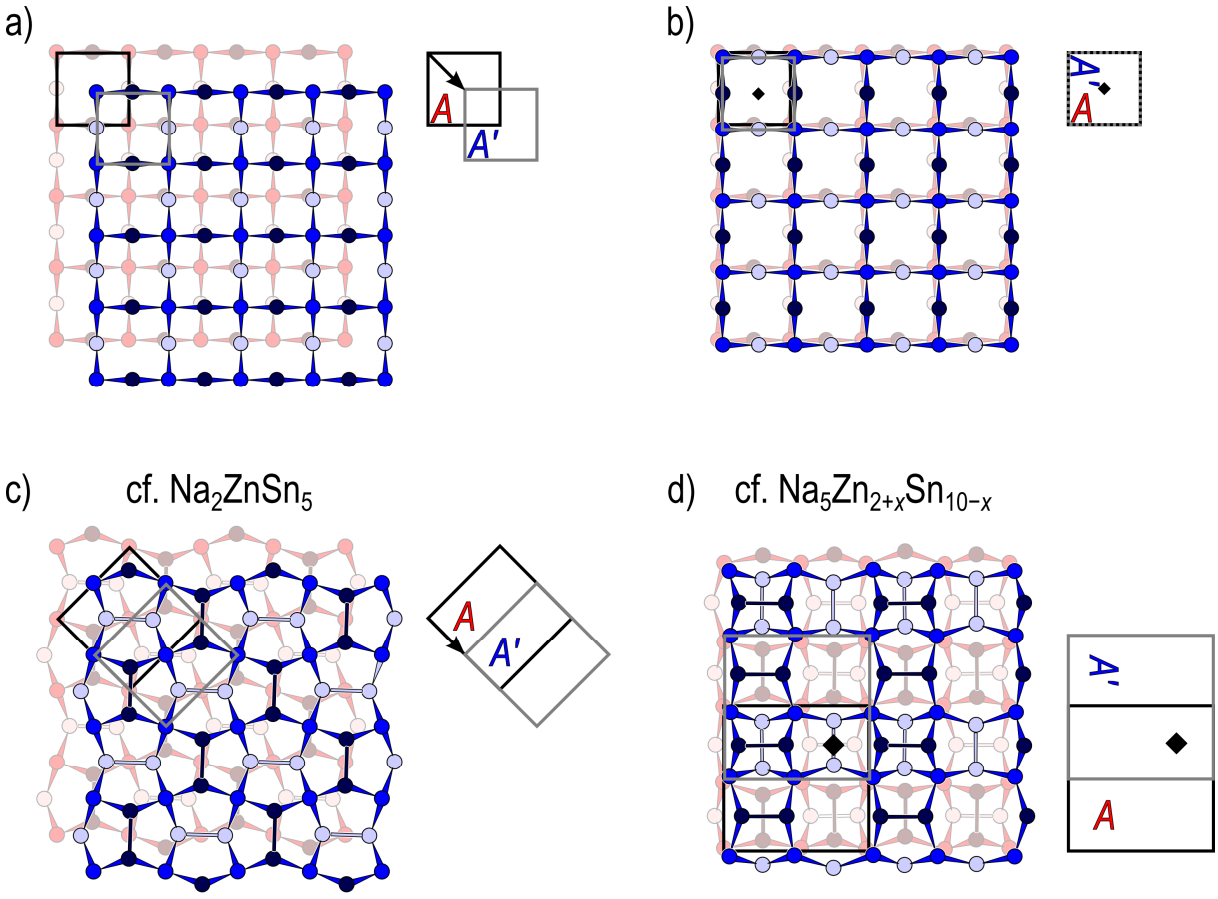

Figure 4. Layer stacking. Representations for two adjacent layers *A* and *A'*. Top view – in case of a) and b) slightly inclined for clarity. Atoms of the lower layer *A* are represented as red spheres, atoms of the upper layer *A'* as blue spheres. Different color shades are used to indicate the positioning of the atoms in the projection direction. With respect to Figures 1 to 3, dark red and blue correspond to black, red and blue to gray, light red and blue to white. a) and b) Stacking of two basic layers of four- and two-connected atoms, a) with on offset of half a diagonal of the square repeating unit of the layer, and b) rotated with respect to each other by 90° (◆ indicates the location of a four-fold symmetry axis). c) Offset stacking of puckered layers of five-membered rings (see Figure 3k) as realized in the network structures of *hP*- and *tI*-Na_2ZnSn_5. d) Stacking of layers as found for $Na_5Zn_{2+x}Sn_{10-x}$ (see Figure 3l), with adjacent layers appearing as rotated with respect to each other (◆ indicates the locating of a four-fold symmetry axis).

Building and Transforming Networks

Utilizing the construction scheme presented herein, a series of four-connected networks may be obtained by combinations of layer designs and stacking modes. Furthermore, the scheme provides an elegant pathway for the interconversion of any two networks of the series that show the same stacking mode sequence – namely via the related basic layers stacked and interconnected as shown in Figures 4a and 4b. Such a pathway, that requires only the change of intralayer bonding patterns while no interlayer bonds need to be broken, has also been presented in the discussion on the structural phase transition from *hP*-Na_2ZnSn_5 to *tI*-Na_2ZnSn_5 [manuscript 6.11].

Conclusion

The construction scheme that is pictured herein allows to anticipate four-connected networks and polymorphic phase transitions that may be considered in theoretical or realized in experimental studies concerned with Zintl phases or allotropes of the group 14 elements C, Si, Ge and Sn.

References

[1] C. Raffy, J. Furthmüller, F. Bechstedt, *Phys. Rev. B* **2002**, *66*, 075201.

[2] J. Gryko, P. F. McMillan, R. F. Marzke, G. K. Ramachandran, D. Patton, S. K. Deb, O. F. Sankey, *Phys. Rev. B* **2000**, *62*, R7707.

[3] A. Ammar, C. Cros, M. Pouchard, N. Jaussaud, J.-M. Bassat, G. Villeneuve, M. Duttine, M. Ménétrier, E. Reny, *Solid State Sciences* **2004**, *6*, 393.

[4] A. M. Guloy, R. Ramlau, Z. Tang, W. Schnelle, M. Baitinger, Y. Grin, *Nature* **2006**, *443*, 320.

[5] A. J. Karttunen, T. F. Fässler, M. Linnolahti, T. A. Pakkanen, *Inorg. Chem.* **2011**, *50*, 1733.

[6] R. Nesper, K. Vogel, P. E. Blöchl, *Angew. Chem. Int. Ed. Engl.* **1993**, *32*, 701; *Angew. Chem.* **1993**, *105*, 786.

[7] A. Grüttner, R. Nesper, H. G. von Schnering, *Angew. Chem. Int. Ed. Engl.* **1982**, *21*, 912.

[8] D. J. Chadi, *Phys. Rev. B* **1985**, *32*, 6485.

[9] J. C. Conesa, *J. Phys. Chem. B* **2002**, *106*, 3402.

[10] F. Kiefer, A. J. Karttunen, M. Döblinger, T. F. Fässler, *Chemistry of Materials* **2011**, *23*, 4578.

[11] H. G. von Schnering, M. Schwarz, R. Nesper, *J. Less. Common Met.* **1988**, *137*, 297.

[12] S. Ponou, S.-J. Kim, T. F. Fässler, *J. Am. Chem. Soc.* **2009**, *131*, 10246.

[13] J. T. Vaughey, J. D. Corbett, *J. Am. Chem. Soc.* **1996**, *118*, 12098.

[14] W. Blase, G. Cordier, R. Kniep, R. Schmidt, *Z. Naturforsch. B* **1989**, *44*, 505.

[15] W. Blase, G. Cordier, *Z. Naturforsch. B* **1988**, *43*, 1017.

[16] C. J. Pickard, R. J. Needs, *Phys. Rev. B* **2010**, *81*, 014106.

[17] D. Connétable, *Phys. Rev. B* **2011**, *83*, 035206.

[18] M. A. Zwijnenburg, K. E. Jelfs, S. T. Bromley, *Phys. Chem. Chem. Phys.* **2010**, *12*.

[19] T. F. Fässler, C. Kronseder, *Angew. Chem. Int. Ed.* **1998**, *37*, 1571; *Angew. Chem.* **1999**, *110*, 1641.

6.13 $SrZn_2Sn_2$ and $Ca_2Zn_3Sn_6$ – Two New *Ae*–Zn–Sn Polar Intermetallic Compounds (*Ae*: Alkaline Earth Metal)

S. Stegmaier, T. F. Fässler,

J. Solid State Chem. **2012**, *192*, 312.

The song is sung.

A Curious Thing – Don’t Tell Me That It’s Over / Amy McDonald